

Groundwater movements around a repository

Repository domain groundwater flow analyses

Part 1 Permeability perturbations

Part 2 Inflow to repository

Part 3 Thermally induced flow

Joe L Ratigan

Anthony S Burgess

Edward L Skiba

Robin Carlwood

Hagconsult AB september 1977

GROUNDWATER MOVEMENTS AROUND A REPOSITORY
REPOSITORY DOMAIN GROUNDWATER FLOW ANALYSES
PART 1 PERMEABILITY PERTURBATIONS
PART 2 INFLOW TO REPOSITORY
PART 3 THERMALLY INDUCED FLOW

Joe L Ratigan
Anthony S Burgess
Edward L Skiba
Robin Charlwood
Hagconsult AB september 1977

Denna rapport utgör redovisning av ett arbete som utförts på uppdrag av KBS. Slutsatser och värderingar i rapporten är författarens och behöver inte nödvändigtvis sammanfalla med uppdragsgivarens.

I slutet av rapporten har bifogats en förteckning över av KBS hittills publicerade tekniska rapporter i denna serie.

TECHNICAL REPORT 5
REPOSITORY DOMAIN GROUNDWATER FLOW
ANALYSES
PART I
PERMEABILITY PERTURBATIONS

GROUNDWATER MOVEMENTS AROUND A REPOSITORY

Technical report 5. Repository Domain Groundwater Flow Analyses

Part I:

Permeability Perturbations

Hagconsult AB
in association with
Acres Consulting Services Ltd
RE/SPEC Inc.

FOREWORD

This report was prepared as one of a series of Technical reports within a study of the groundwater movements around a repository for radioactive waste in the precambrian bedrock of Sweden. It was written in three parts, (I) Permeability Perturbations, (II) Inflow to Repository and (III) Thermally Induced Flow. This is Part I. The contract for this study was between KBS - Kärnbränslesäkerhet (Project Fuel Safety) and Hagconsult AB of Stockholm, Sweden. RE/SPEC Inc. of Rapid City, SD/USA and Acres Consulting Services Ltd of Niagara Falls, Ontario/Canada acted as subconsultants to Hagconsult AB.

The principal author of this report is Mr. Joe L. Ratigan of RE/SPEC Inc. with contributions by Dr. A.S. Burgess of Acres. Review was provided by Dr. Ulf E. Lindblom of Hagconsult AB, Dr. Paul F. Gnirk of RE/SPEC Inc. and Dr. Robin G. Charlwood of Acres.

The opinions and conclusions in this document are those of the author and should not be interpreted as necessarily representing the official policies or recommendations of KBS.

Stockholm September 1977

Ulf E. Linblom
Study Director
Hagconsult AB

TABLE OF CONTENTS

Page

1.	INTRODUCTION	1
2.	PERMEABILITY AS A FUNCTION OF STRESS AND TEMPERATURE	2
2.1	Stress dependency	2
2.2	Temperature dependency	3
3.	LOCAL MODELING PERTURBATIONS	5
3.1	Excavation effects	5
3.2	Thermomechanical stress effects	6
3.3	Temperature effects	8
4.	GLOBAL MODELING PERTURBATIONS	9
4.1	Thermomechanical stress effects	9
4.2	Temperature effects	9
5.	SUMMARY AND CONCLUSIONS	11

REFERENCES

LIST OF FIGURES

Figure

1. Ratios of post excavation horizontal permeability to in situ horizontal permeability for 0° and 90° joint sets.
2. Ratios of post excavation vertical permeability to in situ vertical permeability for 0° and 90° joint sets.
3. Ratios of post excavation normal permeability to in situ normal permeability for 0° and 90° joint sets.
4. Ratios of post excavation tangential permeability to in situ tangential permeability for 0° and 90° joint sets.
5. Ratios of post excavation horizontal permeability to in situ horizontal permeability for 45° and -45° joint sets.
6. Ratios of post excavation vertical permeability to in situ vertical permeability for 45° and -45° joint sets.
7. Post excavation permeability and permeability from thermomechanical normal stresses after 40 years in the tunnel roof.
8. Post excavation permeability and permeability from thermomechanical normal stresses after 40 years in the tunnel rib.
9. Post excavation permeability and permeability from thermomechanical normal stresses after 40 years in the tunnel floor.
10. Ratios of horizontal permeability from thermomechanical normal stresses after 40 years to post excavation horizontal permeability.
11. Ratios of vertical permeability from thermomechanical normal stresses after 40 years to post excavation vertical permeability.

12. Ratios of in situ viscosity to viscosity after 40 years without repository ventilation.
13. Ratios of in situ viscosity to viscosity after 100 years without repository ventilation.
14. Ratios of horizontal permeability with repository ventilation to horizontal permeability without ventilation at 40 years.
15. Ratios of vertical permeability with repository ventilation to vertical permeability without ventilation at 40 years.
16. Ratios of horizontal and vertical permeability resulting from thermomechanical normal stresses at 40 years to in situ values as a function of depth.
17. Ratios of in situ viscosity to viscosity after 40 years and 100 years as a function of depth for instantaneous waste emplacement.
18. Ratios of in situ viscosity to viscosity after 40 years and 100 years as a function of depth for linear waste emplacement.

REPOSITORY DOMAIN GROUNDWATER FLOW ANALYSES - PERMEABILITY PERTURBATIONS

1. INTRODUCTION

Previous analyses within this study (1)^x have provided qualitative evaluations of the perturbation of in situ hydraulic permeability and groundwater flow resulting from (a) the transient temperature fields due to the emplacement of radioactive heat generating waste in a granitic formation (2), and from (b) the stress perturbations due to the excavation of the repository and the thermomechanical loading associated with the aforementioned temperature fields (3). In this report, these perturbations will be treated and analyzed in a quantitative fashion. In particular, relationships have been derived and extracted from the literature which relate hydraulic permeability to rock stress, and viscosity to groundwater temperature. These relationships have been employed to quantitatively evaluate the hydraulic permeability around the repository as a function of the temperature fields presented in (2) and the stress states presented in (3).

The results presented in this report are based on limited data. At this time, no site specific data are available for these effects. To determine these effects, extensive field and laboratory testing and advancement of the state-of-the-art in both field testing methodology and understanding of joint behavior will be required. However, the quantitative results presented in this report can be utilized to quite reliably identify the importance and influence of the temperature and stress perturbations on the rock mass hydraulic permeabilities. In fact, the perturbations of the hydraulic permeability can probably be established with a greater degree of certainty than the values of in situ permeability.

Future sections of this report will present the assumed permeability - stress and permeability - temperature relationships employed and the subsequent perturbations resulting in the local and global repository regions.

^xNumbers in parenthesis refer to references at end of text.

2. PERMEABILITY AS A FUNCTION OF STRESS AND TEMPERATURE

2.1 Stress dependency

The relationships which correlate hydraulic permeability with rock stress as presented in this report should not be interpreted as necessarily accurately representing the in situ conditions. This topic is the subject of current on going research and will perhaps not be well established within the next decade. Previous investigations are inconclusive in relating permeability changes to pre-loading stress states, and in relating permeability to load path in a quantitative manner. A more detailed description of the present state of the art is provided in (4).

Despite the uncertainty in the permeability-stress relationships, one can conclude with a relatively high degree of certainty that within the elastic range of loading and unloading of a rock joint, the hydraulic permeability is a function of the rock stress normal to the joint plane (or equivalently to the joint aperture). It is this relationship (permeability as a function of normal stress) that has been utilized in this study to analyze the effects of stress changes on hydraulic permeabilities.

The empirical relationship between permeability and normal stress which has been utilized in obtaining the results presented in this report has been previously cited in (4). In polynomial form, this relationship can be stated as

$$\log_{10} |K(\sigma_n/\sigma_o)| = -5.57 + 0.362 \log_{10} (\sigma_n/\sigma_o) - 0.978 |\log_{10} (\sigma_n/\sigma_o)|^2 + 0.167 |\log_{10} (\sigma_n/\sigma_o)|^3$$

where

σ_n = stress normal to the joint plane (MPa)

K = hydraulic permeability (m/s)

$\sigma_o = \rho_l g \cdot \rho \cdot l$ (MPa)

g = gravitational acceleration

ρ = density (t/m³)

l = unity (m)

Although other relationships have been obtained in the laboratory and in the field (5), this relationship has been employed since it produces higher hydraulic permeabilities and possesses less normal compressive stress dependency than those presented in (5) for the range of stresses which will occur in and around a repository. In this regard, the formula is conservative, since it results in higher groundwater flows.

2.2 Temperature dependency

A temperature dependency of hydraulic permeability occurs through the perturbation of groundwater viscosity. The differential equation for transient groundwater flow in an isothermal porous media is:

$$\nabla \left| \rho \frac{k_{ij}}{\mu} \nabla p \right| + Q(t, x_i) = \rho c \frac{\partial p}{\partial t}$$

where

ρ = density

k_{ij} = intrinsic permeability tensor

μ = dynamic viscosity

c = specific storage

p = potential

$Q(t, x_i)$ = inhomogenities (fluid source or sink)

reduces to

$$\nabla^2 p = 0$$

in the steady state situation with no inhomogenities. The flux or groundwater flow is merely

$$q_i = K_{ij} \frac{\partial p}{\partial x_j}$$

where

K_{ij} = hydraulic permeability

However, if the steady state groundwater flow is treated in a "quasi-coupled" fashion, the permeability tensor can be estimated to be

$$\frac{K_{ij}}{\mu(T)} \cdot \mu(T_0)$$

where

$\mu(T)$ = dynamic viscosity at temperature T

T_0 = ambient temperature

in order to obtain a first estimate of thermal effects on hydraulic permeability and subsequent groundwater flow. This is the form of the hydraulic permeability - temperature relationship utilized in this study to obtain the results presented in this report.

The function $\mu(T)$ has been taken from (6) and can be stated as

$$\frac{1}{\mu(T)} = 5380 + 3800A - 260A^3 \quad (\text{kg/m, s})$$

where

$$A = (T - 150)/100$$

$$T = \text{temperature } (^{\circ}\text{C})$$

As stated in (6), this relationship is accurate within 3% over a range of temperatures of 0 $^{\circ}\text{C}$ to 300 $^{\circ}\text{C}$.

3. LOCAL MODELING PERTURBATIONS

3.1 Excavation Effects

The excavation of an underground opening will result in a perturbation of the hydraulic permeability around the opening. The excavation method, the subsequent accentuation and attenuation of stresses around the opening, the stress relief and dilatation resulting from failure in shear, all affect hydraulic permeability. Due to the complexity of this interaction, it is extremely difficult (if not impossible) to provide a quantitative analysis of the resulting permeability based upon intuition. Perhaps the same statement can be made even for a qualitative analysis.

Figure 1 and 2 illustrate the ratios R_h and R_v , respectively, around the repository storage tunnel after excavation as

$$R_h = K_h(\sigma_e)/K_h(\sigma_0)$$

$$R_v = K_v(\sigma_e)/K_v(\sigma_0)$$

where

$K_h(\sigma_e)$ = horizontal permeability after excavation

$K_v(\sigma_e)$ = vertical permeability after excavation

$K_h(\sigma_0)$ = in situ horizontal permeability

$K_v(\sigma_0)$ = in situ vertical permeability

σ_0 = in situ stress state

σ_e = stress state after excavation

The in situ permeabilities are those identified in (7) as Case 4

The stresses used in producing these figures are those presented in (3) for the excavation in a rock mass with 0° and 90° joint sets.

Although this simulated excavation resulted in some regions around the opening experiencing strength failure, no explicit accounting of these regions has been utilized in assessing the resulting permeabilities. The stress dependency equation presented in part 2.1 was used in all regions.

The effect of the excavation on the virgin permeabilities is quite pronounced around the storage tunnel periphery; however, the permeability is at the initial magnitude for distances greater than about 2 meters from the tunnel periphery. This dimension would probably be greater if the regions experiencing failure were considered to have experienced joint dilatation.

It is essential to note that the permeabilities presented in the preceding figures are highly dependent upon the assumed in situ stresses and the storage tunnel geometry. For example, if the rib were nearly vertical, the horizontal stresses in the floor would be less and the resulting vertical permeability would be greater. Similarly, if the ratio of in situ horizontal stress to vertical stress were taken to be 1 rather than 2, the horizontal stress at the roof would be less and the resulting vertical permeability greater.

Figures 3 and 4 present the permeability ratios resulting from tunnel excavation based on the assumption that the principal permeability directions and magnitudes are coincident with, and controlled by, the principal stresses. In fact, this may not be the case but it is instructive in displaying the permeability changes normal and tangential to the repository storage tunnel. As can be seen in the figures, the permeability ratio normal to the tunnel periphery ($K_h(\sigma_e)/K_h(\sigma_0)$) or that component which dominates flow into the tunnel, is very low in comparison to the tangential ratio. Physically, this can be explained by noting that the excavation results in an increased tangential compressive stress (above the in situ magnitude) around the tunnel which results in a lower permeability than the initial magnitude. The normal stresses are zero at the tunnel periphery and rapidly increase to in situ magnitudes, resulting in the high tangential permeability near the tunnel and near in situ permeabilities at about 2 m from the tunnel periphery.

The stresses resulting from the assumption of joint sets at 0° and 90° and the stresses from the 45° and -45° joint sets yield very similar permeabilities. These permeability ratio fields $R_h = K_h(\sigma_e)/k_h(\sigma_0)$ and $R_v = K_v(\sigma_e)/K_v(\sigma_0)$ are displayed in contour plot form in Figures 5 and 6, respectively.

3.2 Thermomechanical stress effects

In this section of the report permeabilities resulting from the thermally induced stresses presented in (3) will be presented for regions around the storage tunnel. These permeabilities have been calculated assuming permeability to be a function of the total stress normal to the joint plane. Permeability changes due to viscosity changes resulting from inhomogeneous temperature fields are presented in a later section of this report.

3.3 Temperature effects

In this section of the report permeability changes are evaluated with the functional relationships described in section 2.1 and 2.2 including both normal stress and viscosity effects due to temperature variations. As was the case with the thermomechanical stresses, the temperature effect on the permeability is not nearly as significant as the perturbation of the initial magnitudes caused by excavation. The variation due to temperature perturbation is much smaller than the uncertainty in the predictions of the in situ permeabilities.

Since a ratio of permeabilities with viscosity changes to permeabilities without viscosity changes reduces merely to the function $\mu(T)$ presented in section 2.2, Figures 12 and 13 were constructed with the ratio

$$R = \frac{\mu(T_0)}{\mu(T)}$$

where T_0 = pre-emplacment geothermal temperature

These two figures represent the viscosity ratios at 40 and 100 years after emplacement without ventilation. The greatest magnitudes are in the vicinity of the waste canister and reach a value of about 2.5 after 40 years.

In an effort to quantify the effect that repository ventilation has upon post-emplacment hydraulic permeabilities, the ratios R_h and R_v were calculated as

$$R_h = K_h(\sigma_e + \sigma_{T_v}, T_v) / K_h(\sigma_e + \sigma_{T_{nv}}, T_{nv})$$

$$R_v = K_v(\sigma_e + \sigma_{T_v}, T_v) / K_v(\sigma_e + \sigma_{T_{nv}}, T_{nv})$$

where T_v = temperatures resulting with 30 years of ventilation
 T_{nv} = temperatures resulting without ventilation

The ratios, R_h and R_v are displayed in Figures 14 and 15, respectively, which result from the total stresses and temperatures occurring 40 years after emplacement. Near the tunnel periphery the tangential permeability is greater with ventilation than without, whereas the normal permeability is about 5-20% less with ventilation than without.

4. GLOBAL MODELING PERTURBATIONS

The evaluation of the global permeability perturbations caused by the emplacement of radioactive waste has proceeded in the same manner as that for the local perturbations except that the excavation effects have not been included. The scale of the global model does not allow this level of detail.

The permeability perturbations resulting from the thermomechanical stress and temperature have been evaluated at various depths and consider various waste emplacement sequences.

4.1 Thermomechanical stress effects

The normal stresses utilized in this section of the report for the evaluation of permeability include both the in situ stresses and the thermally induced stresses. Since minimal rock strength failure was exhibited in the global rock mechanics analysis (3), the results presented herein are for all practical purposes independent of the choice of joint orientation. Therefore, the stresses from the 0° and 90° simulations were be employed.

The ratios of the horizontal and vertical permeability in the repository domain occurring 100 years after waste emplacement to the respective in situ values are presented in Figure 16, as a function of depth. The thermomechanical stresses utilized in obtaining these results are those relating to the instantaneous emplacement at 500 m depth (3). As can be seen in the figures, the stress effect on permeabilities is very small. Similar small changes in permeability are noted in both the linear waste emplacement model and the instantaneous waste emplacement at 1000 meters.

4.2 Temperature effects

The permeability changes due to the effect of temperature on viscosity have been analyzed with the temperatures resulting from both the instantaneous and linear waste emplacement sequences. As noted earlier, this perturbation can be represented as the ratio of viscosities. This ratio as a function of depth is displayed in Figure 17 for the instantaneous waste emplacement at 40 and 100 years after emplacement. The viscosity

perturbation in the linear waste emplacement model is illustrated in Figure 18 for 40 and 100 years after initiation of emplacement. The maximum viscosity ratio for these cases is approximately 2.

Perturbations due to viscosity changes at the 1000 meter level repository model are slightly less than those at the 500 meter level model due to the higher initial temperature at 1000 meters.

5. SUMMARY AND CONCLUSIONS

The perturbations of the in situ hydraulic permeability caused by (a) stresses resulting from repository storage tunnel excavation and (b) the thermomechanical stresses resulting from the radiogenic heat have been evaluated. Changes in the permeability due to the temperature dependence of the viscosity have also been studied.

The effects of repository ventilation and waste emplacement sequence on permeability changes have been evaluated for the local and global models, respectively.

It was found that the most significant perturbation in the hydraulic permeabilities was caused by the excavation of the storage tunnels. The change in permeability caused by the temperature and thermomechanical stresses is expected to be small in comparison with expected uncertainty in in situ permeability values. The permeabilities are about 5-20% lower with storage tunnel ventilation than without ventilation.

The perturbed permeability fields will be used in subsequent analyses of groundwater flow.

REFERENCES

1. Lindblom, U.E., Gnirk, P.F., Charlwood, R.G. and Cherry, J., "GROUNDWATER MOVEMENTS AROUND A REPOSITORY, Phase 1. State Of The Art and Detailed Study Plan", Submitted to KBS-Kärnbränslesäkerhet, Stockholm, Sweden, 1977.
2. Ratigan, J.L., "GROUNDWATER MOVEMENTS AROUND A REPOSITORY, Phase 2. Technical Report 3. Thermal Analyses - Part I: Conduction Heat Transfer", Submitted to KBS - Kärnbränslesäkerhet, Stockholm, Sweden., 1977.
3. Ratigan, J.L. "GROUNDWATER MOVEMENTS AROUND A REPOSITORY", Phase 2. Technical Report 4. Rock Mechanics Analyses", To be submitted to KBS - Kärnbränslesäkerhet, Stockholm, Sweden, 1977.
4. Stille, H., Burgess, A.S. and Lindblom, U.E., "GROUNDWATER MOVEMENTS AROUND A REPOSITORY, Phase 2. Technical Report 1. Geological and Geotechnical Conditions", To be submitted to KBS - Kärnbränslesäkerhet, Stockholm, Sweden 1977.
5. Witherspoon, P.A., Amick, C.H., Gale, J.E., Stress-Flow Behavior of a fault zone with fluid injection and withdrawal, Report to U.S. Geological Survey, Contract No. 14-08-001-14583, Report No.77-1.
6. Mercer, J.W. and Pinder, G.F., "Finite Element Analysis of Hydrothermal Systems", Finite Element Methods in Flow Problems, University of Alabama Press, 1974, pp. 401 - 414.
7. Burgess, A.S., "GROUNDWATER MOVEMENTS AROUND A REPOSITORY, Phase 2. Technical Report 5. Repository Domain Groundwater Flow Analyses, Part II: Inflow to Repository, to be submitted to KBS - Kärnbränslesäkerhet, Stockholm, Sweden 1977.

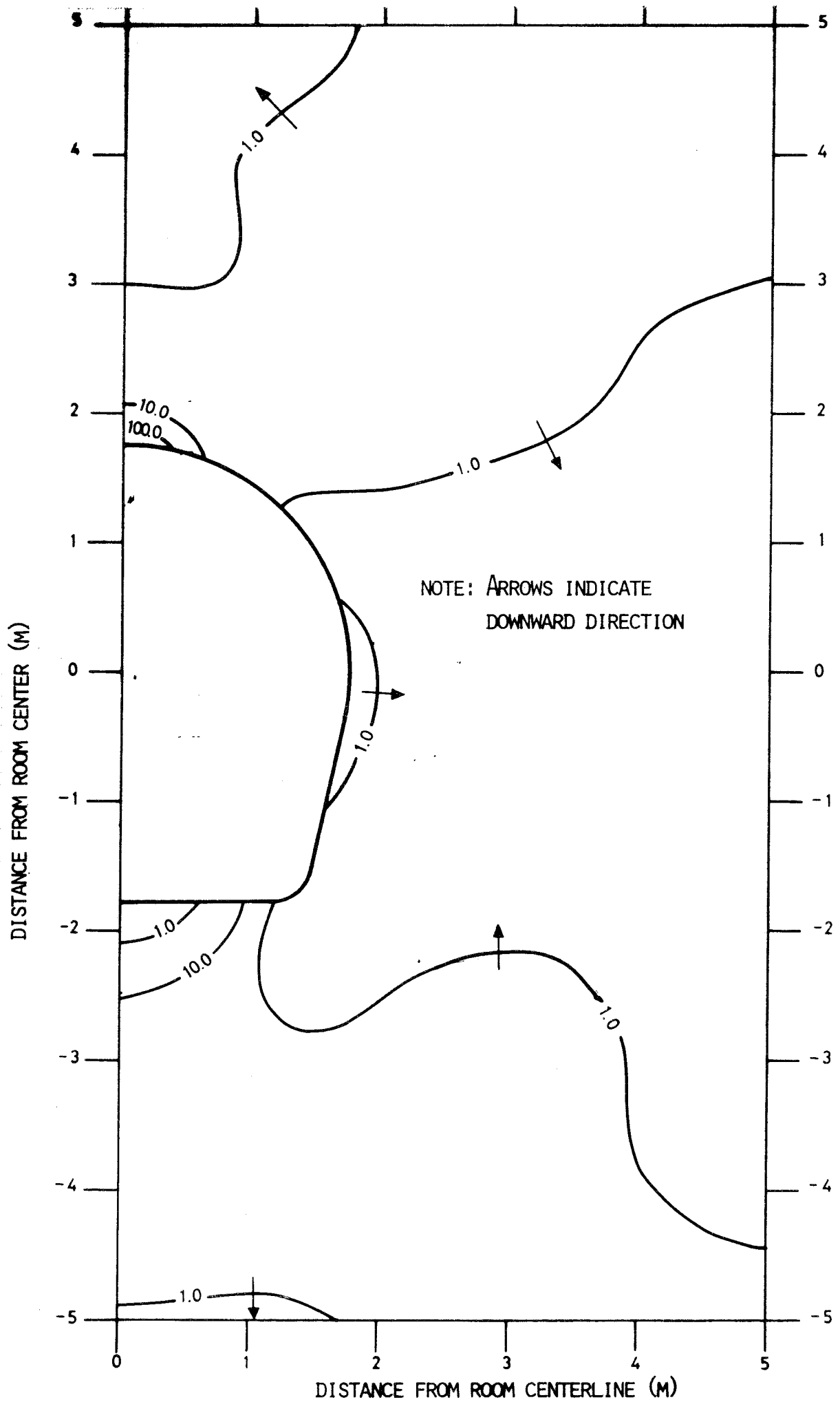


FIGURE 1. RATIOS OF POST EXCAVATION HORIZONTAL PERMEABILITY TO IN SITU HORIZONTAL PERMEABILITY FOR 0° AND 90° JOINT SETS

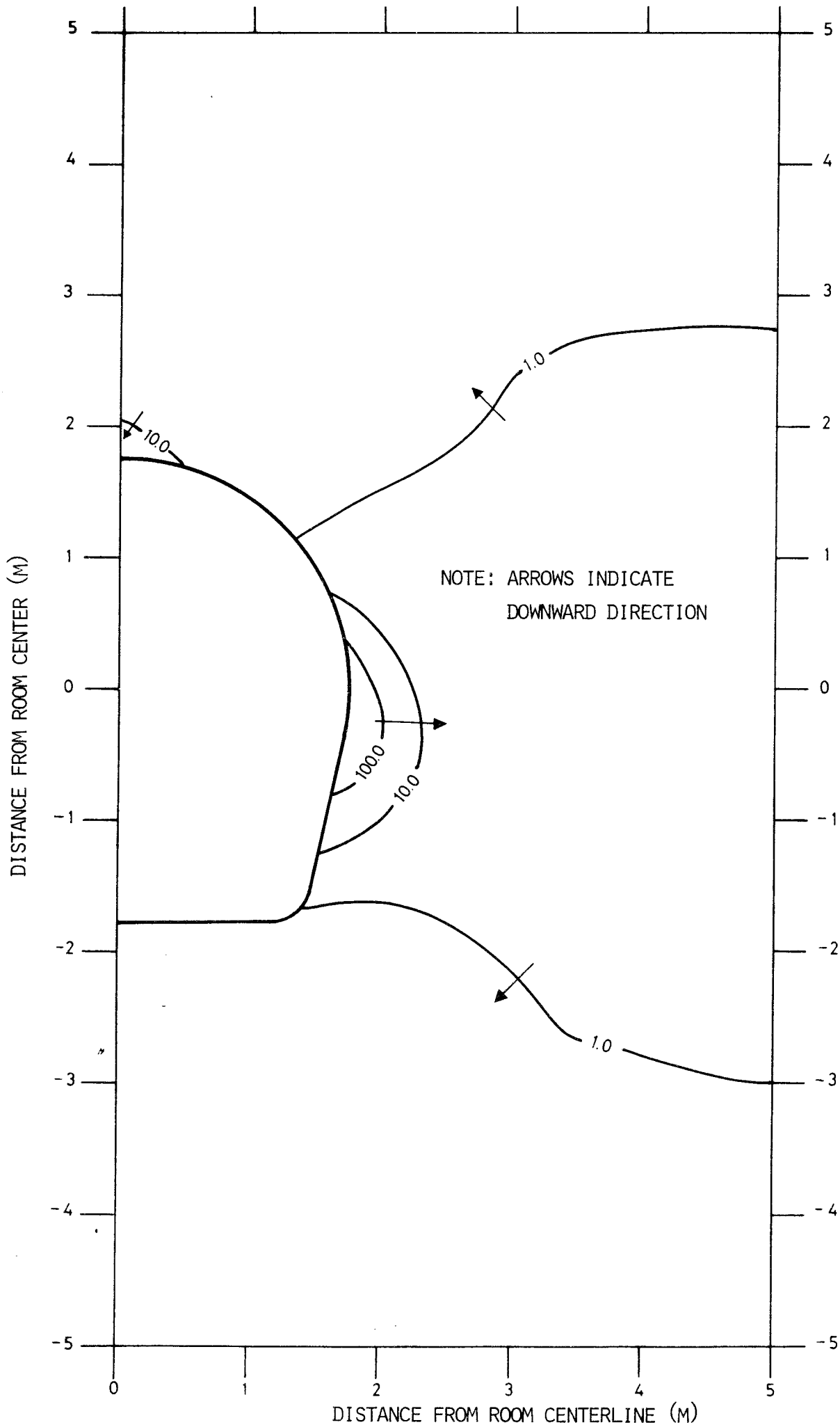


FIGURE 2. RATIOS OF POST EXCAVATION VERTICAL PERMEABILITY TO IN SITU VERTICAL PERMEABILITY OF 0° AND 90° JOINT SETS

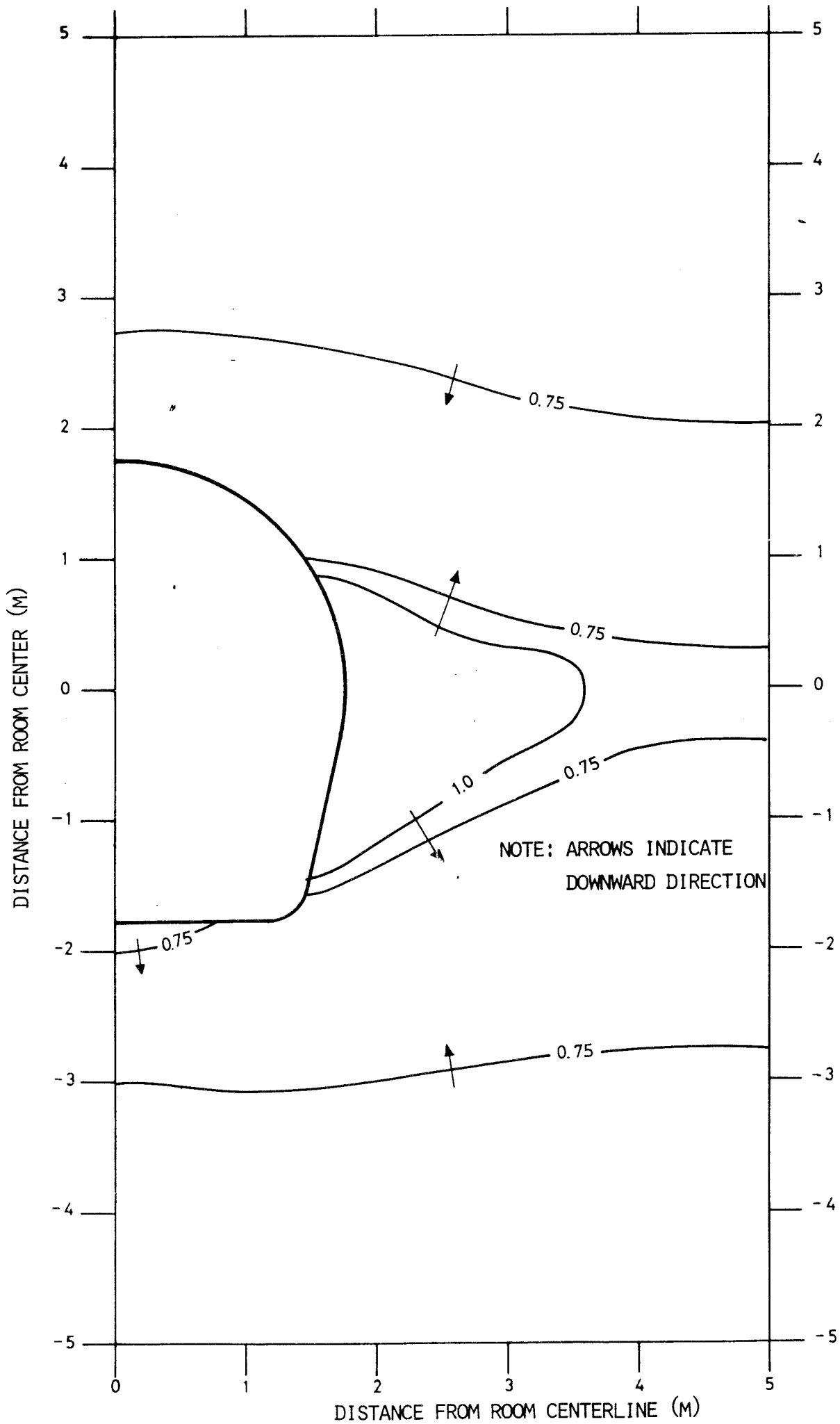


FIGURE 3. RATIOS OF POST EXCAVATION NORMAL PERMEABILITY TO IN SITU NORMAL PERMEABILITY FOR 0° AND 90° JOINT SETS

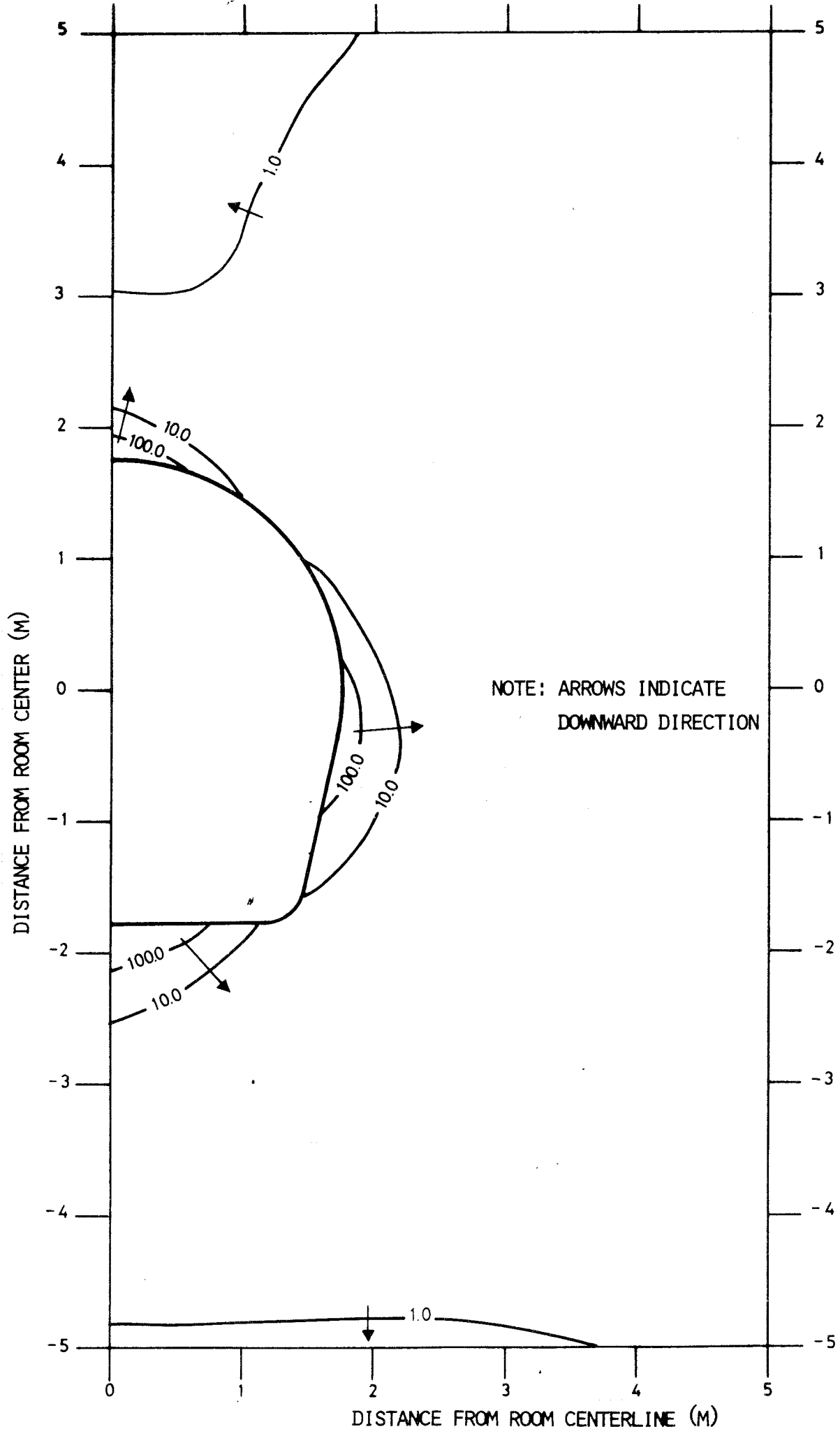


FIGURE 4. RATIOS OF POST EXCAVATION TANGENTIAL PERMEABILITY TO IN SITU TANGENTIAL PERMEABILITY FOR 0° AND 90° JOINT SETS.

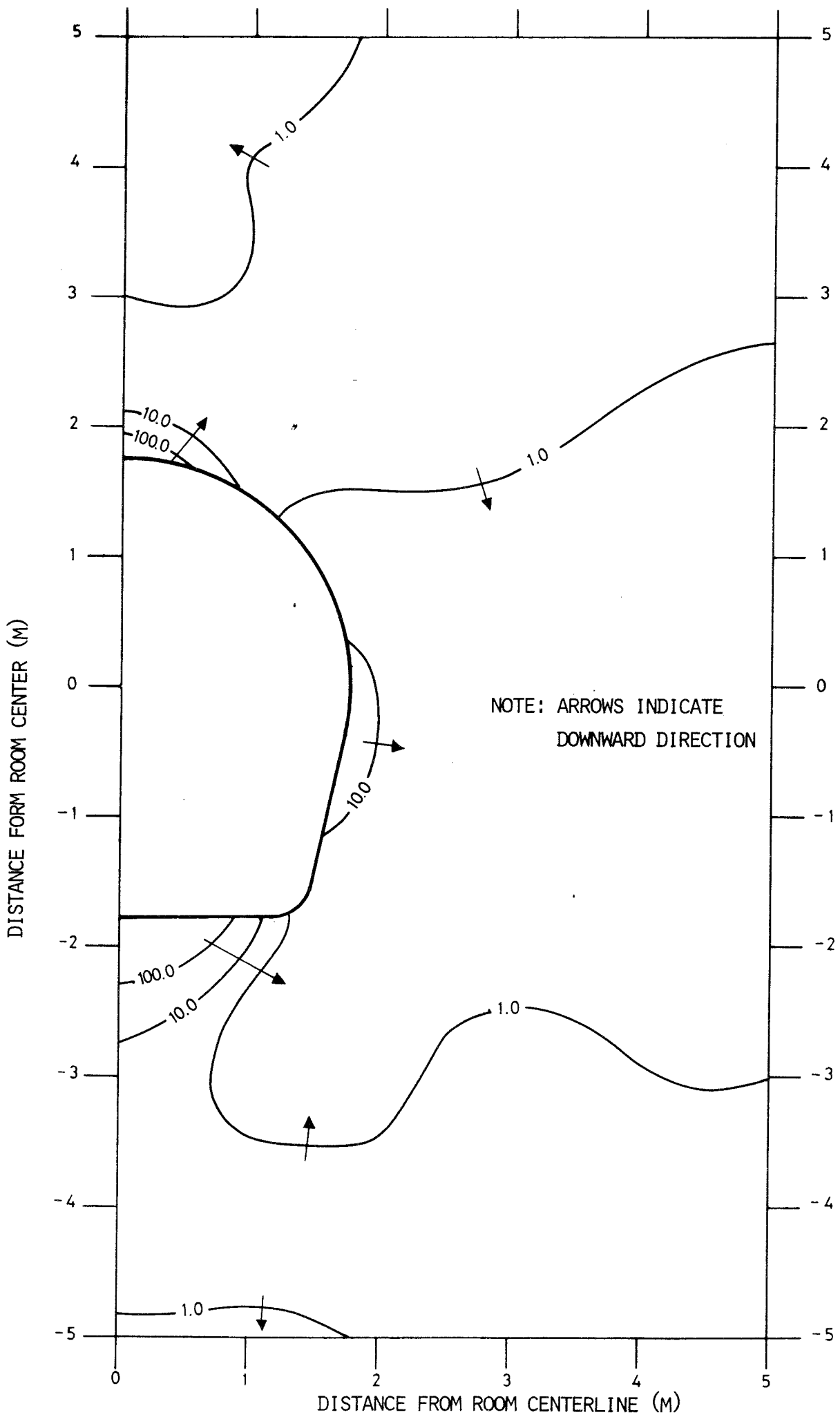


FIGURE 5. RATIOS OF POST EXCAVATION HORIZONTAL PERMEABILITY TO IN SITU HORIZONTAL PERMEABILITY FOR 45° AND -45° JOINT SETS

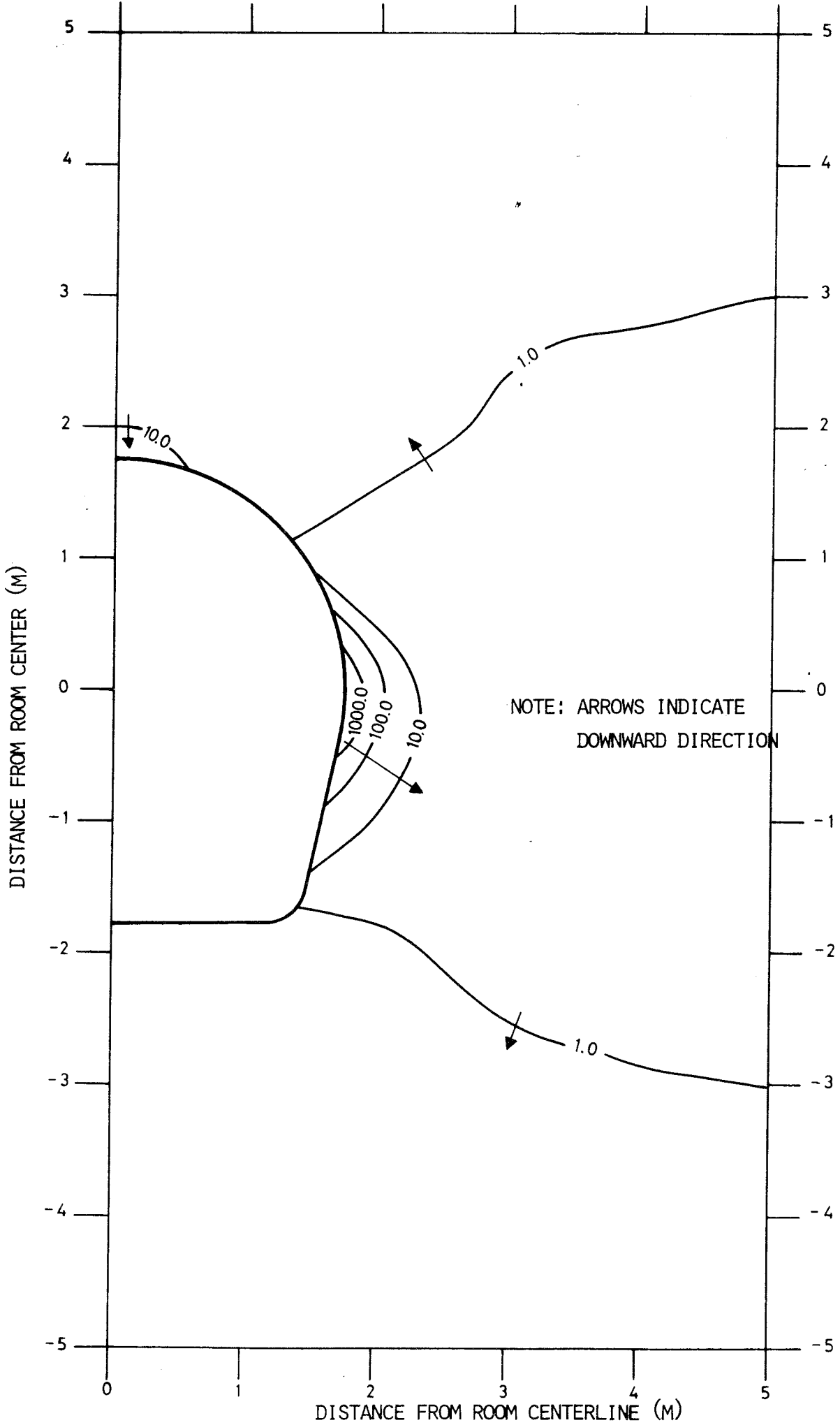


FIGURE 6, RATIOS OF POST EXCAVATION VERTICAL PERMEABILITY TO IN SITU VERTICAL PERMEABILITY FOR 45° AND -45° JOINT SETS

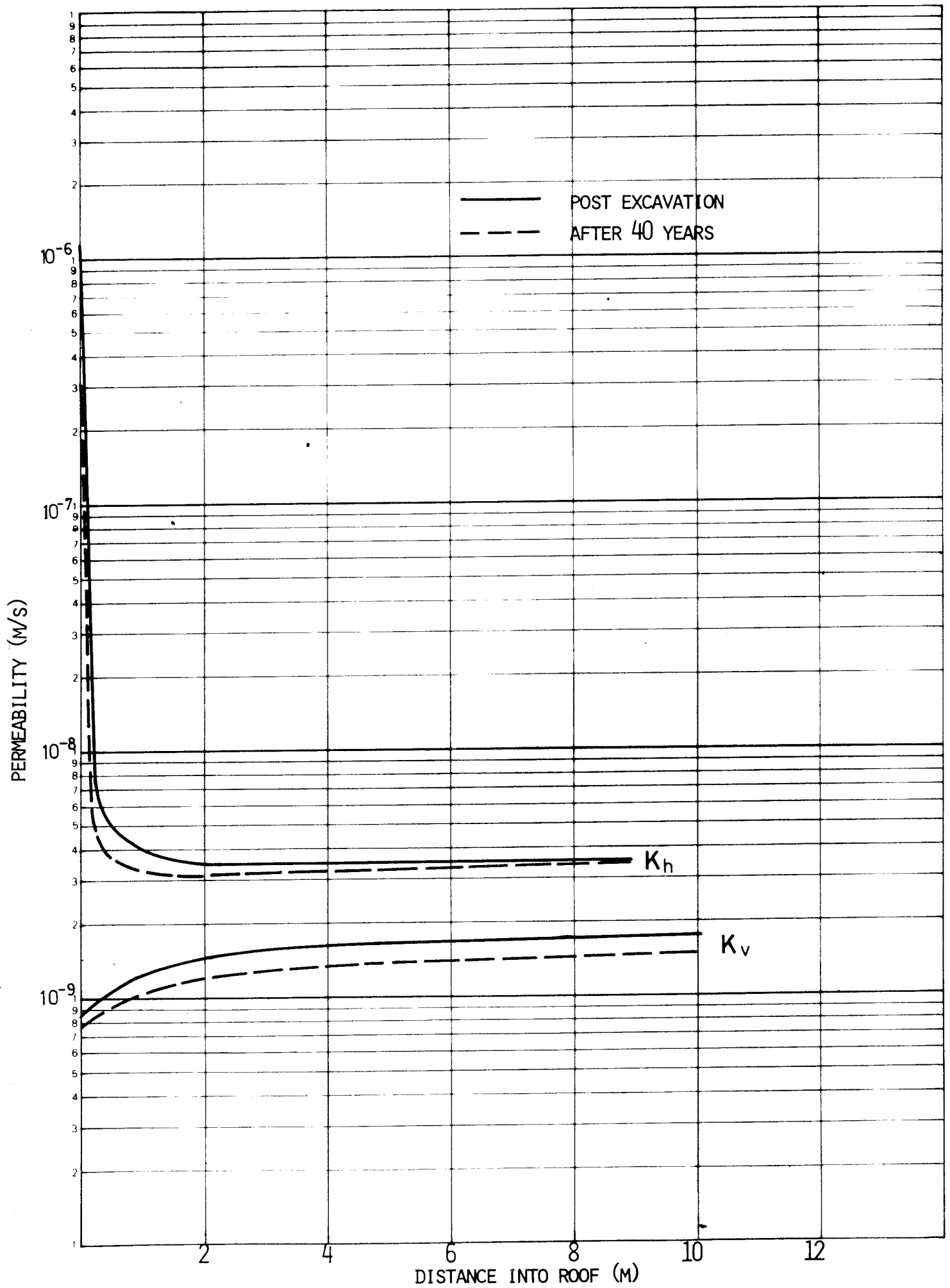


FIGURE 7. POST EXCAVATION PERMEABILITY AND PERMEABILITY FROM THERMOMECHANICAL NORMAL STRESSES AFTER 40 YEARS IN THE TUNNEL ROOF.

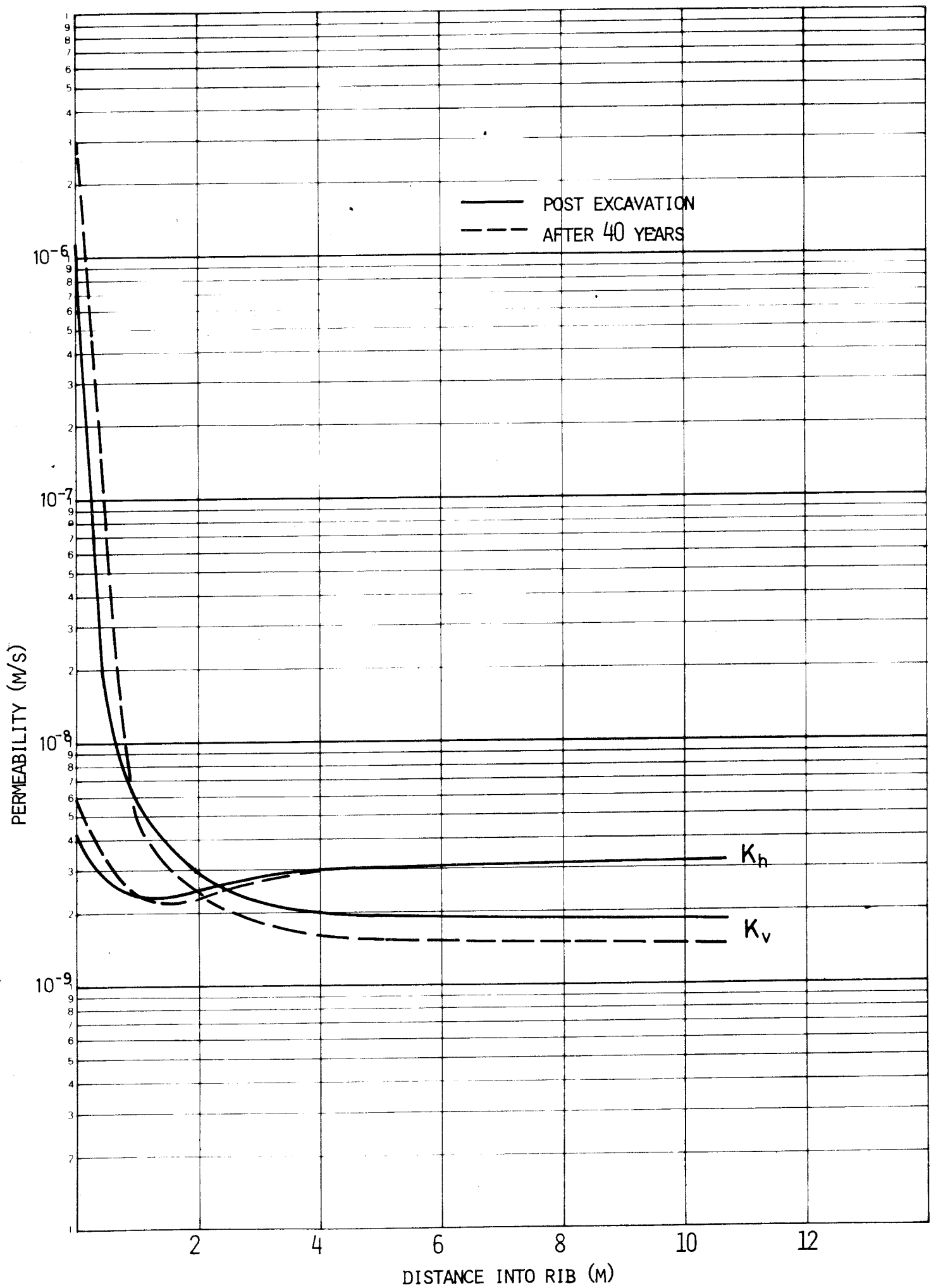


FIGURE 8. POST EXCAVATION PERMEABILITY AND PERMEABILITY FROM THERMOMECHANICAL NORMAL STRESSES AFTER 40 YEARS ON THE TUNNEL RIB.

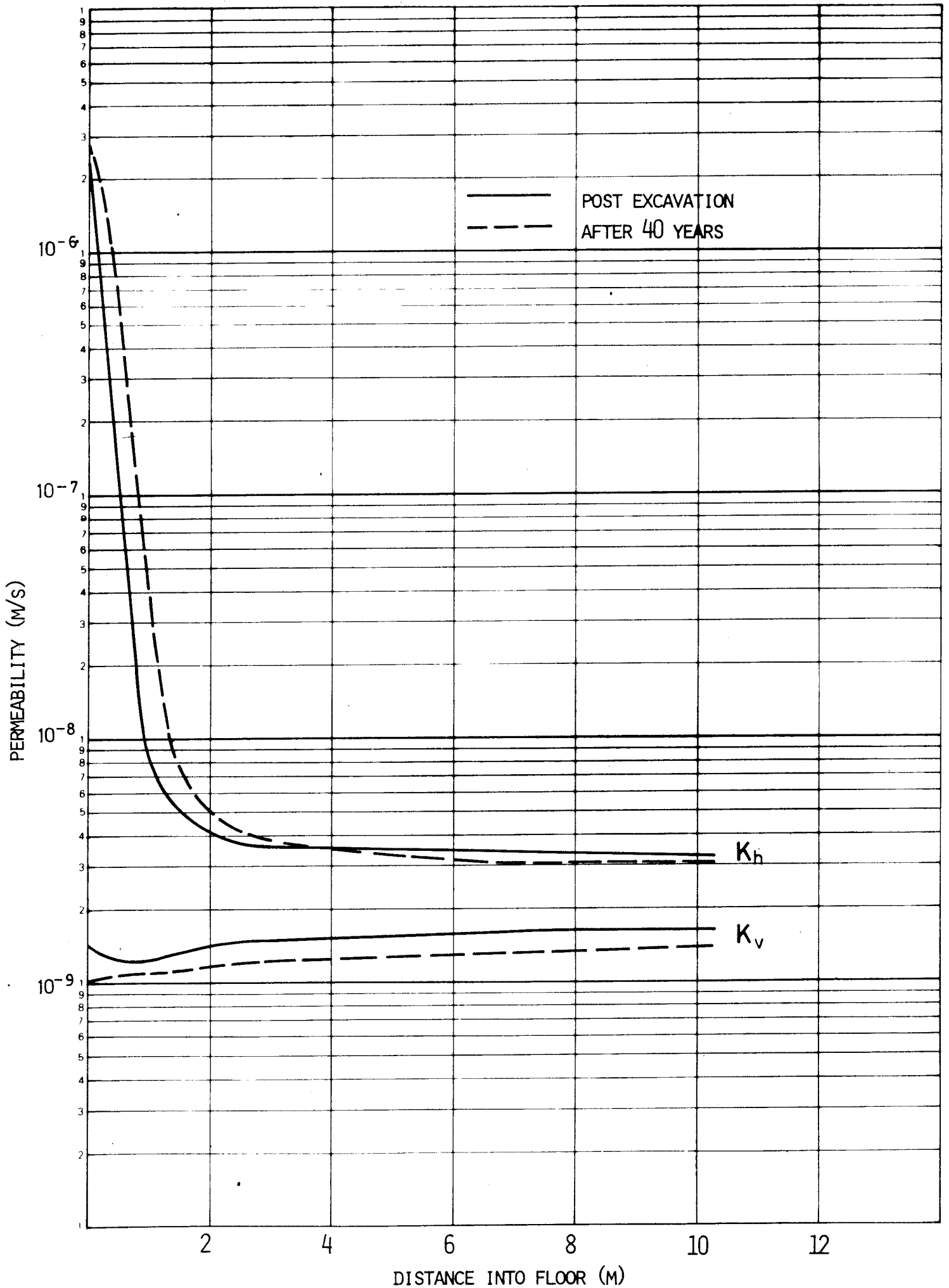


FIGURE 9. POST EXCAVATION PERMEABILITY AND PERMEABILITY FROM THERMOMECHANICAL NORMAL STRESSES AFTER 40 YEARS IN THE TUNNEL FLOOR.

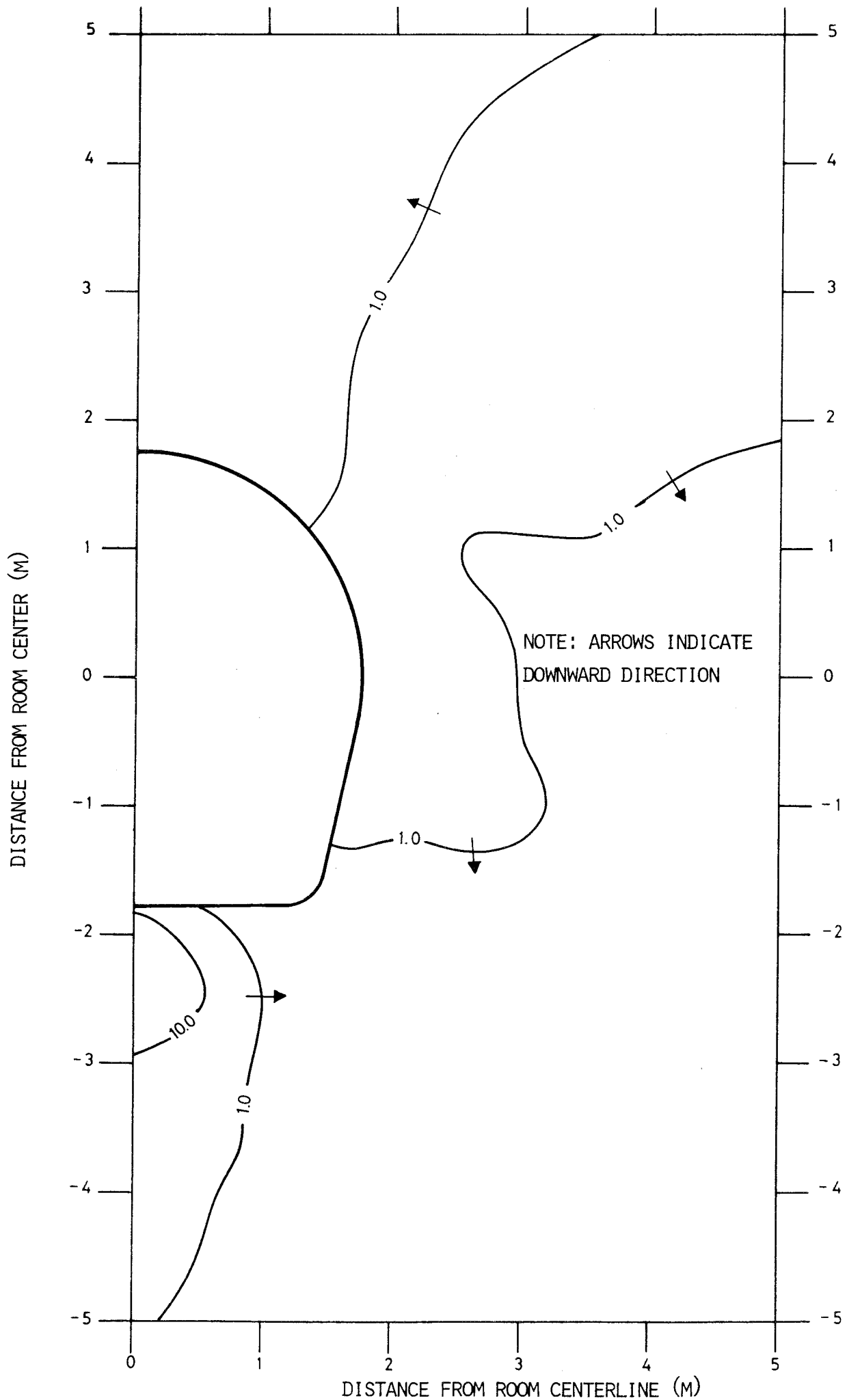


FIGURE 10. RATIOS OF HORIZONTAL PERMEABILITY FROM THERMOMECHANICAL NORMAL STRESSES AFTER 40 YEARS TO POST EXCAVATION HORIZONTAL PERMEABILITY.

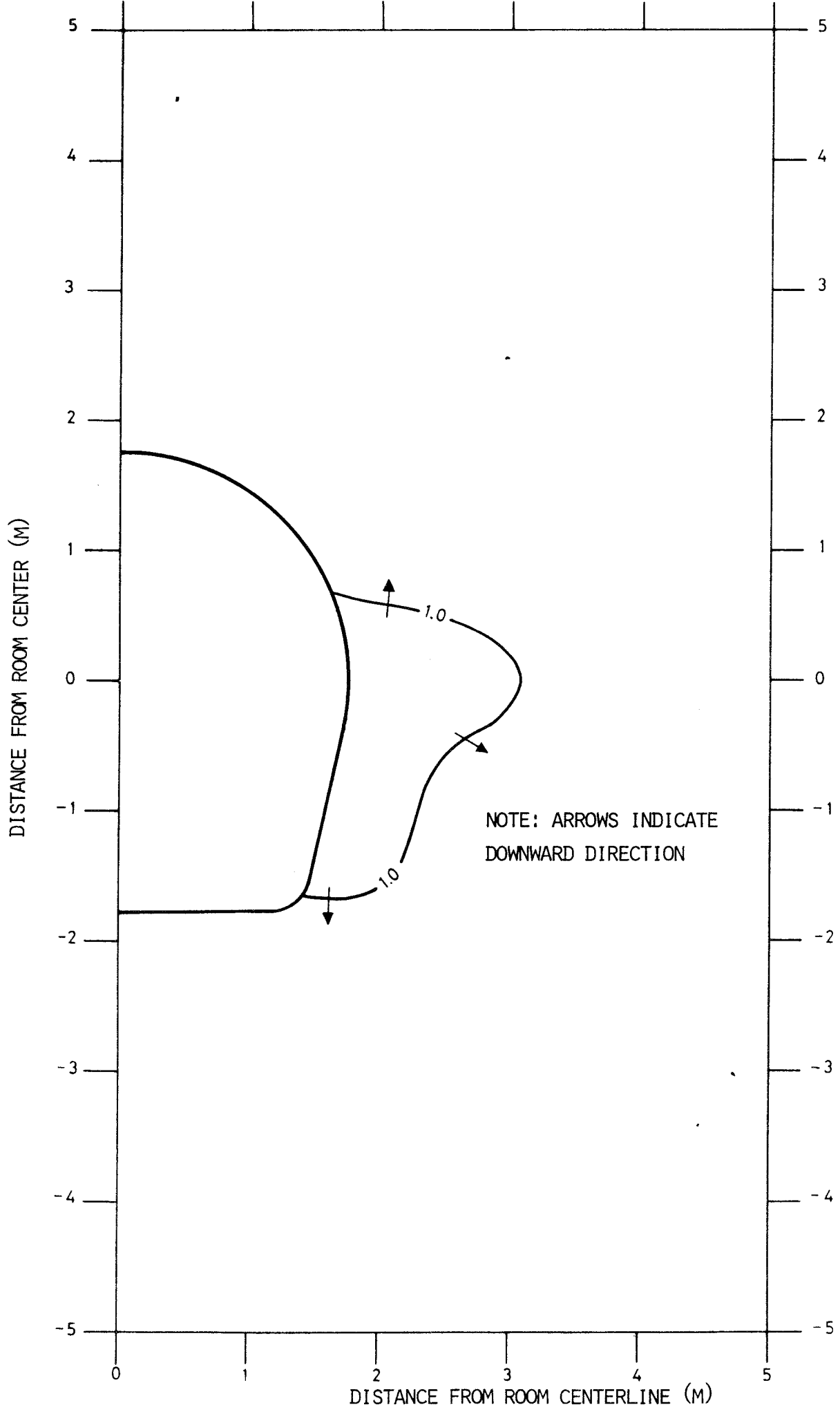


FIGURE 11. RATIOS OF VERTICAL PERMEABILITY FROM THERMOMECHANICAL NORMAL STRESSES AFTER 40 YEARS TO POST EXCAVATION VERTICAL PERMEABILITY

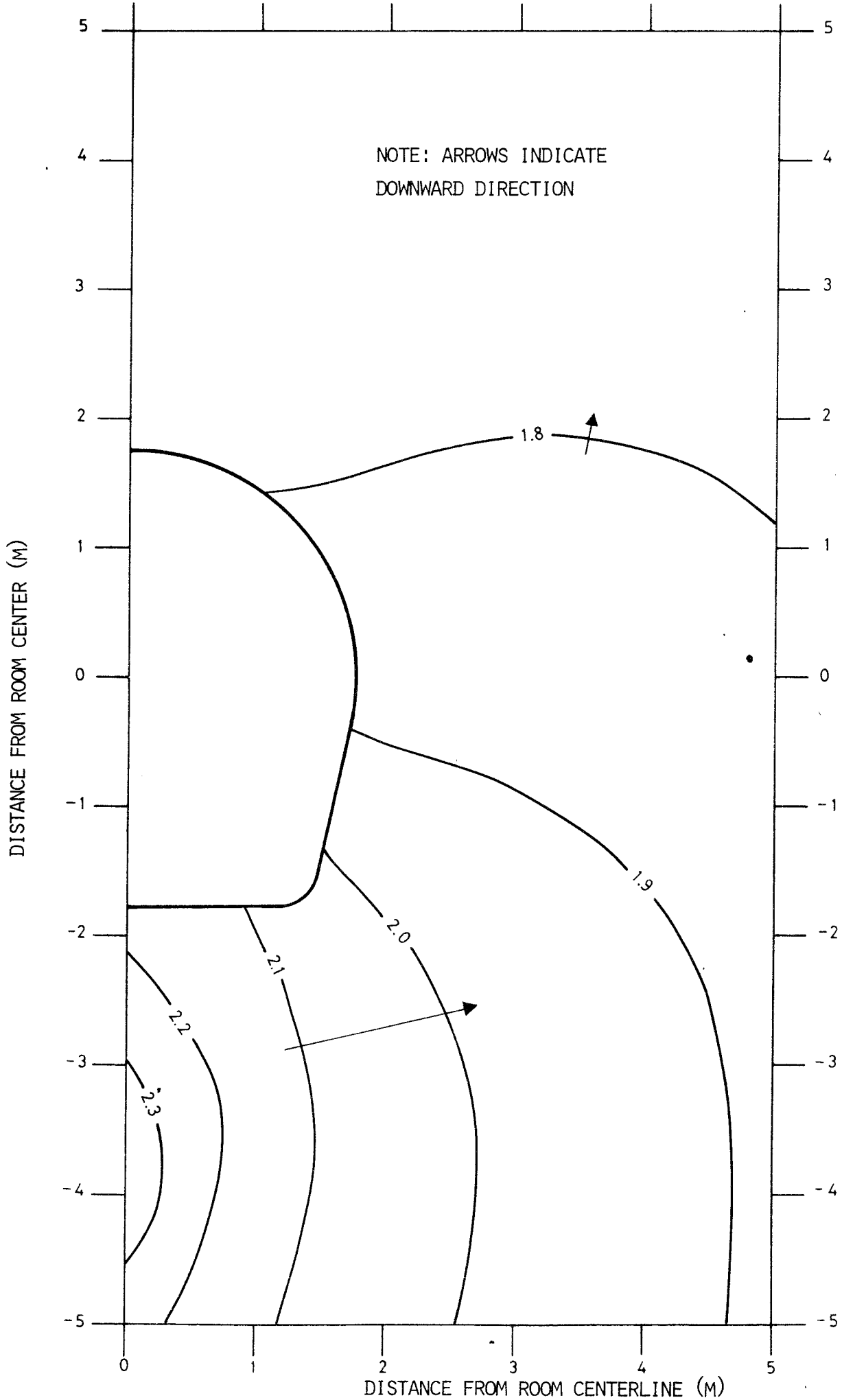


FIGURE 12. RATIOS OF IN SITU VISCOSITY TO VISCOSITY AFTER 40 YEARS WITHOUT REPOSITORY VENTILATION.

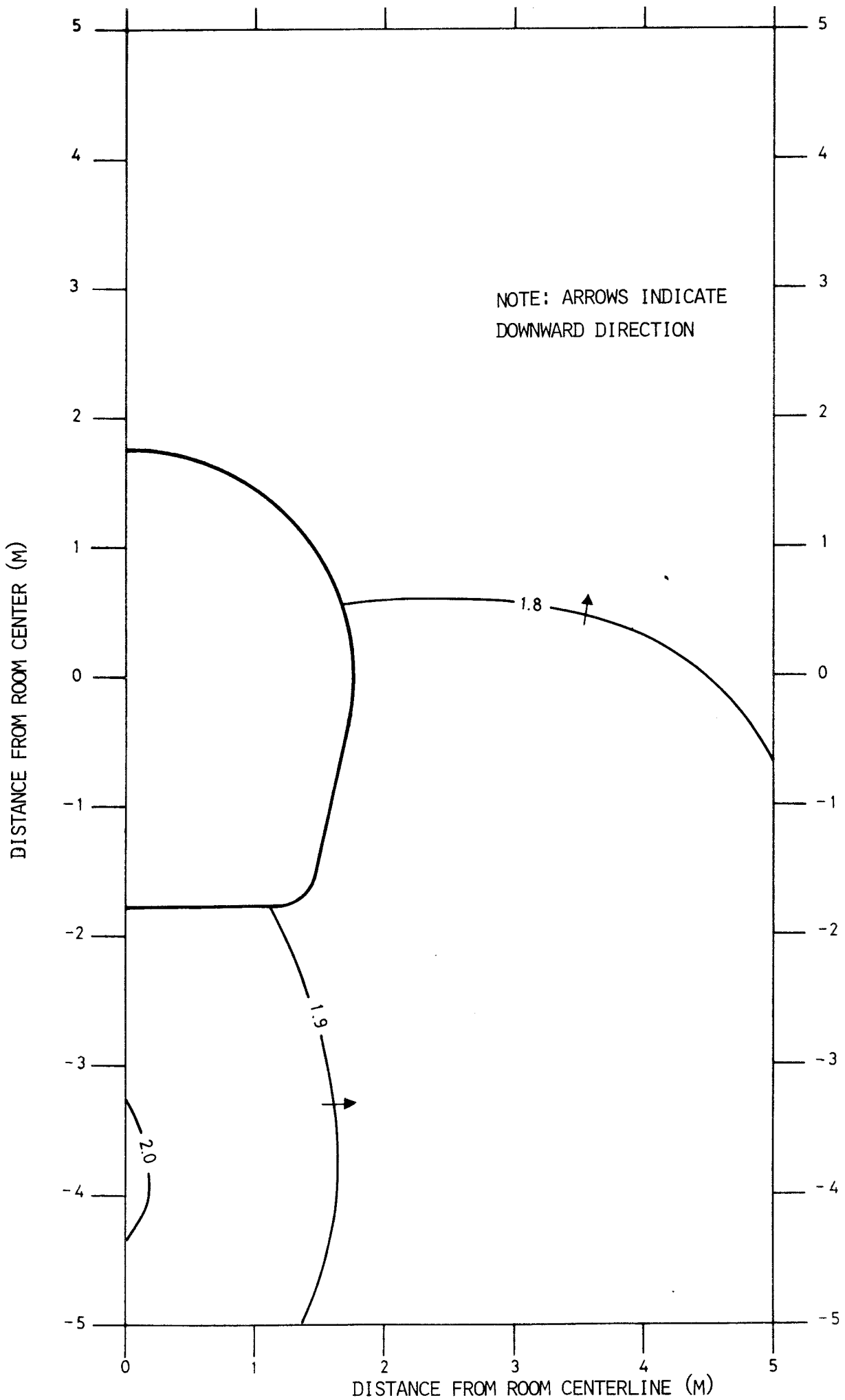


FIGURE 13. RATIOS OF IN SITU VISCOSITY TO VISCOSITY AFTER 100 YEARS WITHOUT REPOSITORY VENTILATION

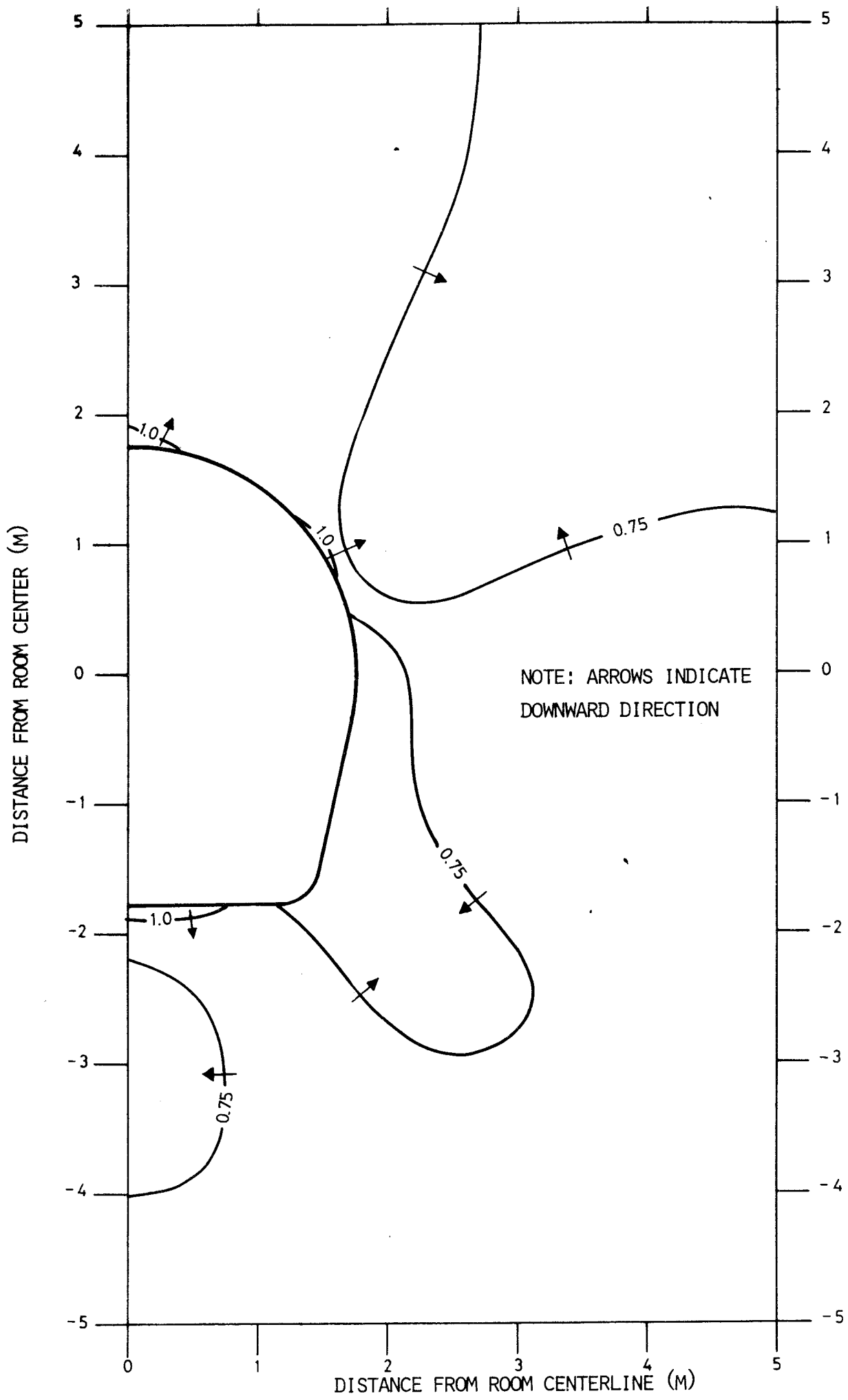


FIGURE 14. RATIOS OF HORIZONTAL PERMEABILITY WITH REPOSITORY VENTILATION TO HORIZONTAL PERMEABILITY WITHOUT VENTILATION AT 40 YEARS

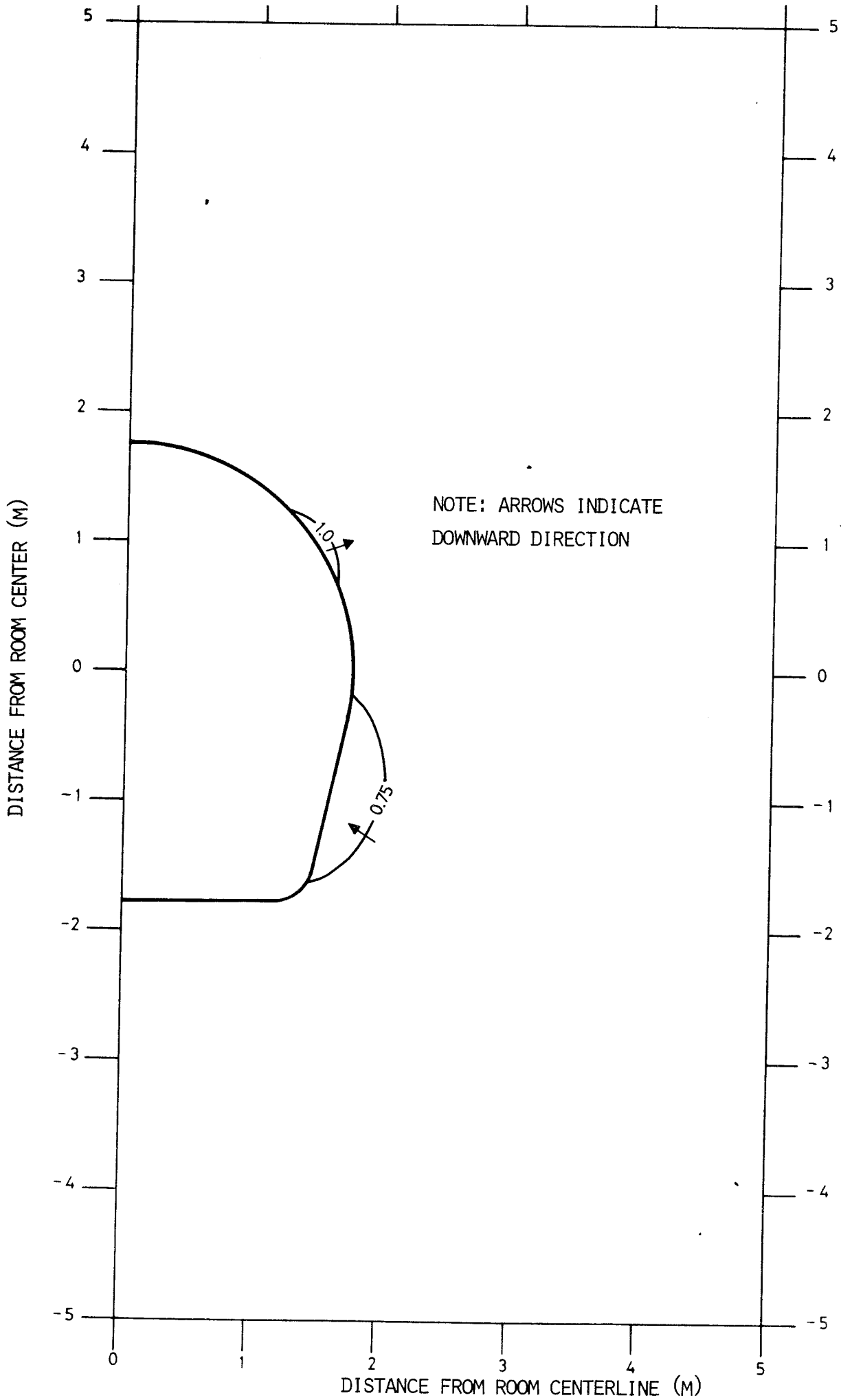


FIGURE 15. RATIOS OF VERTICAL PERMEABILITY WITH REPOSITORY VENTILATION TO VERTICAL PERMEABILITY WITHOUT VENTILATION AT 40 YEARS

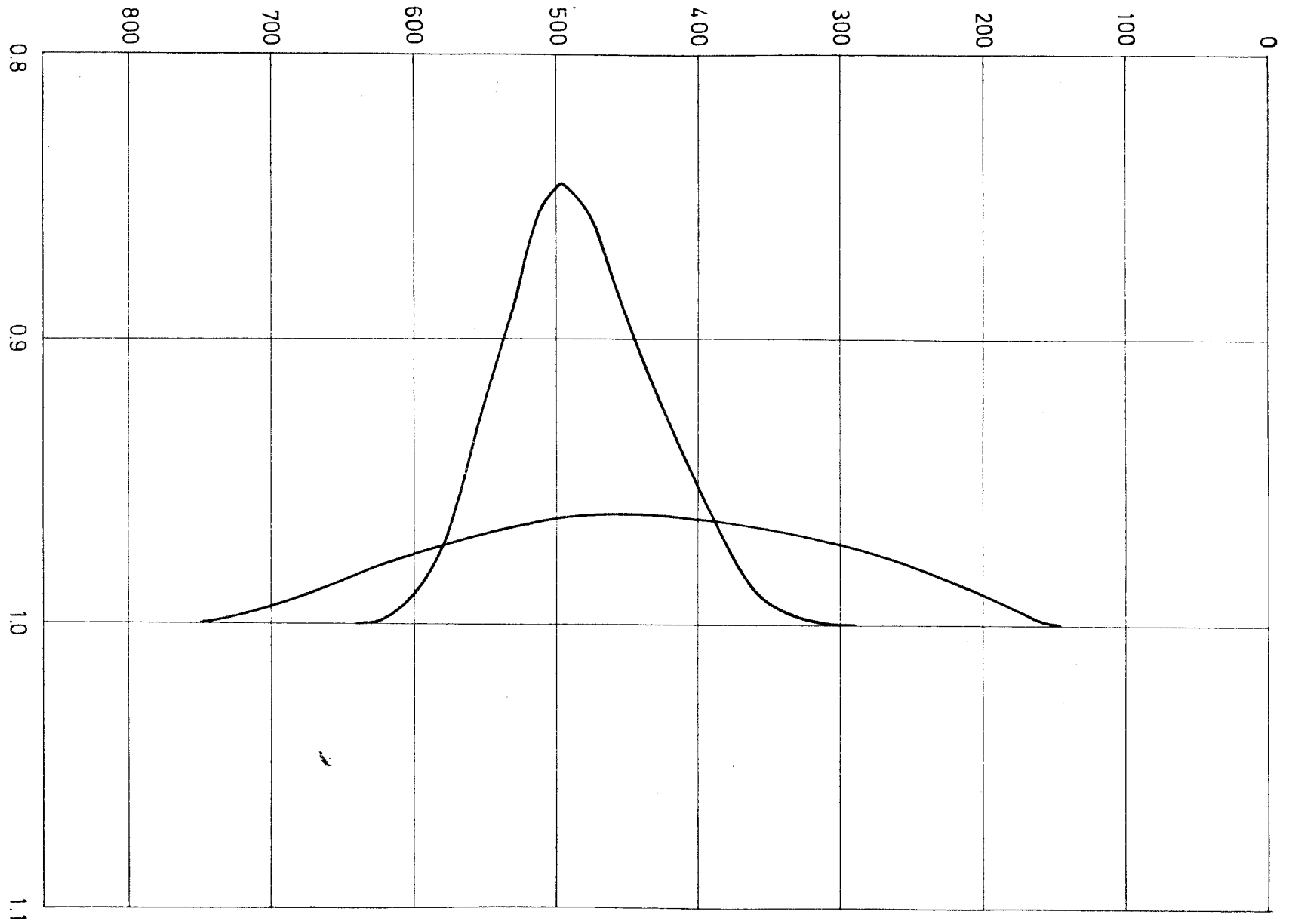


FIGURE 16. RATIOS OF HORIZONTAL AND VERTICAL PERMEABILITY RESULTING FROM THERMOMECHANICAL NORMAL STRESSES AT 40 YEARS TO IN SITU VALUES AS A FUNCTION OF DEPTH

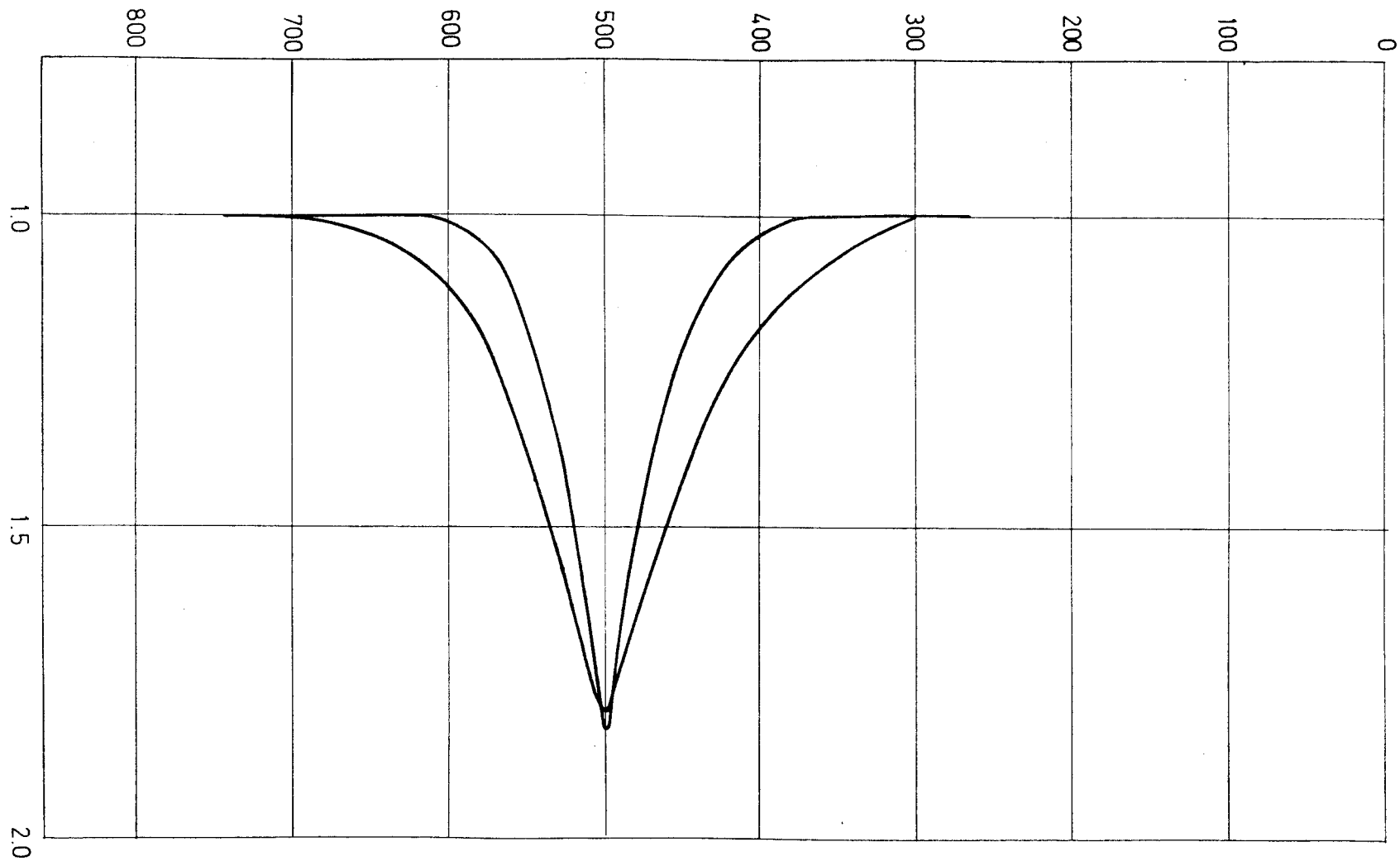


FIGURE 17. RATIOS OF IN SITU VISCOSITY TO VISCOSITY AFTER 40 YEARS AND 100 YEARS AS A FUNCTION OF DEPTH FOR INSTANTANEOUS WASTE EMPLACEMENT

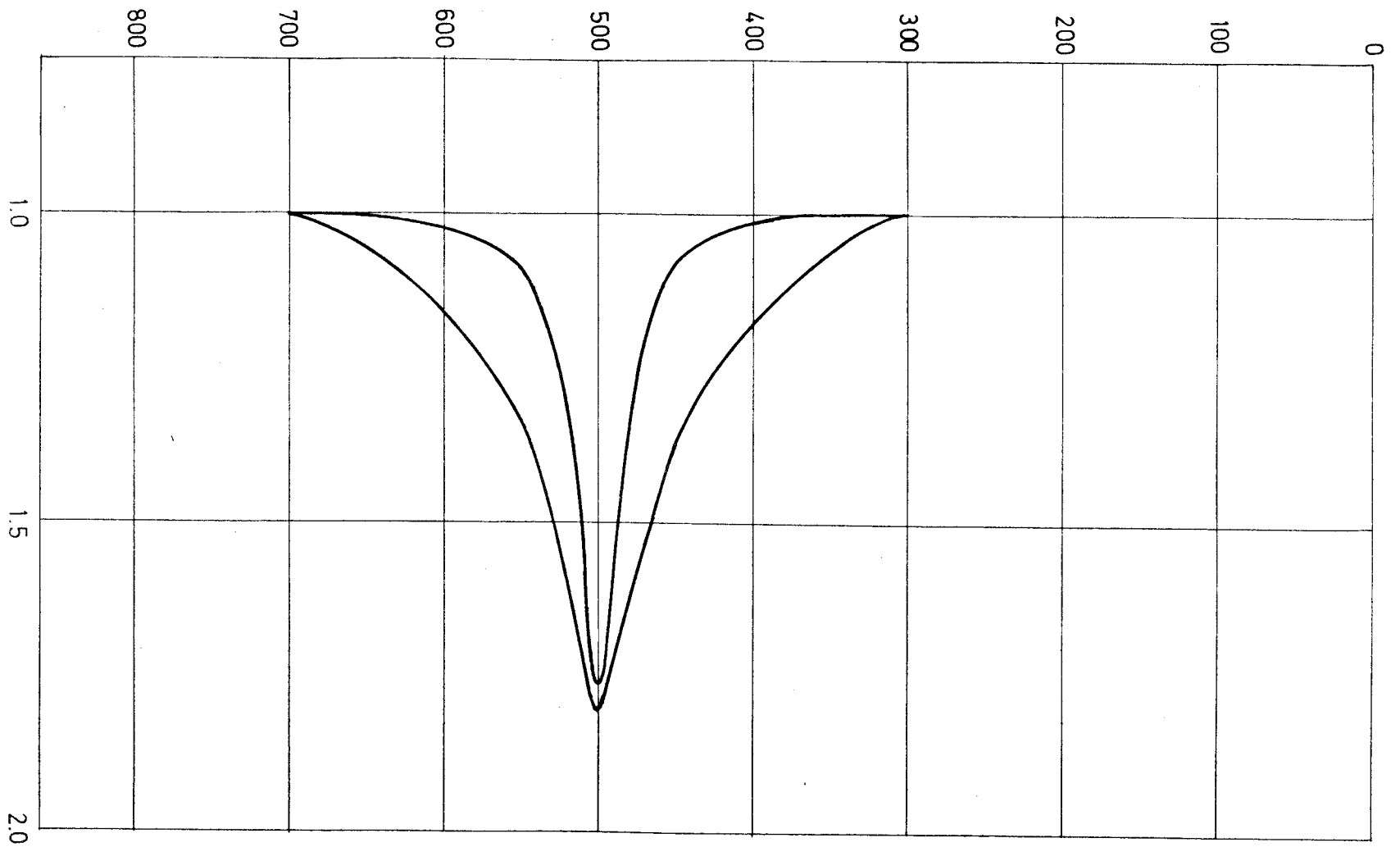


FIGURE 18. RATIOS OF IN SITU VISCOSITY TO VISCOSITY AFTER 40 YEARS AND 100 YEARS AS A FUNCTION OF DEPTH FOR LINEAR WASTE EMPLACEMENT

TECHNICAL REPORT 5
REPOSITORY DOMAIN GROUND-
WATER FLOW ANALYSES
PART II
INFLOW TO REPOSITORY

KBS-Kärnbränslesäkerhet

GROUNDWATER MOVEMENTS AROUND A REPOSITORY

Phase 2.

Technical report 5: Repository Domain Groundwater Flow Analyses

Part II: Inflow to Repository

Hagconsult AB
in association with
Acres Consulting Services Ltd
RE/SPEC Inc.

FOREWORD

This report was prepared as one of a series of technical reports within a study of the groundwater movements around a repository for radioactive waste in the Precambrian bedrock of Sweden. It was written in three parts, (I) Permeability Perturbations, (II) Inflow to the Repository and (III) Thermally Induced Flow. This part is Part II. The contract for this study was between KBS-Kärnbränslesäkerhet (Project Fuel Safety) and Hagconsult AB of Stockholm, Sweden. RE/SPEC Inc. of Rapid City, SD/USA and Acres Consulting Services Ltd of Niagara Falls, Ontario/Canada acted as subconsultants to Hagconsult AB.

The principal authors of this report are Dr Anthony S. Burgess and Dr Edward L. Skiba of Acres. Review was provided by Dr Ulf E. Lindblom of Hagconsult AB and Dr Robin Charlwood of Acres. Input to the study was provided by Dr Håkan Stille and Mr Joe L. Ratigan of the Study Group and by other contributors to the KBS project.

The opinions and conclusions in this document are those of the author and should not be interpreted as necessarily representing the official policies or recommendations of KBS.

Stockholm September 1977

Ulf E. Lindblom
Study Director
Hagconsult AB

TABLE OF CONTENTS

	<u>Page</u>
1. SCOPE AND OBJECTIVES	1
2. METHODOLOGY	2
2.1 General	2
2.2 Inflow with Baseline Permeability Distributions	2
2.3 Inflow with Permeabilities Modified as a Function of Stress	4
2.4 Effect of Inflow upon Thermal Conditions	5
2.5 Reliability of Inflow Period Predictions	5
3. RESULTS	7
3.1 Free Inflow	7
3.2 Inflow with Development of Backpressure	8
3.3 Inflow Effects on Thermal Conditions	9
4. DISCUSSION AND CONCLUSIONS	10
4.1 Comparison with Field Data	10

REFERENCES

LIST OF FIGURES

Figure

1. Finite element meshes for repository domain and local models
2. Nominal permeability and porosity distribution
- 3a Finite element mesh for study of inflow with K as a function
3b of stress
- 4a Permeability ratios
4b
- 5 Case 1 Equipotentials
- 6 Case 2 Equipotentials
- 7 Case 3 Equipotentials
- 8 Case 4 Equipotentials
- 9 Case 5 Equipotentials
- 10 Case 1 Flux patterns
- 11 Case 4 Contours of inflow flux magnitudes
- 12 Case 5 Contours of inflow flux magnitudes
- 13 Effect of backpressure on inflow
- 14 Advective inflow run, seepage fluxes

1. SCOPE AND OBJECTIVES

In this report we present the results of a study of groundwater inflow to the repository, with particular reference to the post-decommissioning period. The objective was to determine the time for the repository to become backflooded (inflow period). After this period, the groundwater flow will return to the regional conditions with the addition of any remaining thermal and/or mechanical perturbations. During the inflow period, groundwater flow by definition is towards the repository. The inflow period may therefore be considered as a containment mechanism.

Finite element methods have been used to determine flow patterns. Coupling of the permeability to stress changes has been incorporated and the effects quantified. The effect of inflow on thermal conditions around and within the repository has also been examined. Some aspects of construction have been assessed, and their influence treated qualitatively. The results of the model simulations have been compared with the limited field data that is available.

For this study, the baseline layout has been used. This consists of rooms approximately 3.5 m diameter, about 1 km in length and spaced at 25 m centre to centre. The repository has been assumed to be located at a depth of 500 m below ground surface.

2. METHODOLOGY

2.1 General

All inflow periods, t_1 , presented below are based upon an unfilled room, i.e. porosity = 1. The inflow period t_n , for a room backfilled with material having a porosity n , may be calculated from

$$t_n = n \times t_1$$

The rock mass with fractures has been treated as an equivalent continuum in the finite element method formulation for flow. To be valid, this assumption requires that the fracture spacing be small compared to the domain modelled. The results from the application of the continuum approximation to room-size models should therefore be considered only as indicative of effects. However, a more sophisticated simulation cannot be used until much more extensive field data is available. The inflow study may be divided into three parts:

- Inflow using estimated initial baseline permeability distributions.
- Inflow using a permeability distribution determined from the insitu stresses and modified by construction stresses.
- The effects of inflow on heat transfer in the repository domain.

2.2 Inflow with Baseline permeability Distributions

For this part of the study, two finite element models have been employed:

- Repository domain model (Figure 1a). This represent a two dimensional vertical section through the repository. The repository centre line has been taken as a line of symmetry.
- Local model (Figure 1b). This also represents a two dimensional vertical section. The room centre line, and the pillar centre line have been taken as lines of symmetry.

The nominal permeability distributions used in the simulations were the same as used for the regional initial conditions. The basis for their selection is described in Technical Report 3 (1) x).

- Case 1. Isotropic, homogeneous. Permeability $K = 1 \times 10^{-8}$ m/s.
- Case 2. Isotropic, non-homogeneous. Permeability decreasing with depth as per empirical function (1)
- Case 3. Anisotropic, non-homogeneous. Vertical permeability = 1.0×10^{-9} m/s. Horizontal permeability decreasing with depth as per empirical function (1).

These permeability distributions are shown in Figure 2.

Throughout the analyses, the effect of singular geological features extending into the repository domain have not been considered. If such features exist then

- a) the repository will be sited to avoid them, or
- b) they will be treated by grouting or other techniques to give them material properties similar to the surrounding rock.

For both the repository domain and local model, the vertical boundaries which are lines of symmetry have been taken as flowlines, i.e. impervious boundaries. In addition, the far field vertical boundary in the global model has been considered as an impervious boundary.

For the repository domain model, the groundwater surface has been assumed coincident with the ground surface. The existence of drawdown was checked by a comparison of the boundary flux with the available recharge flux. For the regions of Sweden where the repository may be located, annual precipitation is typically 500 mm. Infiltration coefficients for typical soil conditions vary from 0.11 to 0.37 (2). Using value of 0.2 a recharge of 100 mm/year is available. This is equal to a boundary flux of 3.17×10^{-9} m/s.

x) Numbers in parentheses refer to references at end of text.

In the inflow simulations, boundary fluxes less than the available recharge flux will be satisfied by infiltration alone. If boundary fluxes are higher than the recharge, drawdown of the groundwater surface will result, until an equilibrium is achieved between horizontal inflow, vertical recharge and downward flow. The extent of the drawdown will depend upon the variation of permeability with depth and the degree of anisotropy. In general, drawdown will be least for the anisotropic condition where the horizontal permeability is relatively high at the surface.

The potential distributions from the repository domain models were used to determine boundary potentials on the local models. The boundary fluxes on the local models were then compared with the repository domain fluxes to assess the influence of geometry effects at the repository level.

At the repository itself, two boundary conditions have been considered:

- Free inflow, i.e. any air within the repository escapes or goes into solution at nominal pressures.
- Inflow with backpressure, i.e. any air within the repository is unable to escape or go into solution and causes pressure rises within the repository.

2.3 Inflow with Permeabilities Modified as a Function of Stress

For this part of the study, a finite element model extending from the ground surface to a depth of 1000 m was used (Figures 3a and 3b). The vertical boundaries were lines of symmetry for the room centre-line and the middistance between adjacent rooms respectively. The technique used for the unmodified permeability distributions, i.e. separate repository domain and local models, was found to be unsatisfactory for this part of study. This was because the repository domain mesh was too coarse in the immediate area of the repository and the significant permeability changes could not be modelled. As a result the boundary conditions for the local model could not be accurately determined.

The initial permeability distribution (Case 4) was made compatible with the initial in-situ stresses for a horizontal to vertical stress ratio of 2. The horizontal permeability at depth z was set equal to the horizontal permeability calculated from the empirical function (1). The vertical permeability at depth z was then equated to the horizontal permeability at depth $2z$. The initial permeability values were then modified using the stress-permeability relationship described in part I of this report (3), for the stress changes due to construction. This is referred to as the Case 5 permeability distribution. The ratios of modified to initial permeability values are given in Figures 4a and 4b.

Boundary conditions for this simulation were the same as those described in section 2.2., with the exception that the backpressure case was not considered.

2.4 Effect of Inflow upon Thermal Conditions

The advection of heat by inflow was studied using the repository domain model with a thermally induced flow finite element technique. Details of the computational method are given in part III of this report (4).

In order to simulate inflow lasting for a significant part of the thermal cycle, the permeability distribution was taken to be isotropic, homogeneous, with a value of 10^{-10} m/s. The initial gross thermal loading was taken as 5.25 W/m^2 , and the thermal conductivity of the rock mass as $2.05 \text{ W/m, } ^\circ\text{C}$.

Boundary conditions for this part of the study were the same as detailed in section 2.2.

2.5 Reliability of Inflow Period predictions

Nominal permeability distributions have been determined by extrapolating to depth permeability values obtained closer to the surface. As a result, apparently short inflow periods result. The inflow period is a function of the permeability in the vicinity of the repository, and of the variation of permeability with depth. In general, the inflow period is

inversely proportional to the permeability in the repository area. Thus an error of one order of magnitude in estimating the permeability would change the inflow period by an order of magnitude.

3. RESULTS

3.1 Free Inflow

The equipotentials for Cases 1 to 5 are shown in Figures 5 to 9 respectively.

The inflow times, inflow rates and upper boundary fluxes are tabulated below. The inflow period is seen to be strongly correlated with the vertical permeability in the vicinity of the repository. The influence of the other factors (anisotropy, horizontal permeability, variation of permeability with depth) on the inflow time can be illustrated by comparing the values of $t_1 \times K_z$ for the different cases. (K_z is the vertical permeability at a depth of 500 m.)

	Flux at ground surface m/s	Inflow rate l/min, km	K_z m/s	Inflow periods year	$t_1 \times K_z$ m
Case 1	12.13×10^{-9}	28.85	10^{-8}	0.64	.20
Case 2	10.14×10^{-9}	17.97	3.7×10^{-9}	1.02	.14
Case 3	1.77×10^{-9}	4.17	10^{-9}	4.39	.14
Case 4	3.66×10^{-9}	6.28	1.7×10^{-9}	3.17	.17
Case 5	3.69×10^{-9}	6.34	1.7×10^{-9}	3.14	.17

For Cases 1 and 3 where K_z is constant with depth, about 65% of the total flux comes from above the repository and 35% from below. For the Cases 2, 4 and 5 in which the vertical permeability decreases with depth the ratio changes to about 85% from above the repository and 15% from below the repository.

From the global model analyses for Cases 1, 2 and 3 the distribution of inflow fluxes laterally across the repository can be assessed. The inflow flux pattern for the homogeneous isotropic permeability distribution (Case 1) is shown in Figure 10.

The total inflow rate is about 50% higher towards the outer limit of the repository, compared with the inner regions. The assumption of vertical flowlines for the local models of Case 1, 2, 3 and for the models for Cases 4 and 5 are therefore valid only for the central areas of the repository. As a result, the inflow periods based on vertical flowlines will be somewhat longer than if the complete repository domain flow pattern were to be used. As discussed in sections 2.2 and 2.3, however, modeling limitations for Cases 4 and 5 required that vertical flowline boundaries be adopted. For comparison purposes, similar conditions have therefore been applied to Cases 1, 2 and 3.

Comparison of inflow periods for Cases 4 and 5 shows that the effect of permeability changes around the room due to construction stresses is very small. This is due to the following reasons:

- The stress changes around the room result in both increases and decreases in the permeabilities in various locations which tend to equalize each other.
- The changes in permeability result in changes in the potential gradients. Thus a decrease in relative permeability results in an increase in gradient in that region.

The effect of the change on the flux is therefore reduced.

Contours of flux magnitudes for Cases 4 and 5 are shown on Figures 11 and 12 respectively. For Case 4, the inflow flux is highest in the roof of the room, and lowest in the floor. The flux distribution for Case 5 is much more variable, reflecting the complex modifications to the insitu permeabilities.

3.2 Inflow with Development of Backpressure

The effect of backpressure within the room was determined for Cases 1, 2 and 3. Figure 13 shows the curves representing both free and pressurized inflow results. The percentages of the room flooded as a function of time and the corresponding decrease in flux due to the backpressure effect are also indicated. The time scale is distorted below the graph for the three permeability cases, the times being inversely proportional to the initial

fluxes. It can be seen that there is only a small difference between the free inflow and backpressure cases. The flux curve, however, demonstrates that for the latter the flux starts to decrease at roughly the free filling time and decays 5 orders of magnitude at 1.26 of the free filling time and 10 orders at 1.54 of the free filling time. The relatively minor nature of the effects of pressurization is a result of the great depth of the repository for which the recharge pressure is nearly 50 atmospheres due to static water head.

3.3 Inflow Effects on Thermal Conditions

The thermal capacity of the tunnels, filled with water by inflow, is $1.61 \times 10^{-6} \text{ J/m}^2, ^\circ\text{C}$. Assuming that the water may reach a temperature of the order of 30°C above ambient and using the initial gross thermal loading (GTL) of 5.25 W/m^2 , the time required for the initial GTL to raise the room-filling water to 30°C is about 0.3 years. Since a great deal more heat than this is available over the years, the thermal capacity provided by the water in the rooms and hence its effect on temperatures in the rock will be minimal. Only in the event of substantial inflow and pumping could the effect be significant, similar to ventilation.

The conclusion is that inflow to the rooms can have little advective effect on temperatures whatever value of permeability is used. The fluid advects some heat into the rooms but provides extra heat storage capacity as well. The temperatures near the waste can only be expected to drop slightly due to inflow of water into the rooms.

In order to quantify the effect of the advective heat transfer due to inflow, a coupled analysis was made. The methodology is described in part III of this report. An arbitrary isotropic homogeneous permeability of 10^{-10} m/s was used in this analysis to provide a case representative of inflow lasting for a significant part of the thermal cycle. For this permeability, the inflow period would be about 65 years. The changes in temperatures due to advection were less than 0.1°C for temperature increases of about 30°C at 70 years. The global water flux associated with this inflow is shown in Figure 14.

4. DISCUSSION AND CONCLUSIONS

4.1 Comparison with Field Data

Field data on inflow to excavations at depths of hundreds of meters is primarily from measurements of inflow into mines. A study of inflow to mines in the Canadian Precambrian Shield is presented by Raven & Gale (5). The inflow rates were normalised by expressing the inflow as liters per minute per kilometer of lateral development in the mine (l/min,km). They concluded that mines with pumped levels within 150 m of the ground surface showed higher inflow rates than mines where the highest pumped level was deeper than 150 m. Values for the latter condition, pertinent to the present study, have been extracted from Raven & Gale and are given in Table 1. Apart from the value of 61.5 for East Malarctic No 5 shaft, the inflows are between 0 and 3 l/min,km.

As part of the field studies for KBS, measurements of inflow rates will be performed at Stripa Mine. A rough estimate made by the author during a site visit indicates an approximate inflow of 3×10^{-2} l/min,km. Permeability test indicate that they are of the order of 5×10^{-11} m/s.

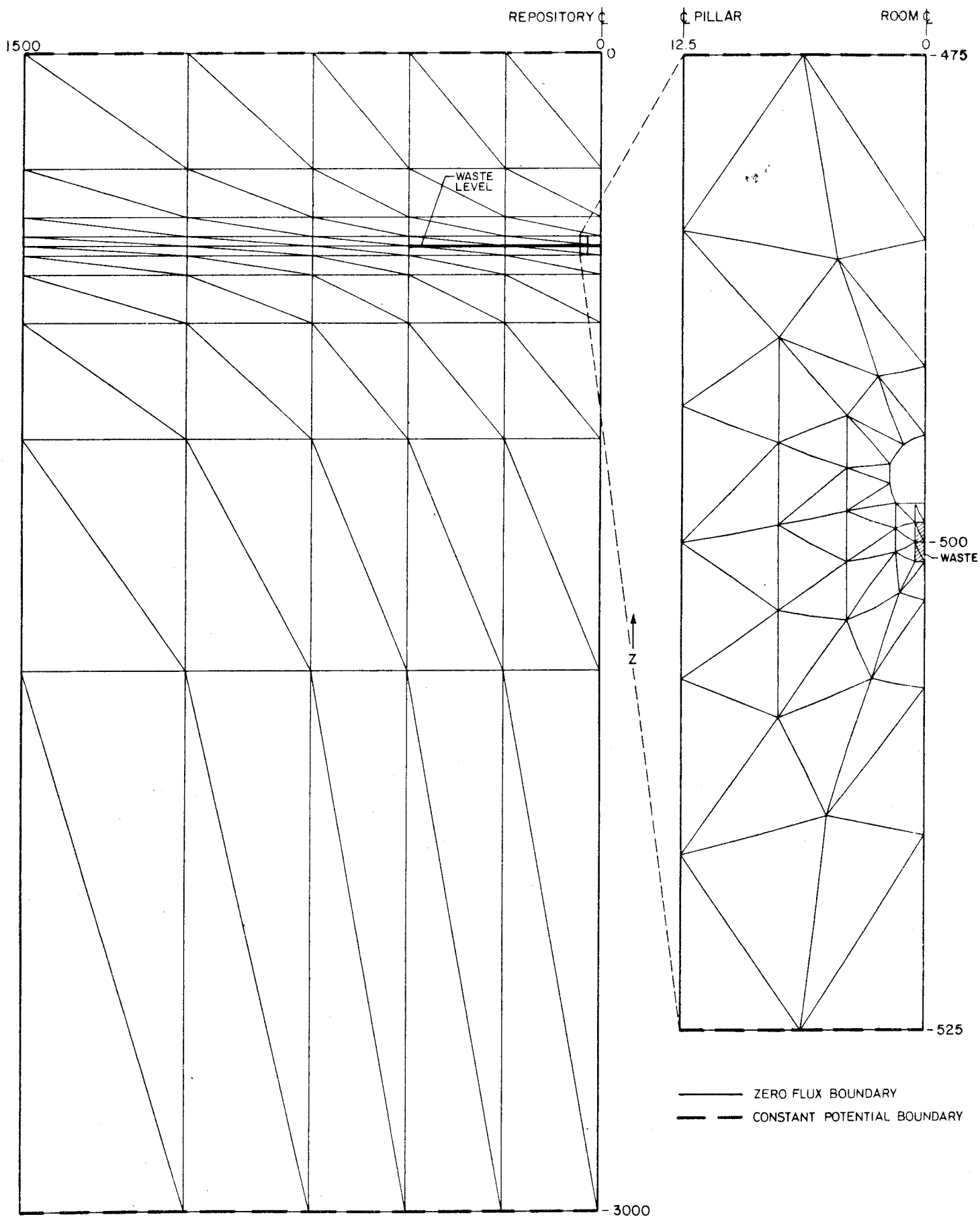
A comparison of these very limited field data with the inflow rates from the model simulations indicates that the model values are relatively high by about an order of magnitude. The final conclusions must await the results of further field data on the permeability distributions.

REFERENCES

1. Burgess, A.S., 1977, "Groundwater Movements Around a Repository", Phase 2, Technical Report 3 Regional Groundwater Flow Analyses, Part I Initial Conditions. To be submitted to KBS-Kärnbränslesäkerhet, Stockholm, Sweden.
2. von Brömssen. F.U., 1970, "Infiltration Coefficients for Groundwater Investigations in Moraine Clay Districts in Central Sweden. Nordisk Hydrologisk Konferens, Lund, Vol.2 pp. 241-249.
3. Ratigan. T.L., 1977, "Groundwater Movements Around a Repository", Phase 2 Technical Report 5, Repository Domain Groundwater Flow Analyses, Part I Permeability Perturbations. To be submitted to KBS-Kärnbränslesäkerhet, Stockholm, Sweden.
4. Skiba, E.L., 1977, "Groundwater Movements Around a Repository", Phase 2, Technical Report 5, Repository Domain Groundwater Flow Analyses, Part III Thermally Induced Flow. To be submitted to KBS-Kärnbränslesäkerhet, Stockholm, Sweden.
5. Raven, K.G. & Gale, J.E., 1977, "Subsurface Containment of Solid Radioactive Waste: a study of the surface and subsurface structural and groundwater conditions at selected underground mines and openings". Canadian Dept. of Energy Mines and Resources, Project 740057, EMR/GSC RW Int Rep No 1/77.

TABLE 1. ESTIMATES OF SEEPAGE WATER PUMPED FROM MINES (5).

MINE & DATE OF SHAFT SINKING	DOMINATE ROCK TYPE(S)	SEEPAGE PUMPED l/min	PERIOD OF PUMPING	DEPTH OF LEVELS PUMPED m	SEEPAGE PUMPED PER KM OF LATERAL DEVELOPMENT l/min,km	MAXIMUM DEPTH OF VISIBLE CONTINUOUS SEEPAGE m
Macassa (1917)	Augito Syenite	115	1971	150-2100	1.5	>915
North (1955)	Norite	3	1975	777-1200	0.2	>1150
New Quirke (1955)	Meta Conglo- merate Quartzite	0	1975	260-683	0	520
Strathcona (1964)	Granite Gneiss Norite	0	1975	365-915	0	365
Millenbach (1969)	Andesite, Quartz Feld- spar Porphyry	45	1975	716-1224	3.0	355
Langmuir (1971)	Meta Volcanic	6	Oct 1975	154-378	0.6	>378
East Malartic No.5 shaft (1969)	Greywacke Syenite	0 680	1975 April-May 1975	1160-1475	0 61.5	>1160



(a) REPOSITORY DOMAIN HALF MESH

(b) LOCAL HALF MESH

FIGURE 1. FINITE ELEMENT MESHES FOR REPOSITORY DOMAIN AND LOCAL MODELS

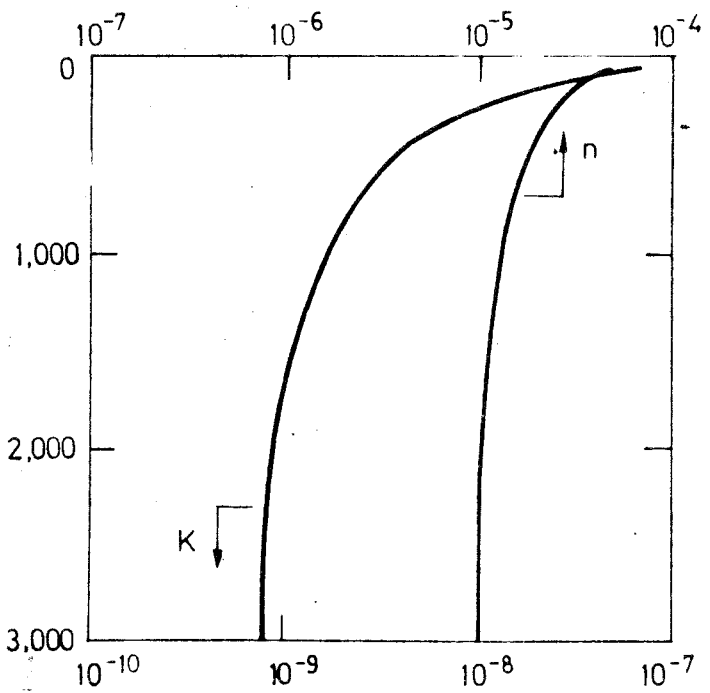
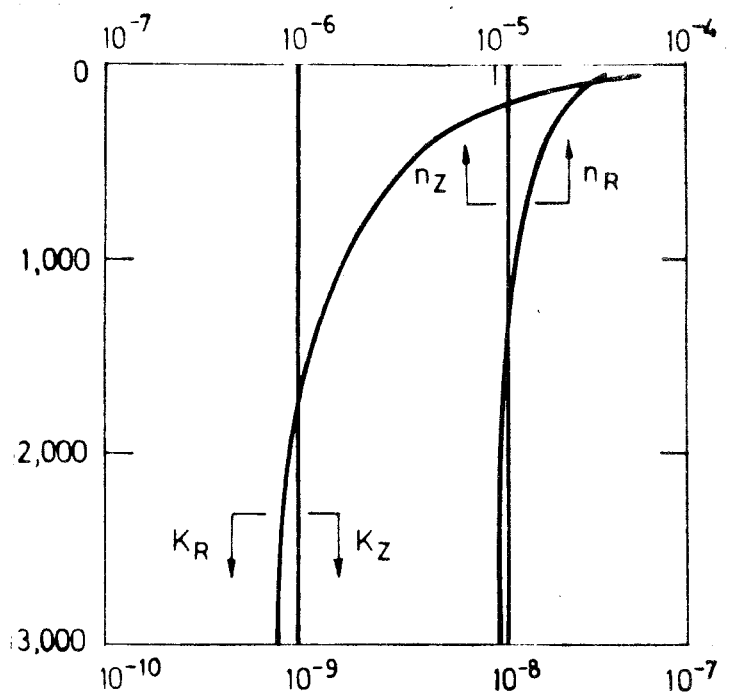
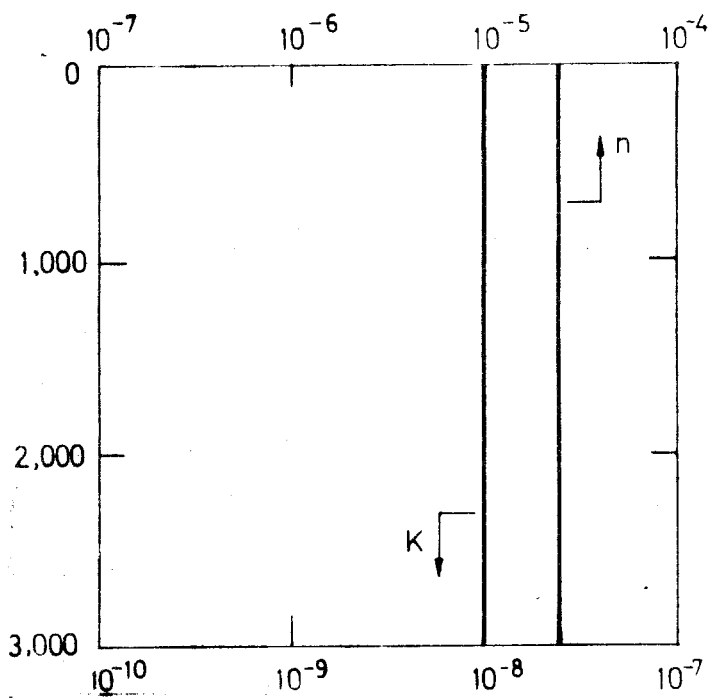


FIGURE 2. NOMINAL PERMEABILITY AND POROSITY DISTRIBUTIONS

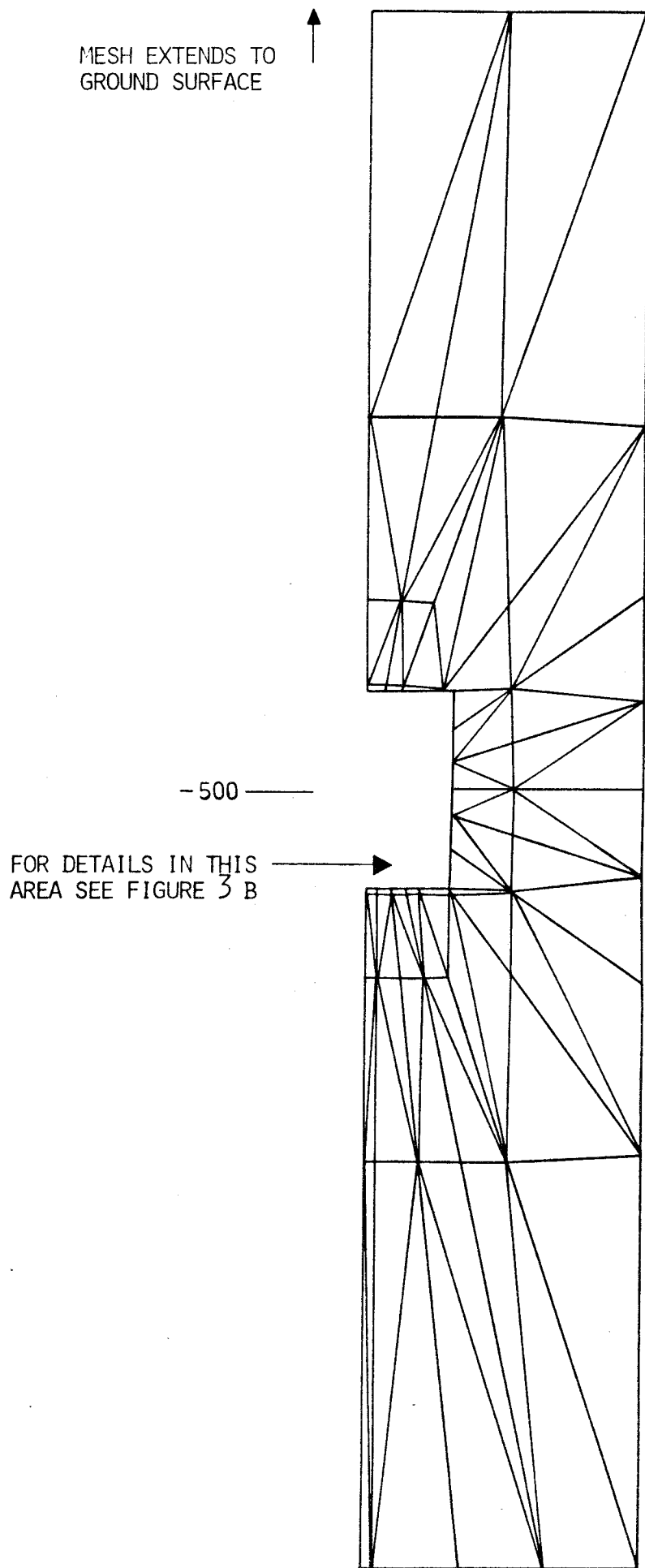


FIGURE 3 A. FINITE ELEMENT MESH FOR STUDY OF INFLOW WITH K AS A FUNCTION OF STRESS.

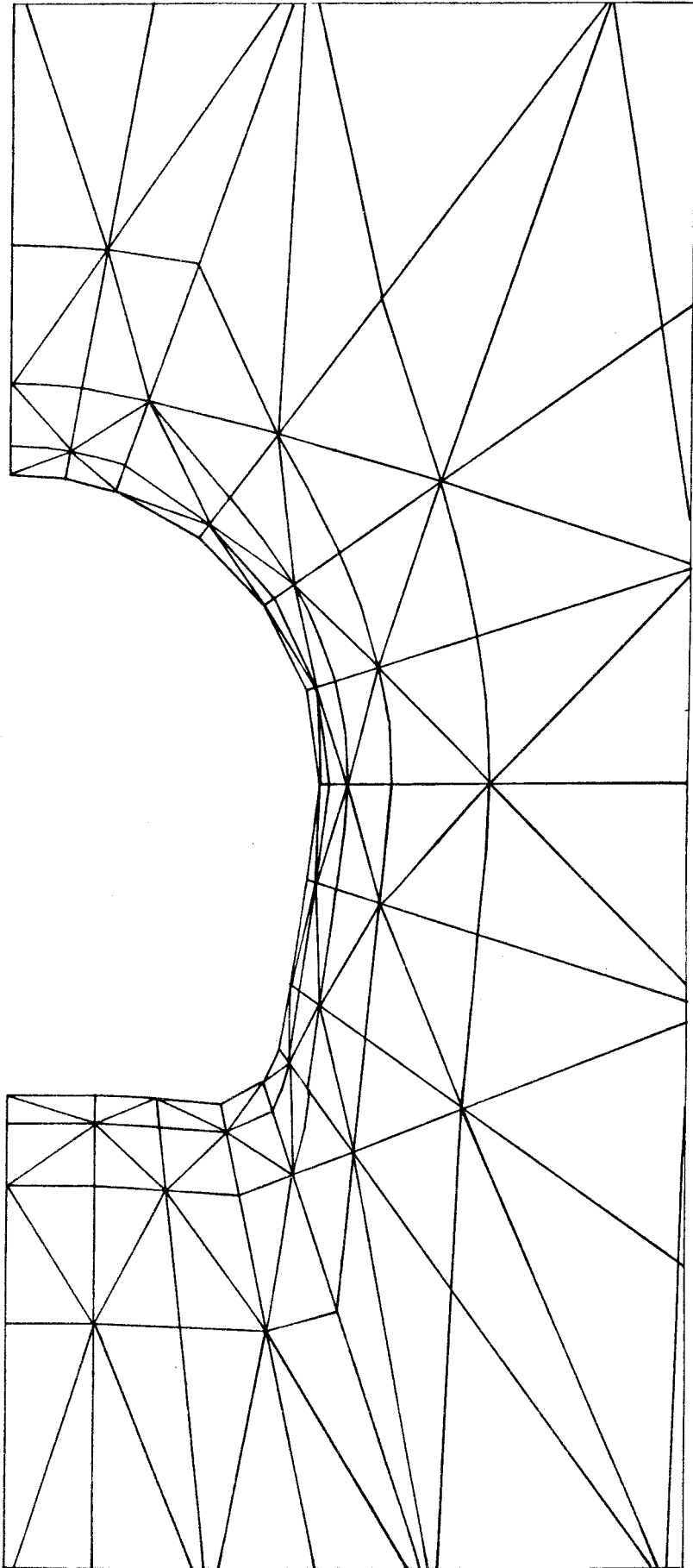


FIGURE 3 B. FINITE ELEMENT MESH FOR STUDY OF INFLOW WITH K AS A FUNCTION OF STRESS.

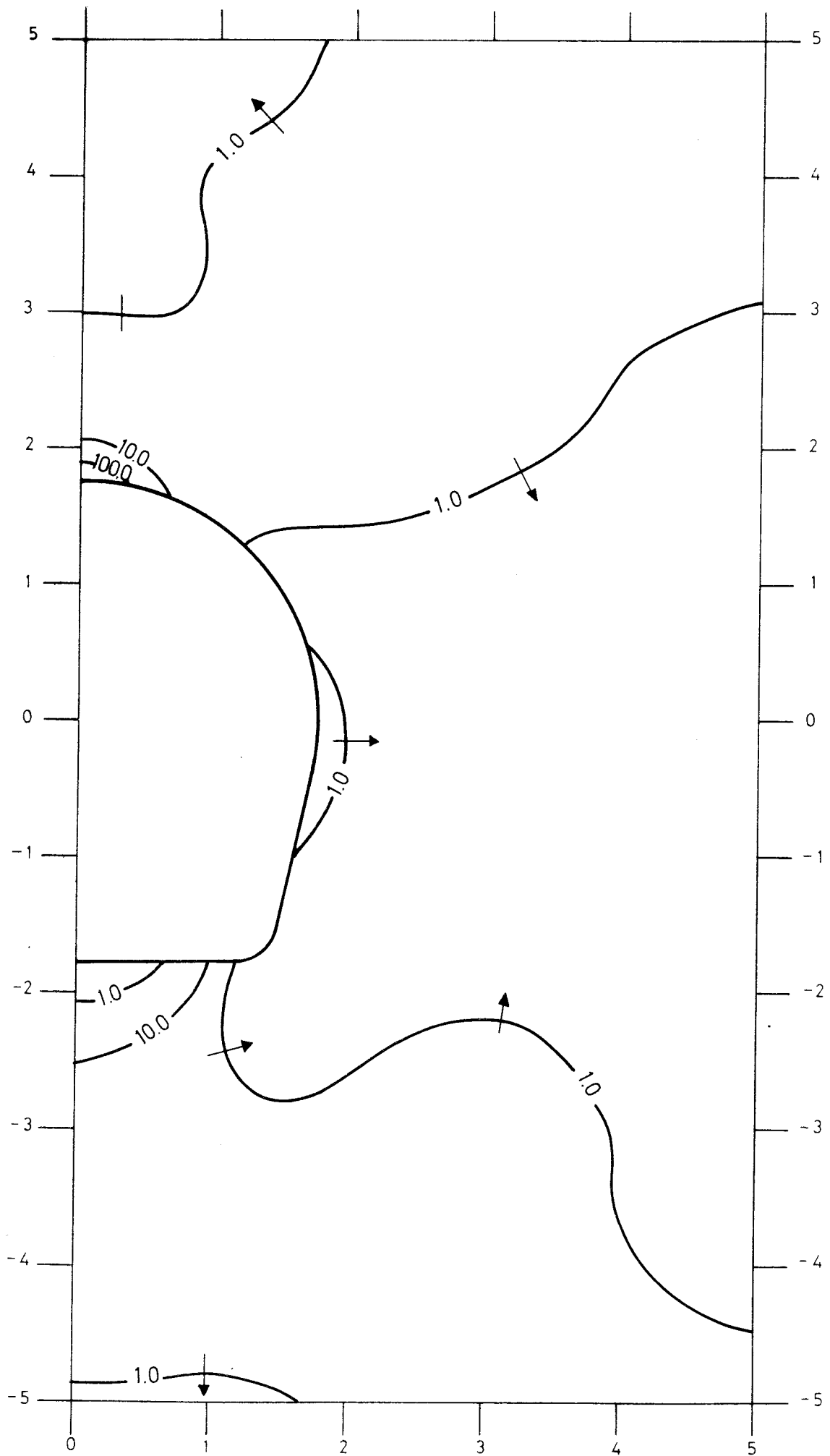


FIGURE 4 A. PERMEABILITY RATIOS

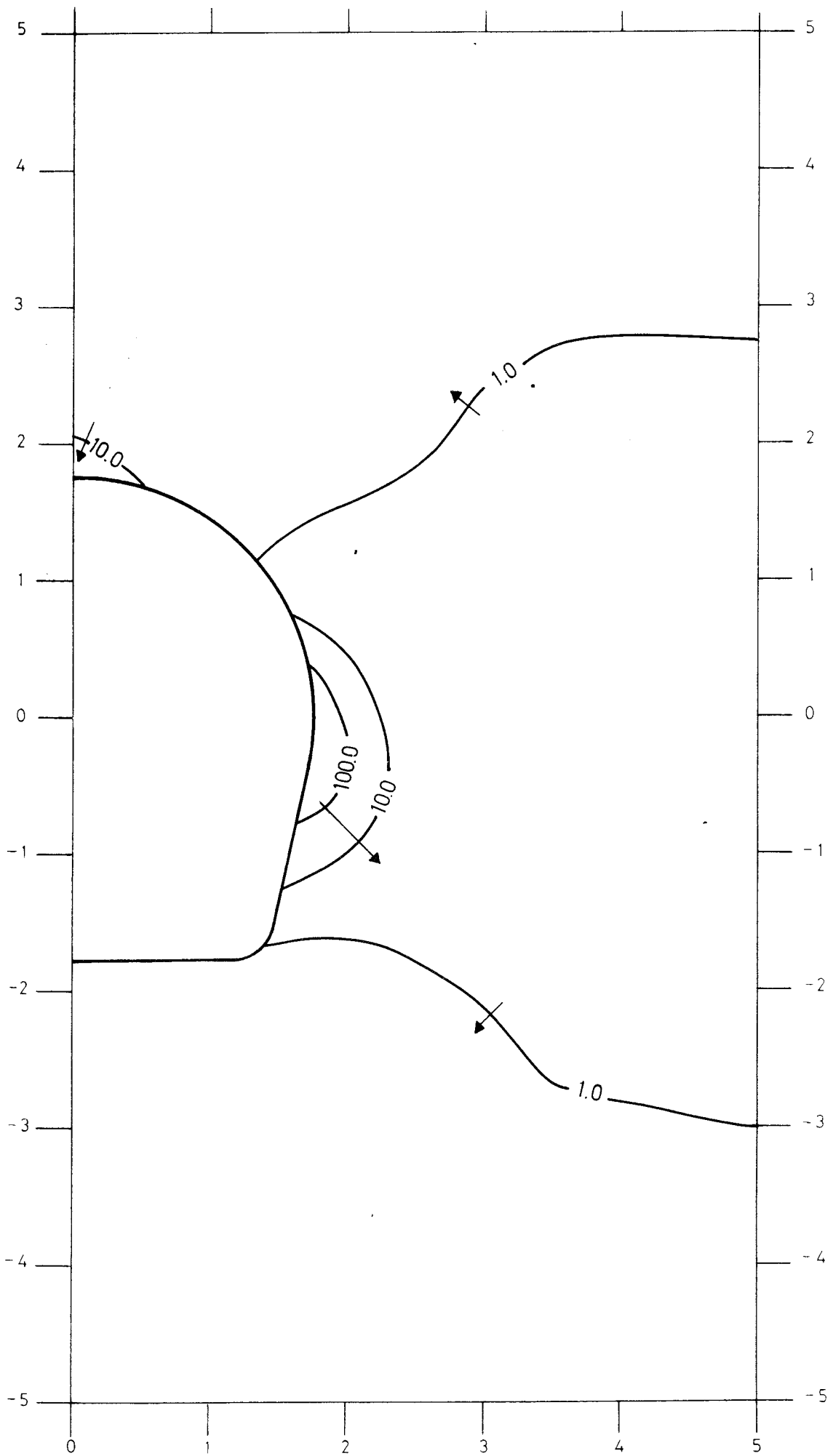


FIGURE 4 B. PERMEABILITY RATIOS.

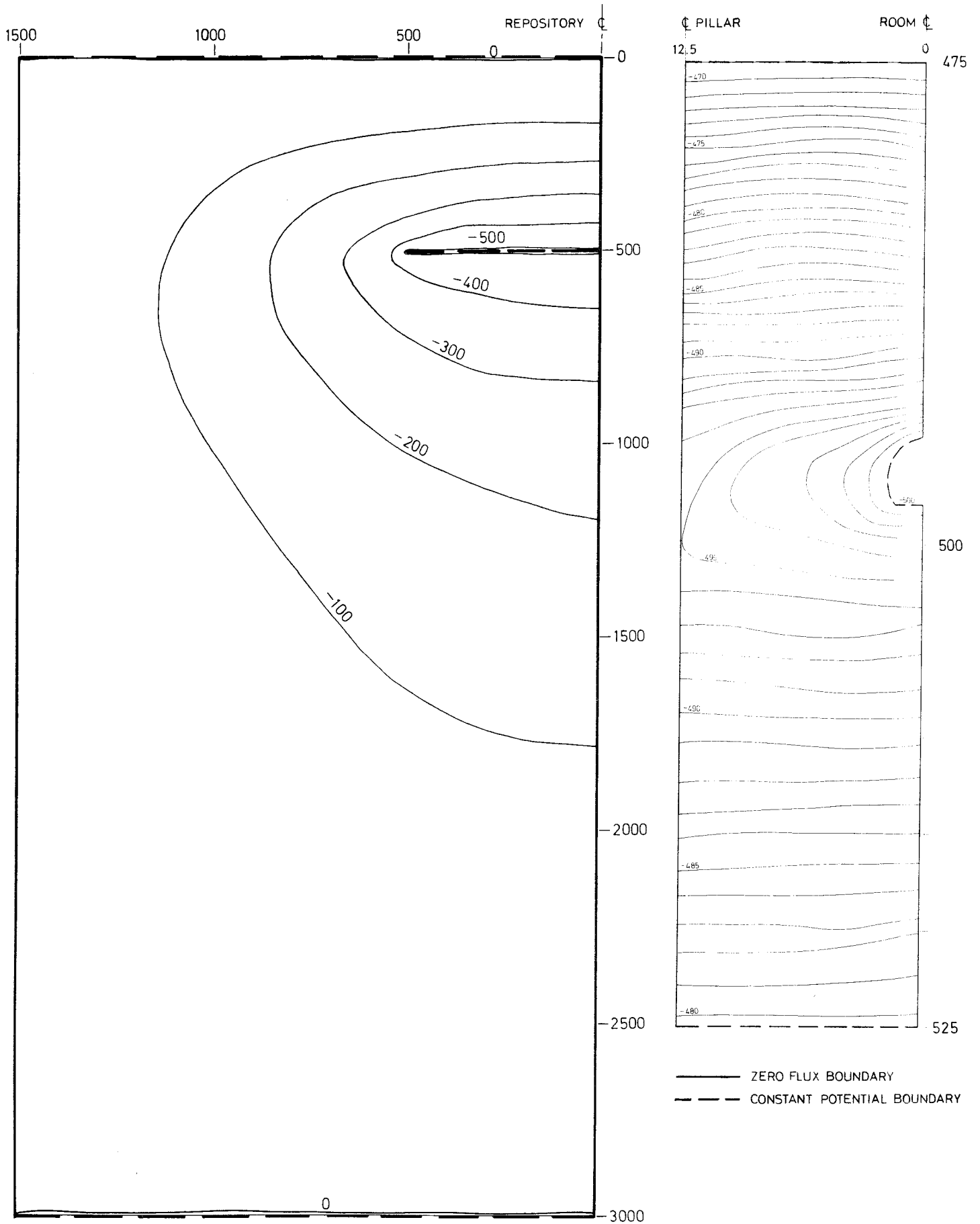


FIGURE 5. CASE 1 EQUIPOTENTIALS

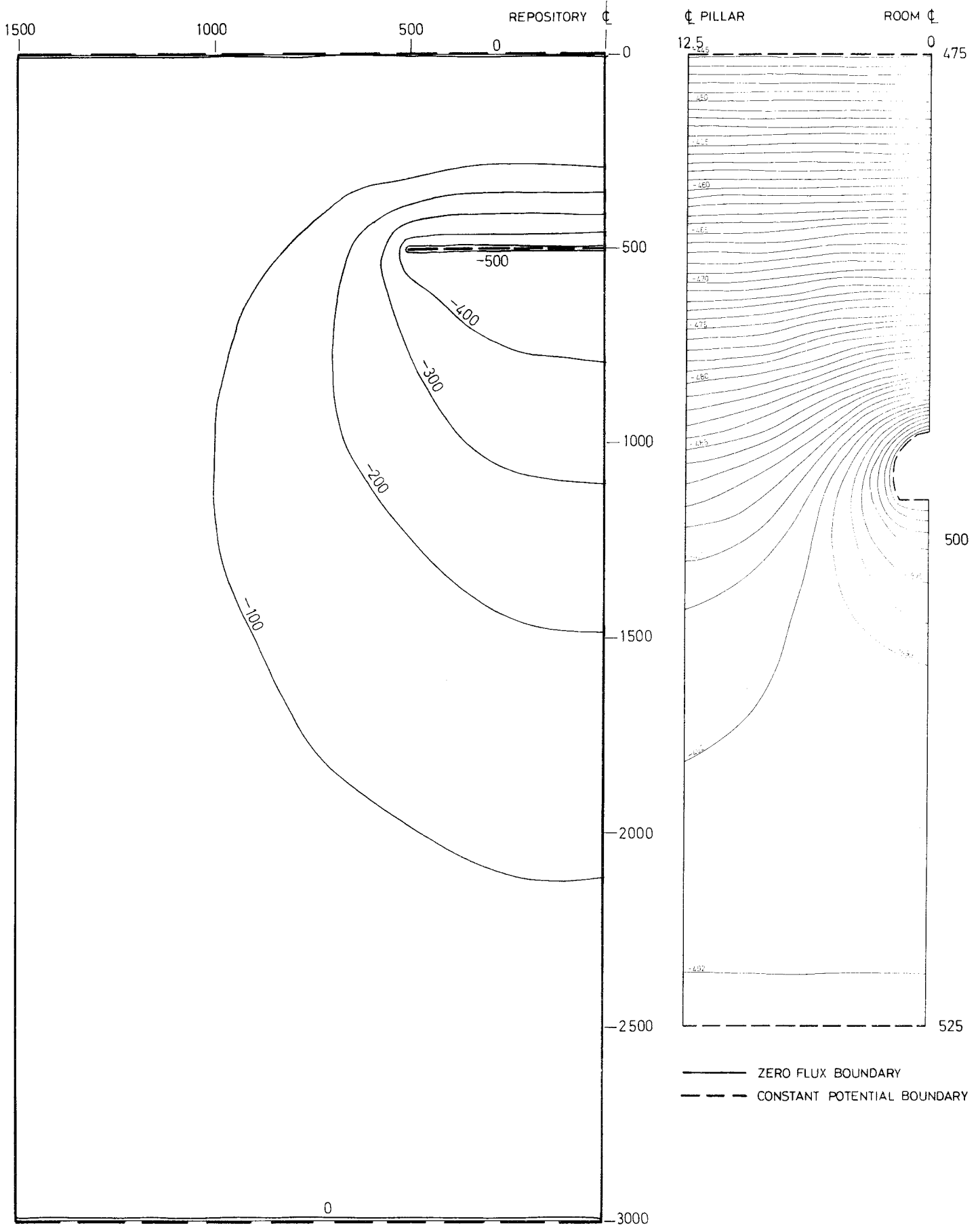


FIGURE 6. CASE 2 EQUIPOTENTIALS

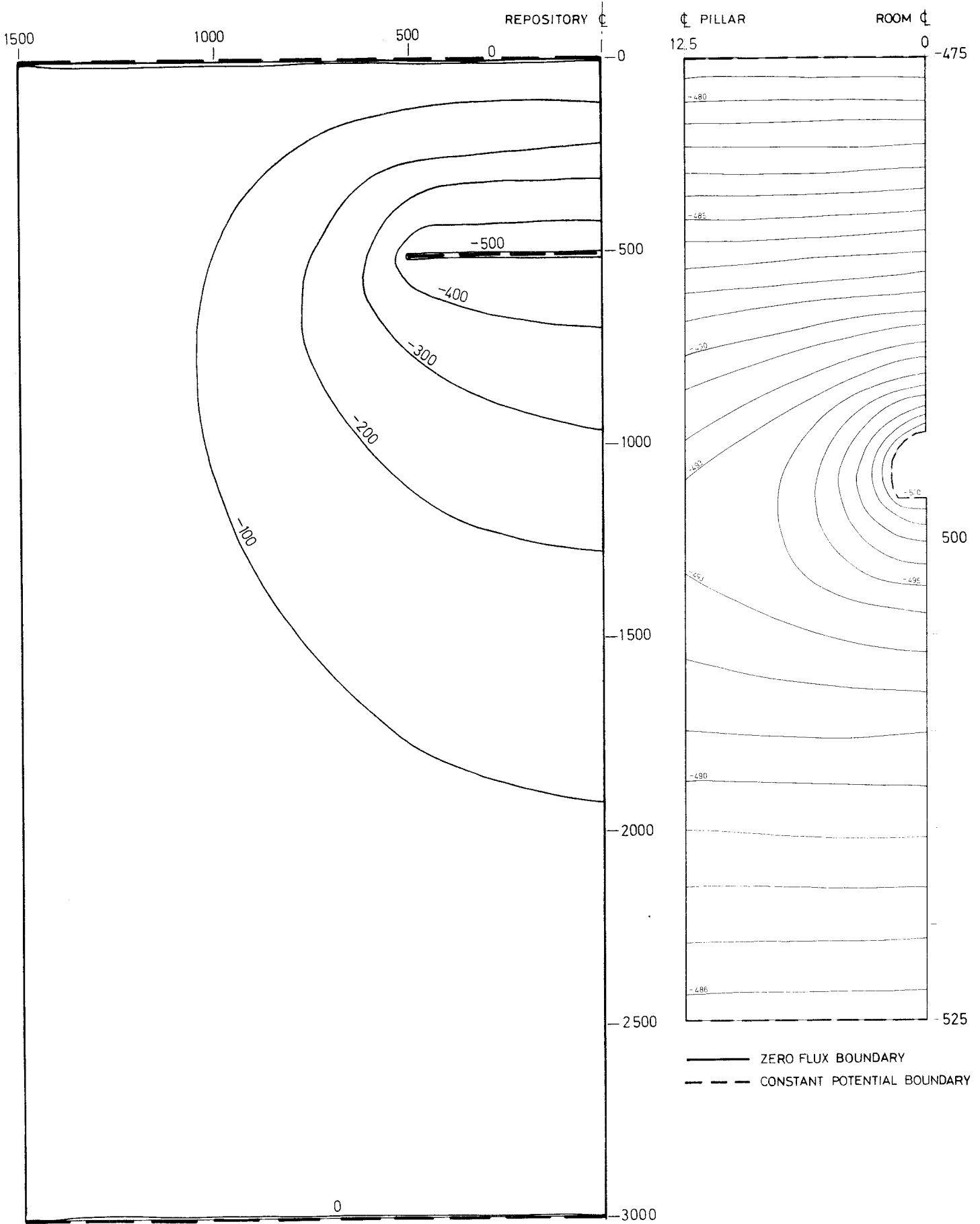


FIGURE 7. CASE 3 EQUIPOTENTIALS

INFLOW FL5-2 NON PERTURBED K VALUES EQUIPOTENTIALS

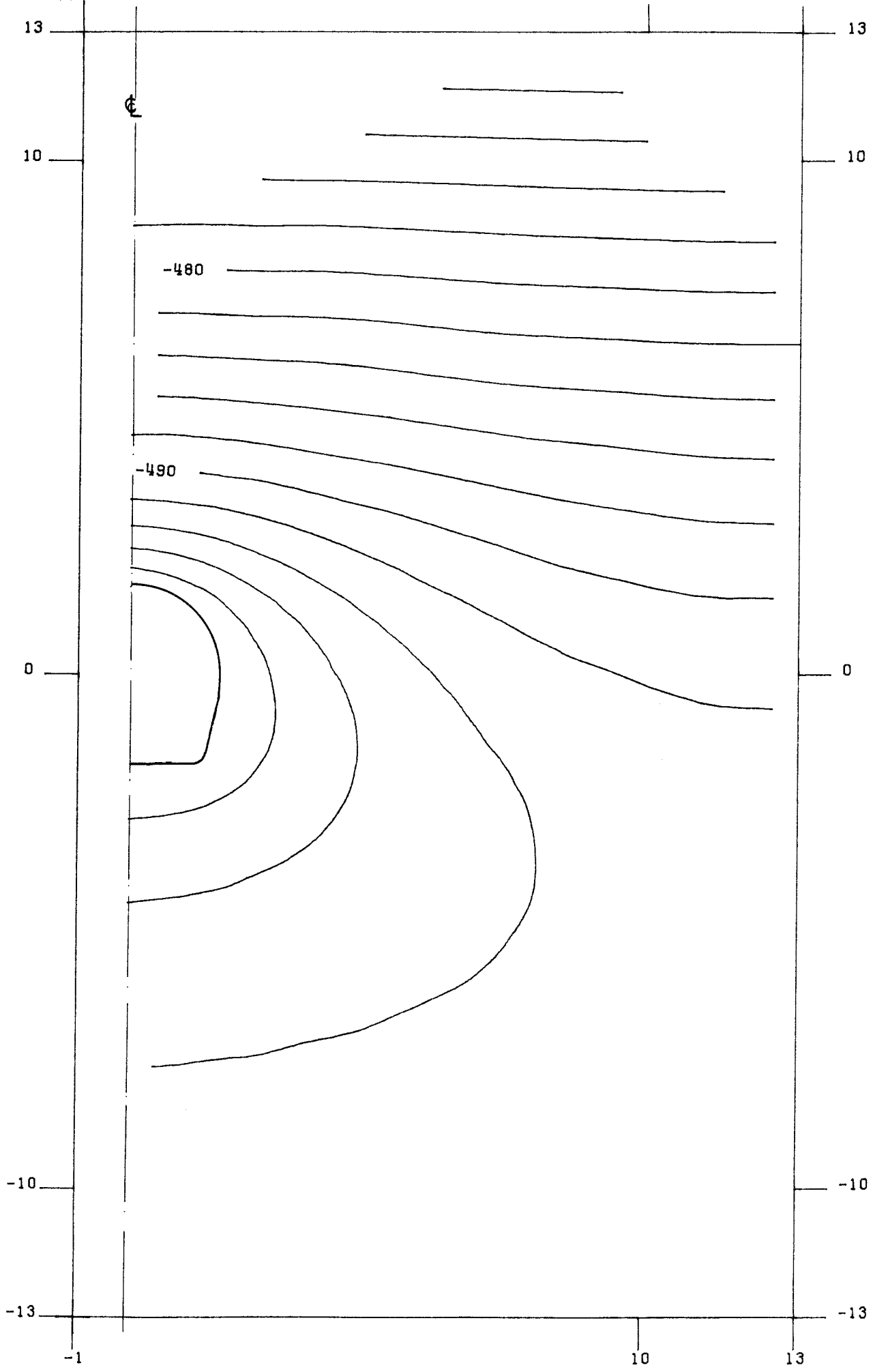


FIGURE 8. CASE 4 EQUIPOTENTIALS

INFLOW FL5-4 STRESS MODIFIED K VALUES EQUIPOTENTIALS

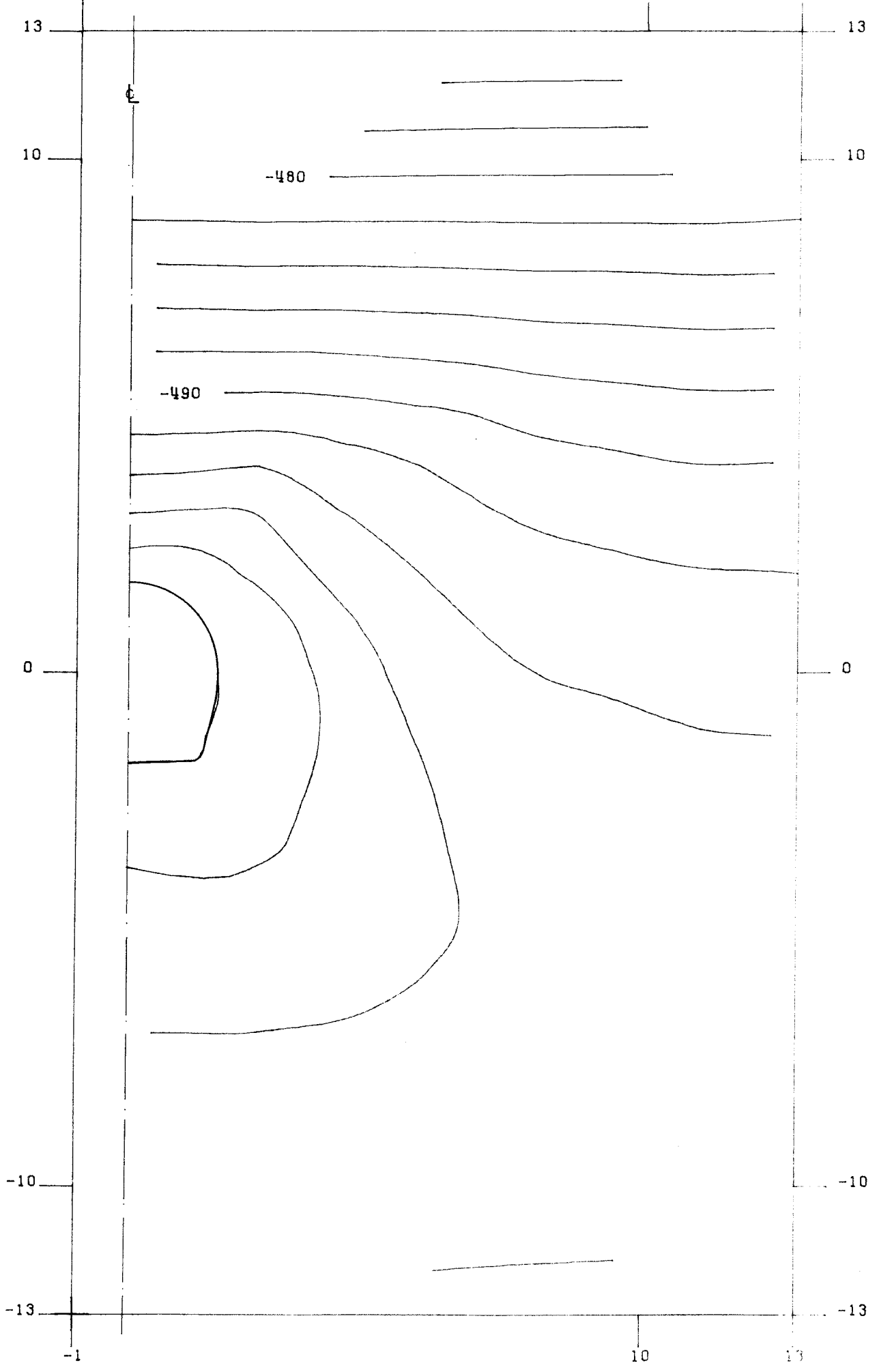


FIGURE 9. CASE 5 EQUIPOTENTIALS

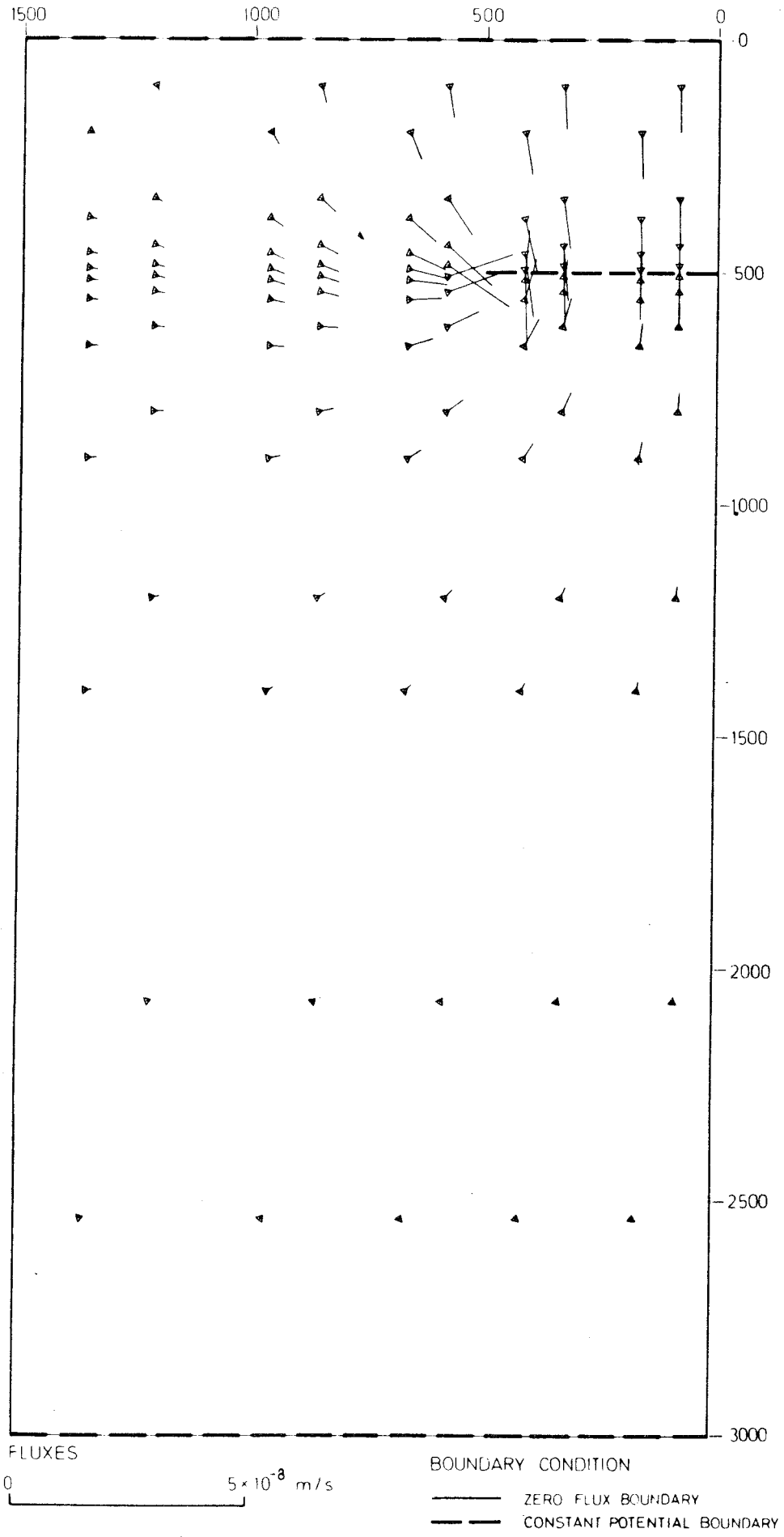


FIGURE 10. CASE 1 FLUX PATTERNS

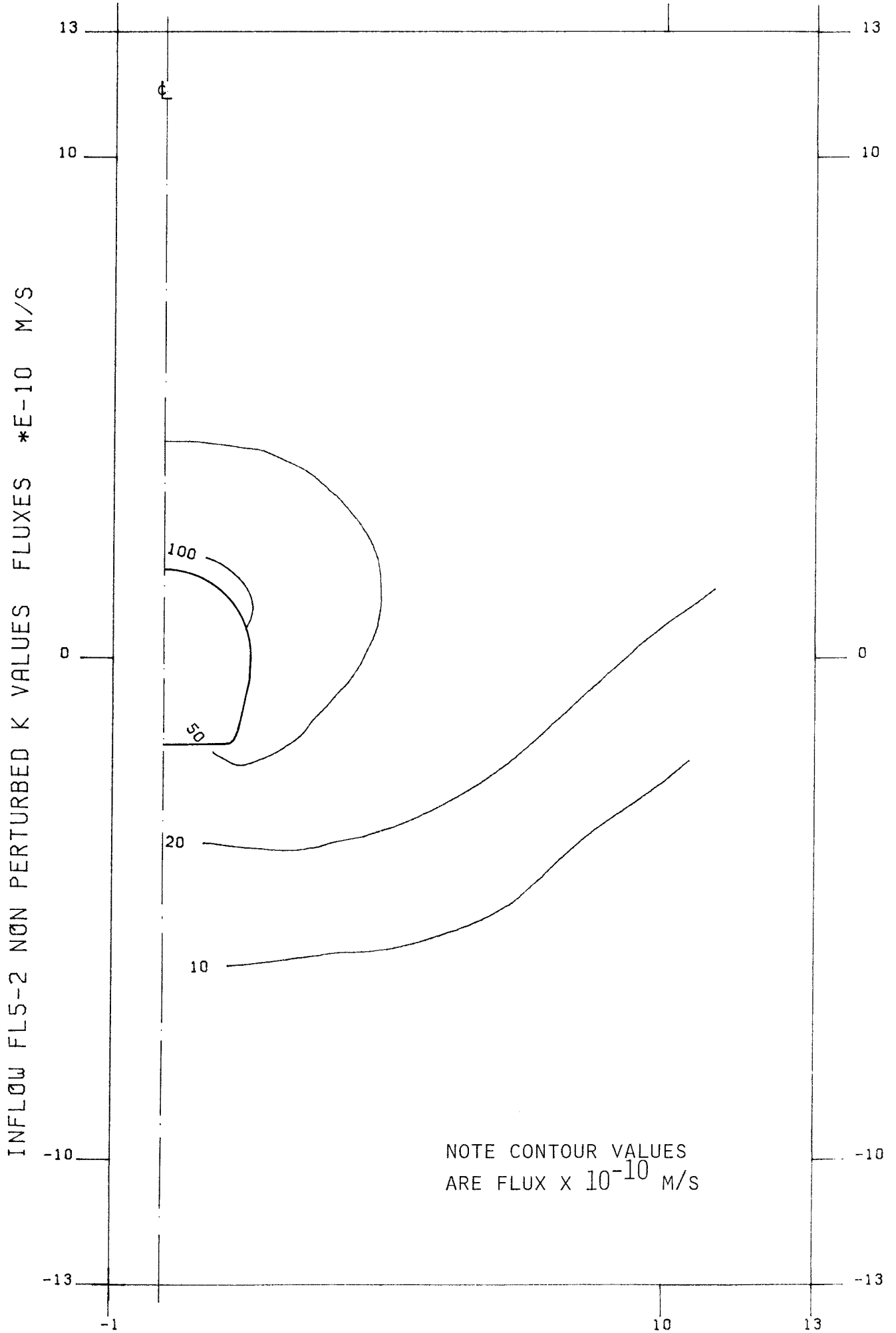
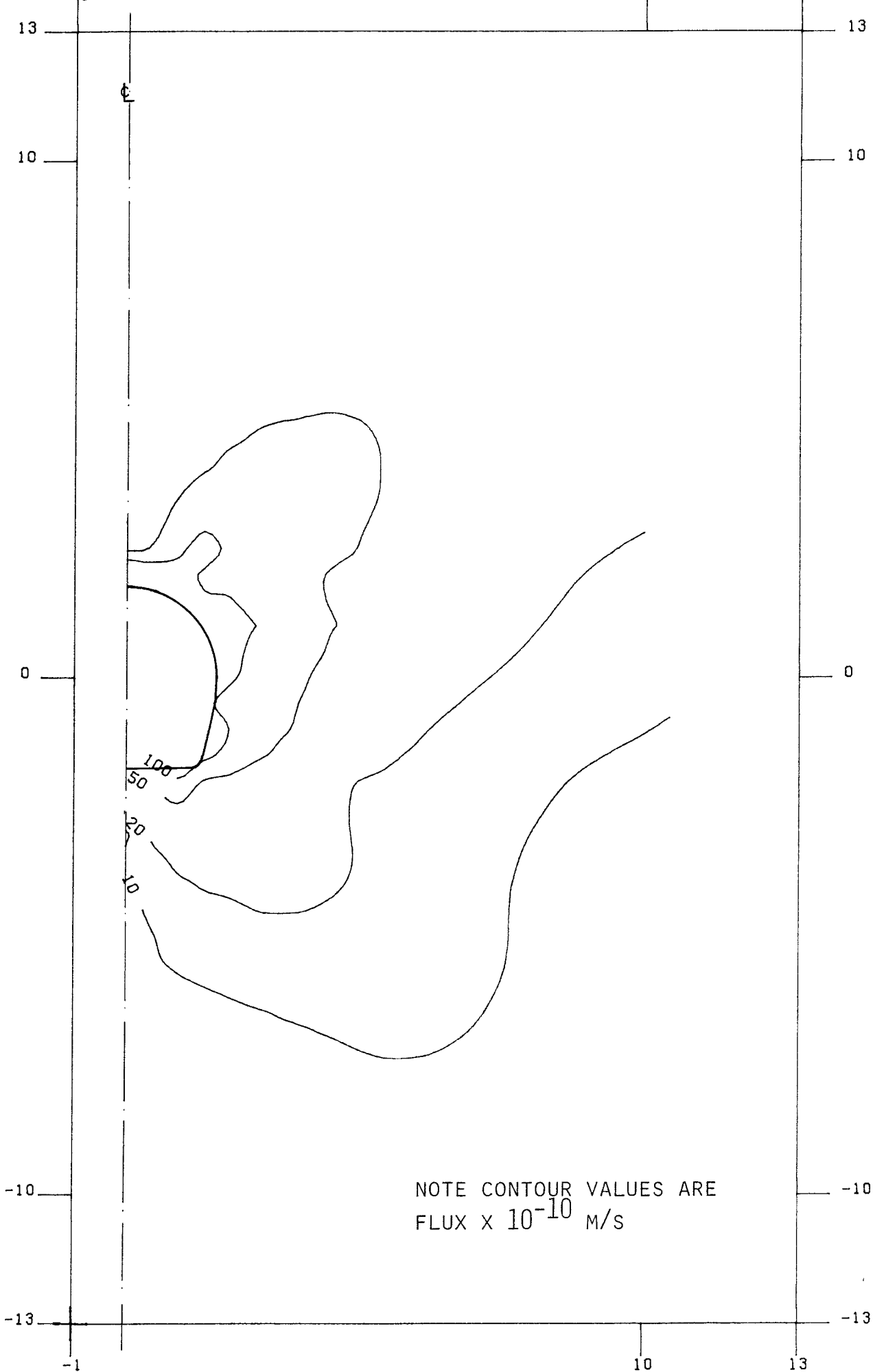


FIGURE 11. CASE 4 CONTOURS OF FLUX MAGNITUDES

INFLOW FL5-4 STRESS MODIFIED K VALUES *E-10 M/S



NOTE CONTOUR VALUES ARE
FLUX X 10^{-10} M/S

FIGURE 12. CASE 5 CONTOURS OF INFLOW FLUX MAGNITUDES

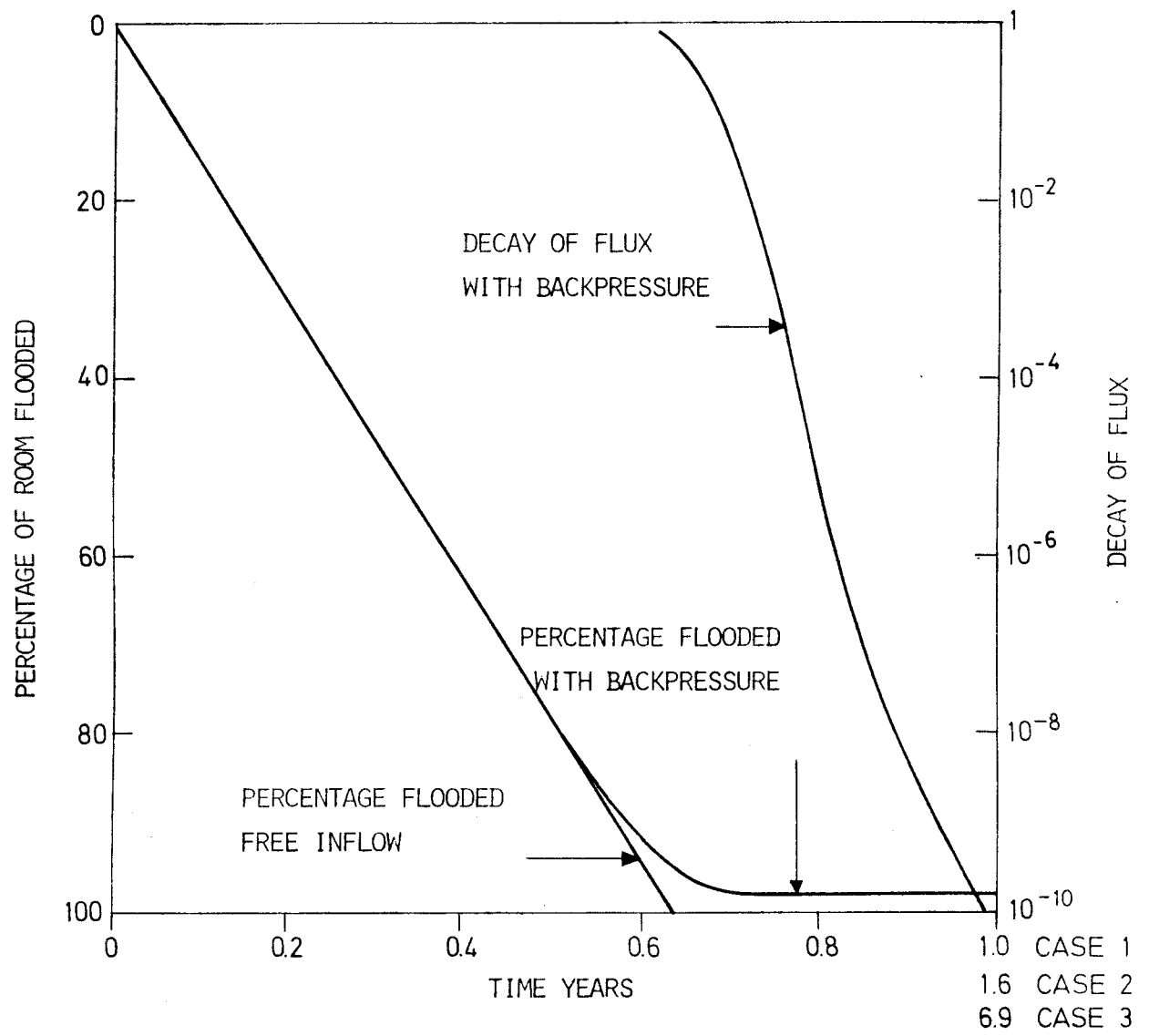


FIGURE 13. EFFECT OF BACKPRESSURE ON INFLOW

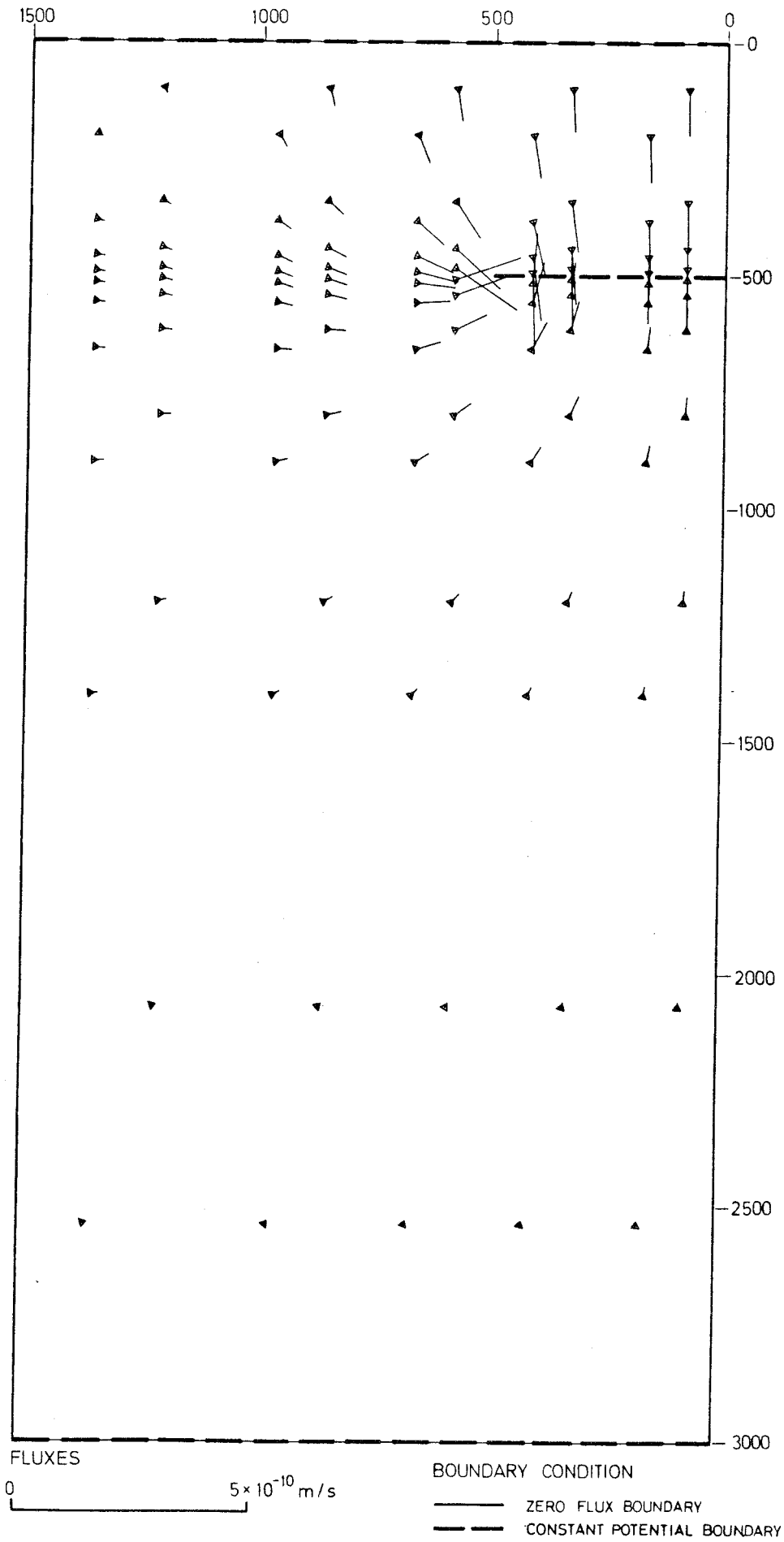


FIGURE 14. CASE 1 ADVECTIVE INFLOW RUN, SEEPAGE FLUXES

TECHNICAL REPORT 5
REPOSITORY DOMAIN GROUNDWATER
FLOW ANALYSES
PART III
THERMALLY INDUCED FLOW

KBS ~ Kärnbränslesäkerhet

GROUNDWATER MOVEMENTS AROUND A REPOSITORY

Phase 2. Technical Report 5: Repository Domain Groundwater Flow
Analyses.

Part III - Thermally Induced Flow

Hagconsult AB
in association with
Acres Consulting Services Ltd
RE/SPEC Inc.

FOREWORD

This report was prepared as one of a series of technical reports within a study of the groundwater movements around a repository for radioactive waste in the Precambrian bedrock of Sweden. It was written in 3 parts, (I) Permeability Perturbations, (II) Inflow to Repository and (III) Thermally Induced Flow. This is part III. The contract for this study was between KBS - Kärnbränslesäkerhet (Project Fuel Safety) and Hagconsult AB of Stockholm, Sweden. Acres Consulting Services Limited of Niagara Falls, Ontario, Canada and RE/SPEC Incorporated of Rapid City, South Dakota, U.S.A. acted as subconsultants to Hagconsult AB.

The principal authors of this report are Mr. Edward L. Skiba and Dr. Robin G. Charlwood of Acres, with contributions by Dr. A.S. Burgess of Acres and Mr. J.L. Ratigan of RE/SPEC. Review was provided by Dr. Ulf E. Lindblom of Hagconsult AB.

The opinions and conclusions in this document are those of the authors and should not be interpreted as necessarily representing the official policies or recommendations of KBS.

Stockholm, October 1977

Ulf E. Lindblom
Study Director
Hagconsult AB

TABLE OF CONTENTS

FOREWORD

1. INTRODUCTION

2. INPUT PARAMETERS AND MODELING
 - 2.1 Layout and Thermal Loading
 - 2.2 Flow Assumptions
 - 2.3 Flow Geometries and Boundary Conditions

3. THERMALLY INDUCED FLOW
 - 3.1 Conduction Baseline Results
 - 3.2 Thermally Induced Flow
 - 3.3 Effect of inflow on Thermally Induced Flow

4. THERMALLY INDUCED FLOW WITH REGIONAL FLOW

5. SUMMARY AND CONCLUSIONS

REFERENCES

APPENDIX A - Model Description

APPENDIX B - Model Validation

1. INTRODUCTION

The overall objective of this study is to assess the groundwater flow around a radioactive waste repository as produced by various possible mechanisms. The pre-excitation flow due to the regional gradient is the subject of a previous report in this series (1)^x) This report deals with the time period following loading of the repository, in which the mechanism of natural convection may produce flows which are temporary perturbations to the regional flow. The natural convection ends when the waste-generated temperature perturbation disappears and the regional geothermal gradient is reestablished.

Inflow into the repository will occur during the construction and emplacement phases and will continue until the repository zone is recharged. Inflow, which is discussed separately (2), is shown to be much stronger than the thermally induced flows and consequently thermally induced flows are not significant until the recharge period is over. The interaction between these mechanisms is discussed in this report. Following these time periods of transient perturbations, regional flow again dominates water transport, albeit somewhat influenced by the residual effects of the repository tunnelling and associated excavation and fracturing of the rock. This long-term era flow is the subject of another report in this series (3).

The specific objective of this report is to define flow patterns during the thermal era, using baseline properties, with the intention of identifying groundwater flow fields which may be of interest in subsequent safety analyses. These flows and temperature fields are computed with full coupling between heat transfer and ground-water flow and are referred to as thermally induced flow analyses. Conduction heat transfer results are also presented for comparison with the thermally induced flow results and the magnitude of advective heat transfer is discussed.

x) Numbers in paranthesis refer to references at end of text

After a brief presentation of the assumptions, geometries and material properties used in this short-term study, the bulk of this report is devoted to thermally induced flow and coupled thermally induced and cross flow. Conclusions are presented section by section and summarized later. The appendices contain the development of the theory for the thermally induced flow model and validation runs.

2. INPUT PARAMETERS AND MODELING

2.1 Layout and Thermal Loading

The repository layout consists of 41 tunnels each 1 km long on 25 m centers, covering an area 1 km square at a depth of 500 m (4). For the study of thermally induced flow, nine thousand canisters of 40 year old highlevel waste (HLW), reprocessed at 10 years, were assumed to be instantaneously emplaced at 4 m spacing along the tunnels. This results in a gross thermal loading (GTL) of 5.25 W/m^2 (525 W/canister divided by $100 \text{ m}^2/\text{canister}$), at time of emplacement. The decay of this gross thermal loading is presented in Figure 1 for 1,000 years. After 1,000 years, the thermal loading is almost negligible since it falls to 0.0003 W/m^2 at 10,000 years which is considerably less than the approximate geothermal heat flux of 0.04 W/m^2 .

Nonetheless, the theoretical potential for thermally induced flows will remain as long as temperature gradients exist around the repository. The geothermal gradient is not represented in the modeling. Instead, an initial condition of zero temperature everywhere is assumed. The pre-emplacement temperatures in the conduction report were 5°C at surface and a $20^\circ\text{C}/\text{km}$ rise with depth giving 15°C at the repository depth of 500 m. Since the isotherms due to the geothermal loading are nominally horizontal, they do not directly cause thermally induced flow (5). Horizontal inhomogeneity of the geothermal gradient may be found in thermally active regions but is not considered here as a generator of flow.

The conceptual model considered consists of a large block of "intact" rock bounded by singular features. The intact rock is assumed to be traversed by joint sets and thus permeable and is the subject of these analyses. Flow mechanisms in the singular features are not studied in this report.

2.2 Flow Assumptions

Initially, we assume saturated, one-phase flow with fixed fluid and permeability parameters. Laminar Darcy flow is assumed valid for an equivalent porous analogue to the jointed medium. The regional groundwater flow report (1) in this series describes the details of the derivation of the three permeability and porosity distributions presented in Figure 2. They are:

- Case 1) $K = 10^{-8}$ m/s, homogeneous and isotropic
- Case 2) $K(Z)$, isotropic, non-homogeneous, decreasing with depth.
- Case 3) $K_R(Z)$, anisotropic, non-homogeneous horizontal, decreasing with depth, but K_Z , vertical, constant at 10^{-9} m/s

These are used to determine the volumetric flux of fluid, and in conjunction with their corresponding porosities, the fluid velocity. The porosities are computed from the permeabilities using a formulation derived by Snow (6) for parallel fracture sets at given spacing of 1.8 m. Flow patterns derived using any of the above permeability distributions are also valid for other conditions providing the same relative permeability distribution in space is maintained. Fluxes and velocities may then be scaled homogeneously with the new permeability values. Flux is scaled linearly with the K scale for given fracture spacing and velocities scale as $K^{2/3}$. Thus, a decrease by a factor of 1,000 in K decreases fluxes by 1,000 but velocities only by 100 for the same fracture spacing.

The other material properties used in this report are shown in Figure 3.

2.3 Flow Geometries and Boundary Conditions

The modeling has been divided into two scales for examining global and local effects. These two model geometries are found in Figure 4. The two dimensional global model has been constructed with symmetry at the repository centreline, making the centre boundary impermeable to flow of heat and fluid. For thermally induced flow modeling the other three boundaries are also impermeable to fluid flow but are maintained at 0°C , the initial condition for temperature. The model size is felt to be large enough to preclude interference in thermal distributions to at least 1,000 years. Beyond this time, growing interference will occur. However, since

near repository temperatures are decreasing anyway and the loading is negligible, the interference is estimated to be tolerable. The lateral dimension and depth are also felt to be sufficient to allow ample room for return flow to complement the thermally induced flow through the repository itself, and therefore, to be non-restrictive. The global model size is representative of the expected intact zone. Any larger model would have to include singular features, which are considered beyond the scope of the present study and the state-of-the-art for thermally induced modeling.

The local model is a half room and pillar section with symmetry boundaries on both vertical sides, impervious to heat or fluid flow. In all local model runs, the time dependent boundary conditions on potential and temperature, required for the top and bottom, are obtained from the corresponding global model run. The room is assumed to be backfilled with a saturated impervious material.

For the combination of thermally induced flow and global crossflow considered later in this report, the thermally induced flow results were transposed across the symmetry plane and the crossflow applied by superposition to produce the flow patterns.

3. THERMALLY INDUCED FLOW

3.1 Conduction Baseline Results

The isotherms predicted with the conduction global (GLOBAL/HT-1) and local (LOCAL/HT-1) model runs are contained in Figures 5 to 7 at 40, 200 and 1,000 years after emplacement. The isotherms are not plotted for times greater than 1000 years since there is evidence of boundary interference with the isotherms. The repository temperature estimates at long times, however, seem quite good compared with the analyses presented in the thermal analyses report (4). Figure 8 shows two important temperature histories with time, the average repository temperature and the drill hole periphery temperature. These compare well with the temperatures attained in the conduction heat transfer report. The only essential difference in these runs is the backfill in the tunnel of the local model, but this appears to have little influence on the resulting temperatures. The runs to 1,000 years were carried out with the same time steps as in the conduction heat transfer report, and repeated with larger time steps (3 times larger). The results were comparable to within 0.5°C at all locations at all times. The longer time steps were used for subsequent analyses.

3.2 Thermally Induced Flow Results

In order to assess the relative importance of thermally induced flow in comparison with regional cross flow, the models were analysed with and without regional cross flow. All thermally induced flow analyses for zero cross flow showed no significant deviation from the conduction temperatures discussed previously. All temperatures were within 0.1°C of the conduction temperatures at all times, thus demonstrating that advective heat transport is negligible as far as temperature predictions are concerned.

Velocity plots are contained in Figures 9 to 13 for the GLOBAL/HT-2 and LOCAL/HT-2 runs using the Case 1 permeability, K homogeneous and isotropic at 10^{-8}m/s , at 40, 200, 1,000, 10,000 and 100,000 years after emplacement. Similar results are presented in Figures 14 to 18 for the GLOBAL/HT-3 and

LOCAL/HT-3 runs using the Case 3 permeabilities, $K(Z)$ horizontally, and K uniform vertically. For the global thermally induced flow runs, Figure 29 displays the average vertical transport velocities above the repository. Local velocities are larger near the repository. Global runs were attempted for the Case 2 permeabilities, $K(Z)$ isotropic, but the vertical permeability was so large near the surface that numerical instability developed at the large time steps used in the runs and the results were invalidated. All the results show a mild degree of numerical instability at low times (40 and 200 years for Case 1 and 40 years for Case 3) which damps out for longer times and yields results which are stable. The runs to 1,000 years were performed with one iteration per time step, but the run extensions to 100,000 years used two iterations per time step, allowing the use of large steps while preserving stability. Since heat advection is so low in this problem, it would seem advisable to neglect it in further runs, which would increase the stability of the buoyant flow produced. This numerical stability, or instability, is not to be confused with the physical instability of vertically stratified systems (Bénard cells). Since a horizontal gradient of temperature and density always exists in our system, there is no minimum temperature difference which must be exceeded in the classical sense for thermally induced flow to commence (5). Other inhibiting mechanisms, due to the fractured nature of our medium or partial saturation, may exist, but are not obvious and have not been considered here. Experimental and numerical comparisons of fractured and analogous porous media undergoing thermal flow loading must be conducted to answer the many questions which may arise on this matter.

The nature of the flows themselves warrant some comment. Globally, a cell, rising through the repository and descending around it, develops at short times and persists, only dropping an order of magnitude over 100,000 years. A local cell also develops beside the waste canister and tunnel but it begins to weaken substantially by 1,000 years. The inherent problem with these flows is that the local cell channels flow over the canister itself and the global cell provides direct transport to the surface. For the nominal conductivities used herein the expected travel times from the repository to the surface are presented below. It must be noted that these are for the conditions of no regional crossflow. This condition is likely only beneath a large body of water well away from the shore.

Table 2.

Thermally induced flow - travel time to surface assuming no cross flow

Travel time	starting at 1,000 years	starting at 100,000 years
Case 1 ($K_z = 10^{-8}$) isotropic homogeneous	200 years	2,000 years
Case 3 ($K_z = 10^{-9}$) anisotropic non-homogeneous	1,000 years	10,000 years

If these permeabilities are decreased by 3 orders of magnitude, the times increase by a factor of 100 assuming a similar fracture frequency. These decreased permeabilities are quite limiting to the flow. Note that the increased horizontal permeability of Case 3 near the surface appears to have little influence on the travel time to the surface. The expected increase in travel time for a one order decrease in K is $10^{2/3} = 4.64$, close to that found numerically.

An interesting effect of the anisotropy and non-homogeneity is noted in the location of the eye of the global cell. For both cases, the eye moves outward from the repository at long times. In Case 1 (isotropic), the eye drops below the repository several hundreds of meters. The increased horizontal permeability of the anisotropic Case 3, near the surface, appears to permit the eye to remain at repository level at long times, in contrast to the isotropic case.

3.3 Effect of Inflow on Thermally Induced Flow

Inflow is expected to be capable of dominating hydrothermal flow for a considerable period of time. This could be evaluated by comparing downward inflow velocities (2) and upward thermally induced flow velocities directly above the global repository level, see below.

Relative strengths of inflow and thermally induced flow

	<u>Flux (m/s)</u>	<u>Velocity (m/s)</u>
Case 1 Inflow	1.213×10^{-8}	4.89×10^{-4}
Case 1 T/I flow	1.463×10^{-11}	5.90×10^{-7} (100 years)
Case 3 Inflow	1.77×10^{-9}	1.08×10^{-4}
Case 3 T/I flow	2.165×10^{-12}	1.32×10^{-7} (100 years)

According to the table, the inflows are stronger than the thermally induced flows by a factor of 830 for Case 1 and 820 for Case 3. In both cases, inflow and thermally induced flows are equally controlled by the vertical hydraulic permeability and scale equally as K is scaled in value. It is anticipated that for any K and n distributions, the ratio of inflow to thermally induced flow will be near to 800 or roughly 3 orders of magnitude. These results are for free inflow and initial pressurizing inflow as well. On the tail of the pressurizing inflow will still dominate hydrothermal flow for a period roughly equal to its free inflow time without pressurizing. This domination time could extend to hundreds of years (640 for $K_z = 10^{-11}$ m/s), but the value of K required for domination of inflow to 100,000 years would be incomprehensibly low (0.64×10^{-13} m/s). This result would indicate that thermally induced flow could be expected to occur, despite inflow, at some time during the life of the repository.

4. THERMALLY INDUCED FLOW

Regional gradient flow and thermally induced flow can only be expected to interact significantly if the two flows are of comparable magnitude. Figures 19 to 23 present the interaction for the Case 1 K distribution with a regional gradient of $2 \cdot 10^{-3}$ (1). Since the hydrothermal and cross flow are essentially non-advective of heat, superposition of solutions was used to produce these plots. At 1,000 years, the cross flow is about one order of magnitude stronger than the average thermally induced flow; however, at 100,000 years, this increases to two orders of magnitude. The time for flow due to cross flow from the edge of the repository to the edge of the geometry (1,000 m) is about 40 years. Thus, it is evident that the cross flow, while it cannot completely suppress the hydrothermal flow, sweeps the flow horizontally and may reduce or eliminate the possibility of direct surface discharge of contaminants due to vertical hydrothermal flow, even for small regional gradients.

Figures 24 to 28 present similar plots for the Case 3 anisotropic K distribution in which the horizontal permeability is greater than the vertical. In fact, it is evident that the regional flow dominates even more here since it is determined by the horizontal permeability, not the vertical. Time to exit at the vertical boundary is 70 years since the regional gradient velocity is about 0.45×10^{-6} m/s as compared to 0.8×10^{-6} m/s for Case 1 at the repository. The velocities may be scaled by $K^{2/3}$ and the times by $K^{-2/3}$ if scaling of K is desired. This will not effect the relative strenghts of the regional and thermally induced flows, however, if the same isotropy or distribution of anisotropy with depth is maintained during scaling.

Quantity of water flowing past canister is = (flux x cross section area of canister perpendicular to flux). The highest quantity will be for horizontal flow. Flow through pillars unimportant for leaching. Either needs more explanation or should be deleted.

5. SUMMARY AND CONCLUSIONS

Thermally induced flows have been predicted to occur using a fully coupled thermal/flow finite-element program. It is assumed that flow in the host rock in the region of the repository can be modelled by Darcy's law with a bouyant term under fully saturated conditions.

Thermally induced flow does not cause significant advective heat transfer for expected values of rock mass permeabilities. In the future thermally induced flow analyses may be done with bouyant coupling only using temperature fields computed on the basis of conduction only if the gross thermal loading is not significantly increased. This will enhance analytical stability and output accuracy.

If regional flow is not present, natural convection cells will develop. There will be global cells which could conceivably transport contaminants to the surface. Figure 29 displays the calculated average vertical transport velocities above the repository assuming no cross-flow. The predicted travel times are in the range of 1,000 years depending on the rock mass permeability. Local cells may also develop which will have the effect of channelling the flow close to the waste cannisters.

The theoretical model indicates that in the absence of cross flow natural convection cells can be initiated with small temperature gradients. The concept of a critical gradient for flow initiation does not apply in this problem. If partially saturated conditions exist, these may inhibit thermal flows. The fully saturated case analysed here is thought to give higher velocities and hence conservative results for safety analyses.

The inflow period may last for many years, depending on the nature of flow around and into the repository. While inflow lasts, it is expected that the inflow velocities will be 2 to 3 orders of magnitude larger than the velocities caused by natural convection alone. Consequently, inflow would prevent thermally induced flows from moving upwards to the surface during the recharge period. Natural convection flows can, however, start once inflow is essentially complete.

It is expected that a regional groundwater gradient of $2 \cdot 10^{-3}$ will exist which will cause the convection flows to be swept almost horizontally, indicating that the most likely point of exit from the host rock is into a singular feature at depth and not up to the surface above the repository.

The quantity of groundwater flowing through the repository due to regional gradients is increased by the thermally induced flow effects. These flow quantities may affect leach rate predictions depending on whether it is determined by concentration in the water or by the diffusion rate in the glass matrix. The local thermally induced flows may tend to channel flow near the canisters, although this tendency may be somewhat reduced by the regional flow.

REFERENCES

1. Burgess, A.S., 1977. "GROUNDWATER MOVEMENTS AROUND A REPOSITORY Phase 2. Technical Report 3. Regional Groundwater Flow Analyses. Part I: Initial conditions". Submitted to KBS-Kärnbränslesäkerhet Stockholm, Sweden.
2. Burgess, A.S., 1977 "GROUNDWATER MOVEMENTS AROUND A REPOSITORY Phase 2. Technical Report 5, Repository Domain Groundwater Flow Analyses. Part II: Inflow to Repository". Submitted to KBS - Kärnbränslesäkerhet Stockholm, Sweden.
3. Burgess, A.S., 1977, "GROUNDWATER MOVEMENTS AROUND A REPOSITORY Phase 2. Technical Report 3. Regional Groundwater Flow Analyses. Part II: Long-Term Residual Conditions". Submitted to KBS-Kärnbränslesäkerhet Stockholm, Sweden.
4. Ratigan, J.L., 1977 "GROUNDWATER MOVEMENTS AROUND A REPOSITORY Phase 2. Technical Report 2. Thermal Analyses, Part I: Conduction Heat Transfer". Submitted to KBS-Kärnbränslesäkerhet Stockholm, Sweden.
5. Sorey, M.L., 1975, "Numerical Modelling of Liquid Geothermal Systems". United States Department of Interior Geological Survey, Report 75-613, Menlo Park, California.
6. Snow, D.T., "Rock Fracture Spanings, Openings, and Porosities" J. Soil Mechanics & Foundations Division, ASLE, SMI, January 1968. p 73-91.
7. Mercer, J.W. and Pinder, G.F., "Finite - Element Analysis of Hydrothermal Systems". Finite - Element methods in Flow Problems, University of Alabama Press, 1974, p.401-414.

A P P E N D I C E S

A.1 INTRODUCTION

This appendix describes FINI 520, a two-dimensional, planar and axis-symmetric, transient (or steady-state) finite element saturated thermally induced flow code developed at Acres Consulting Services Limited, Niagara Falls, Ontario, Canada, in 1977.

The available elements are an anisotropic isoparametric quadratic head/temperature triangle with 6 nodes (12 degrees of freedom) and a line loading element with 3 nodes (6 degrees of freedom).

Matrices and vectors are computed by numerical quadrature. Conductivity Material properties are principal values of anisotropic thermal and flow permeability and principal angles. bulk density and bulk specific heat, fluid density and fluid specific heat, thermal expansion coefficient and porosity.

The model starts from a specified set of initial conditions and proceeds stepwise through a number of solutions during the course of a transient run. Several iterations must be performed to get steady-state solutions.

Boundary conditions include specified head/temperature at nodes, nodal loads (fluid/heat source), element internal loads and surface loads. The surface loads are specified normal seepage velocity/heat flux and specified head/temperature outside a film. All specified values and loads are variable linearly over time spans of one to several time steps and may be started and stopped independently whenever desired.

Pore velocities are computed in a post-processor attached to the main program itself and plotting of meshes, isotherms, equipotentials and pore velocities is accomplished by a follow-up program, FINI 511, that accesses several of the disc files produced by the main code.

The program is divided into several overlay segments to minimize core storage requirements. Within each overlay the coding is broken into subroutines containing logical segments. In addition, extensive

A.2 FORMULATION AND DEVELOPMENT

The basic equations for porous thermally induced flow are the motion equation for fluid flow and the heat transport equation, as discussed separately below. Later in this section, they are combined to form the system matrix equations and boundary condition compatibility is described.

A.2.1 Groundwater Flow

The equation of motion for the liquid phase in a nonisothermal, single-component, groundwater flow system may be written as:

$$\frac{\partial}{\partial x_p} \left(\frac{\rho g k_{pq}}{\mu} \left(\frac{\partial P}{\partial x_q} + \rho g \delta_{q1} \right) \right) - \rho g \left(n \beta^P + \alpha^P \right) \frac{\partial P}{\partial t} - n \rho g \beta^T \frac{\partial T}{\partial t} + \rho g Q^\phi = 0 \quad (1)$$

where x = linear dimension,

ρ = fluid density,

g = gravitational constant,

k = intrinsic permeability tensor,

μ = dynamic viscosity,

P = pressure,

δ = Kronecker delta and direction 1 is upward,

n = porosity,

β^P = fluid compressibility,

α^P = matrix compressibility,

t = time,

β^T = fluid thermal expansion coefficient (negative),

T = temperature, and

Q^ϕ = volumetric rate of fluid source.

The equation of state of the fluid is

$$\rho = \rho_o + \rho_o \beta^T (T - T_o) + \rho_o \beta^P (P - P_o) \quad (2)$$

where the subscript o denotes evaluation at the reference state.

We use the Boussinesq approximation (7) in which properties are assumed at the reference condition (T_o, P_o) , except in the temperature buoyancy term, and neglect pressure buoyancy. Since time dependence in this problem may be relegated mainly to heat transport, the motion equation may be considered quasi-steady. We get:

$$\frac{\partial}{\partial x_p} \left(K_{pq}^\phi \left(\frac{\partial P}{\rho g \partial x_q} + \delta_{q1} + \beta^T (T - T_o) \delta_{q1} \right) \right) + Q^\phi = 0 \quad (3)$$

where $K^\phi = \rho g \frac{k}{\mu}$ = hydraulic permeability tensor, and (4)

$$\phi = \frac{P}{\rho g} + z = \text{hydraulic potential or head.} \quad (5)$$

$$\left(\text{Note: } \frac{\partial \phi}{\partial x_q} = \frac{\partial P}{\rho g \partial x_q} + \delta_{q1} \right)$$

The final equation becomes:

$$K_{pq}^\phi \frac{\partial^2 \phi}{\partial x_p \partial x_q} + K_{pq}^\phi \beta^T \frac{\partial T}{\partial x_p} \delta_{q1} + Q^\phi = 0 \quad (6)$$

The seepage flux is defined by:

$$q_p^\phi = -K_{pq}^\phi \left(\frac{\partial \phi}{\partial x_q} + \beta^T (T - T_o) \delta_{q1} \right) \quad (7)$$

and the pore velocity by:

$$v_p = q_p^\phi / n \quad (8)$$

In sealed flow cases, T_o for neutral buoyancy cannot be determined a priori and must be calculated as the average temperature in the mesh. With substantial throughflow, T_o is fixed at the inflow supply temperature.

A.2.2 Heat Transport

The energy equation describing heat transport in a porous medium containing only a solid and one liquid phase is:

$$\frac{\partial}{\partial x_p} \left(K_{pq}^T \frac{\partial T}{\partial x_q} \right) - n \rho c_v \frac{\partial T}{\partial x_p} - \bar{\rho} \bar{c}_v \frac{\partial T}{\partial t} + Q^T = 0 \quad (9)$$

where $K^T = (nK_f^T + (1 - n)K_s^T)$ = thermal conductivity tensor with fluid and solid components,

c_v = fluid specific heat,

$\bar{\rho}$ = bulk density,

\bar{c}_v = bulk specific heat,

such that $\bar{\rho} \bar{c}_v = (n \rho_f c_{vf} + (1 - n) \rho_s c_{vs})$, and

$Q^T = (nQ_f^T + (1 - n)Q_s^T)$ = volumetric heat source

including $\rho c_v Q^{\phi} T_b$ for source of fluid at temperature T_b .

All properties are rigorously defined at reference conditions.

A.2.3 Galerkin Functionals

In the finite element discretization of the modeled region, the physical space is broken up into elements, in each of which the potential and temperature fields are described by a simple relationship:

$$\phi = \phi_i N_i, \quad T = T_i N_i \quad (10)$$

The ϕ_i and T_i are solution values at specified discretization points or nodes and the N_i are distribution functions associated with each node attached to the element.

The T_i are also assumed to vary linearly over time steps so that accounting for the time variation expands equation 10b into:

$$T = T_{i k}^k M_{i k} N_i \quad (11)$$

in which the M_k are time distribution functions associated with the old and new solutions spanning the time interval in question.

A weighted-residual method may be used with finite elements to formulate a set of linear algebraic equations representative of the modeled system. In this model, we use Galerkin weighting in which the residuals, multiplied by the distribution functions previously mentioned, are integrated over time and space and set equal to zero.

The form of the flow Galerkin pseudo-functional is:

$$\chi_\phi = \int_R \left(K_{pq}^\phi \frac{\partial^2 \phi}{\partial x_p \partial x_q} + K_{pq}^\phi \beta^T \frac{\partial T}{\partial X_p} \delta_{q1} + Q^\phi \right)^\dagger \phi \, dR \quad (12)$$

† The residual is not varied in the derivation of the matrix equations below.

Integration-by-parts and the divergence theorem yield a quadratic formulation:

$$\begin{aligned} \chi_\phi = \int_R \left(-K_{pq}^\phi \frac{\partial \phi^\dagger}{\partial x_p} \frac{\partial \phi}{\partial x_q} + \left(K_{pq}^\phi \beta^T \frac{\partial T}{\partial x_p} \delta_{q1} + Q^\phi \right) \phi \right) dR \\ + \int_S \left(K_{pq}^\phi \frac{\partial \phi^\dagger}{\partial x_p} i_q \right) \phi \, dS \end{aligned} \quad (13)$$

where the second integral is a boundary flux term used to express natural boundary conditions (impermeable) or imposed seepage fluxes and specified head outside a film. i_q is the outward-facing normal to the surface S . This term is omitted for impermeable boundaries or those with fixed potential and is replaced for other boundaries by:

$$\int_S \left(q^\phi - \alpha^\phi (\phi - \phi_a) \right)^\dagger \phi \, dS \quad (14)$$

where the imposed seepage flux q^ϕ is positive for fluid inflow. α^ϕ is the film transfer coefficient and ϕ_a is the ambient potential outside the film. The impermeable condition implies that the boundary is a streamline.

The energy Galerkin pseudo-functional is:

$$\chi_T = \int_R \left(K_{pq}^T \frac{\partial^2 T}{\partial x_p \partial x_q} - n \rho c_v v_q \frac{\partial T}{\partial x_q} - \bar{\rho} \bar{c}_v \frac{\partial T}{\partial t} + Q^T \right)^\dagger T \, dR \quad (15)$$

Integrating-by-parts and using the divergence theorem we get:

$$\begin{aligned} \chi_T = \int_R \left(-K_{pq}^T \frac{\partial T^\dagger}{\partial x_p} \frac{\partial T}{\partial x_q} + n \rho c_v v_q T^\dagger \frac{\partial T}{\partial x_q} - \bar{\rho} \bar{c}_v \frac{\partial T^\dagger}{\partial t} T + Q^T T \right) dR \\ + \int_S \left(K_{pq}^T \frac{\partial T}{\partial x_p} - n \rho c_v v_q T \right)^\dagger i_q T \, dS \quad (16) \end{aligned}$$

Surface integrals drop out if surface throughflow is zero or if T is specified on the boundary. Thermal load boundaries may exist in which the first surface integral term is replaced by:

$$\int_S \left(q^T - \alpha^T (T - T_a) \right)^\dagger T \, dS \quad (17)$$

analogous to the fluid case.

In cases of fluid inflow with specified temperature T_b , the second term should be replaced by:

$$\int_S \left(-n \rho c_v v_q T_b i_q \right)^\dagger T \, dS \quad (18)$$

to account for the heat brought in by the forced inflow of fluid.

The boundary conditions on potential/fluid flow and temperature/heat flux are only compatible in certain combinations. In general, if there is fluid throughflow, the temperature at the boundary must be specified. Otherwise, any temperature boundary condition is permitted.

Seepage fluxes and pore velocities are by equation (7) a function of the choice of T_0 , the nonbuoyant reference temperature. A bad choice of T_0 can produce velocities that are totally unrealistic.

A good choice of T_0 is the boundary temperature if it is known. If it is not known, or highly variable over the boundary, it may not be possible to maintain the impervious nature of boundaries in the model run and the results may be invalidated. The model permits the use of a specified single value for T_0 or for the use of the average temperature in the modeled region, calculated in the program automatically. More involved determinations of T_0 may be required, e.g. when the neutral buoyancy temperature is a function of position in the mesh, and this must be added in special subroutines created for that purpose.

A.2.4 Matrix Equation

When the first variations of these pseudo-functionals are taken as:

$$\partial \chi_\phi / \partial \phi_i = 0, \quad \partial \chi_T / \partial T_i = 0 \quad (19)$$

The following matrix equations result at time ℓ , where Δt = time step length:

(a) for fixed α^ϕ and α^T :

$$\begin{aligned} & \left(\frac{2}{3} \begin{pmatrix} \bar{K}^T & + & \bar{\alpha}^T & & 0 \\ & 0 & & \bar{K}^\phi & + & \bar{\alpha}^\phi \end{pmatrix} + \frac{1}{\Delta t} \begin{pmatrix} \bar{C}^T & 0 \\ 0 & 0 \end{pmatrix} \right) \begin{pmatrix} T_j \\ \phi_j \end{pmatrix}^\ell = \\ & \left(-\frac{1}{3} \begin{pmatrix} \bar{K}^T & + & \bar{\alpha}^T & & 0 \\ & 0 & & \bar{K}^\phi & + & \bar{\alpha}^\phi \end{pmatrix} + \frac{1}{\Delta t} \begin{pmatrix} \bar{C}^T & 0 \\ 0 & 0 \end{pmatrix} \right) \begin{pmatrix} T_j \\ \phi_j \end{pmatrix}^{\ell-1} \\ & + \frac{1}{3} \begin{pmatrix} \bar{Q}^T & + & \bar{q}^T & + & \bar{\alpha}^T T_a \\ \bar{Q}^\phi & + & \bar{q}^\phi & + & \bar{\alpha}^\phi \phi_a \end{pmatrix}^{\ell-1} + \frac{2}{3} \begin{pmatrix} \bar{Q}^T & + & \bar{q}^T & + & \bar{\alpha}^T T_a \\ \bar{Q}^\phi & + & \bar{q}^\phi & + & \bar{\alpha}^\phi \phi_a \end{pmatrix}^\ell \\ & \begin{pmatrix} nTv & \bar{V} \\ q & q \\ K & \frac{\partial T}{\partial x} \\ p & \beta T \\ \beta & \beta \end{pmatrix}^{\ell-1} \end{aligned} \quad (20a)$$

(b) for variable α^T and α^ϕ :

delete $\bar{\alpha}^T$ and $\bar{\alpha}^\phi$ on L.H.S. and
 replace $\bar{\alpha}^T$ and $\bar{\alpha}^\phi$ on R.H.S. by $3\bar{\alpha}^T$ and $3\bar{\alpha}^\phi$. (20b)

(c) for steady-state solutions:

$$\begin{pmatrix} \bar{K}^T + \bar{\alpha}^T & 0 \\ 0 & \bar{K}^\phi + \bar{\alpha}^\phi \end{pmatrix} \begin{pmatrix} T_j \\ \phi_j \end{pmatrix}^\ell =$$

$$\begin{pmatrix} \bar{Q}^T + \bar{q}^T + \bar{\alpha}^T T_a \\ \bar{Q}^\phi + \bar{q}^\phi + \bar{\alpha}^\phi \phi_a \end{pmatrix}^\ell + \begin{pmatrix} nT v_q \bar{V}_q \\ K_{p1}^\phi \frac{\partial T}{\partial x_p} \beta^T \bar{\beta} \end{pmatrix}^{\ell-1}$$
(20c)

where ℓ denotes the ℓ th iteration for steady-state runs. At least three iterations must be performed for steady-state runs in order to load the buoyancy and advection terms.

The buoyancy and advection terms are written out fully above to indicate that T , v_q and $\partial T / \partial x_p$ must be evaluated for each element from the old solution before these terms are added into the load vector. All other loads are specified and not solution dependent. This solution dependence of advection and buoyancy requires the use of an iterative process in solution of steady-state cases, but for transient problems, the nonlinearity can be assimilated into the normal time-stepping solution procedure.

The component matrices are:

$$\bar{K} = \sum_e \int_e K_{pq} N_{j,x_p} N_{i,x_q} dR, \text{ where } \sum \text{ is a sum over elements,}$$

$$\bar{\alpha} = \sum_e \int_e \alpha N_j N_i dS, \text{ where } S \text{ is the external boundary,}$$

$$\bar{\alpha} = \sum_e \int_e \alpha N_i dS,$$

$$\begin{aligned} \bar{C} &= \sum_e \int_e \bar{\rho} \bar{c}_v N_j N_i dR \quad , \\ \bar{Q} &= \sum_e \int_e Q N_i dR + Q_i \quad , \text{ where } Q_i \text{ is a nodal load,} \\ \bar{q} &= \sum_e \int_e q N_i dS \quad , \\ \bar{V}_m &= \sum_e \int_e \rho c_v N_{i,x_m} dR \quad , \text{ and} \\ \bar{\beta} &= \sum_e \int_e N_i dR \quad . \end{aligned}$$

These matrices are presented for the general case. In 2-dimensional planar geometry (dR) is ($dx dy$). For axisymmetry, replace (dR) by ($2\pi r dz dr$), (dS) by ($2\pi r dS$) and (Q_i) by ($2\pi r Q_i$).

A.2.5 Units

The program is written in dimensionless form so that any compatible set of units for the input data will be acceptable.

As an example consider the following: In metric units, the desirable units of length and time may be the metre and second respectively. The values of K^T , $\bar{\rho}$ and \bar{c}_v (ρ and c_v , as well) must be given in the input data so that the thermal diffusivity $K^T / \bar{\rho} \bar{c}_v$ has units of (m^2/sec). K^T in ($W/m^{\circ}C$), $\bar{\rho}$ in (kg/m^3) and \bar{c}_v in ($W \text{ sec}/kg^{\circ}C$) will achieve this and are compatible. It is important to note that the nodal locations must be given in the length unit desired, (m) in this example. Also, thermal loading units must be compatible: volumetric heat generation Q^T in (W/m^3), boundary heat flux q^T in (W/m^2), thermal convection coefficient α^T in ($W/m^2 \text{ }^{\circ}C$), ambient temperature T_a in ($^{\circ}C$) and nodal load Q_i^T in (W). For flow parameters, K^{ϕ} is in (m/sec), n is dimensionless and β^T is in ($^{\circ}C^{-1}$). The constituent units for K^{ϕ} are k in (m^2), μ in ($kg/m \text{ sec}$), ρ in (kg/m^3) and g in (m/sec^2). The loading units are: volumetric source Q^{ϕ} in (sec^{-1} , actually $m^3/m^3 \text{ sec}$), boundary normal seepage flux q^T in (m/sec), film coefficient α^{ϕ} in (sec^{-1}), film external potential ϕ_a in (m) and nodal source Q_i^{ϕ} in (m^3/sec).

use is made of disc storage and all data passed from overlay to overlay is written to disc and reread in the newly loaded overlay. This not only minimizes storage but facilitates restarts during long runs or multiple runs and simplifies debugging.

APPENDIX B
Model Validation

B.1 Thermal validation

Validation of the model for heat transport was carried out with an analytical solution to a 1-dimensional problem. The initial conditions are zero temperature everywhere in the positive x region at time $t = 0$ and the boundary conditions are $T(0) = 1$ and $T(\infty) = 0$ for $t > 0$. The analytical solution is:

$$T = \frac{1}{2} \left[\operatorname{erfc} \left(\frac{x - vt}{(4Kt)^{\frac{1}{2}}} \right) + \exp \left(\frac{xv}{K} \right) \operatorname{erfc} \left(\frac{x + vt}{(4Kt)^{\frac{1}{2}}} \right) \right]$$

where v is the velocity and K is the thermal conductivity. The problem was solved for $v = 5$, $K = 1$, $0 \leq x \leq 1$, and with 25 time steps of 0.002 to 0.05. The boundary condition $T(1) = 0$ was an approximation of $T(\infty) = 0$ so the solution is reported here to $x = 0.5$. Table B.1 gives the analytical and model results for various x values at $t = 0.05$. The agreement is excellent.

Table B.1 Thermal validation results

<u>x</u>	<u>T analytical</u>	<u>T model</u>
0	1.0	1.0
0.05	0.9565	0.9532
0.10	0.9037	0.9052
0.15	0.8422	0.8380
0.20	0.7732	0.7747
0.25	0.6988	0.6931
0.30	0.6212	0.6211
0.35	0.5422	0.5347
0.40	0.4646	0.4631
0.45	0.3912	0.3823
0.50	0.3228	0.3191

This problem is strongly advective and adequately tests thermal capacity, conductivity and advection terms, all the transport terms in the heat transfer equation.

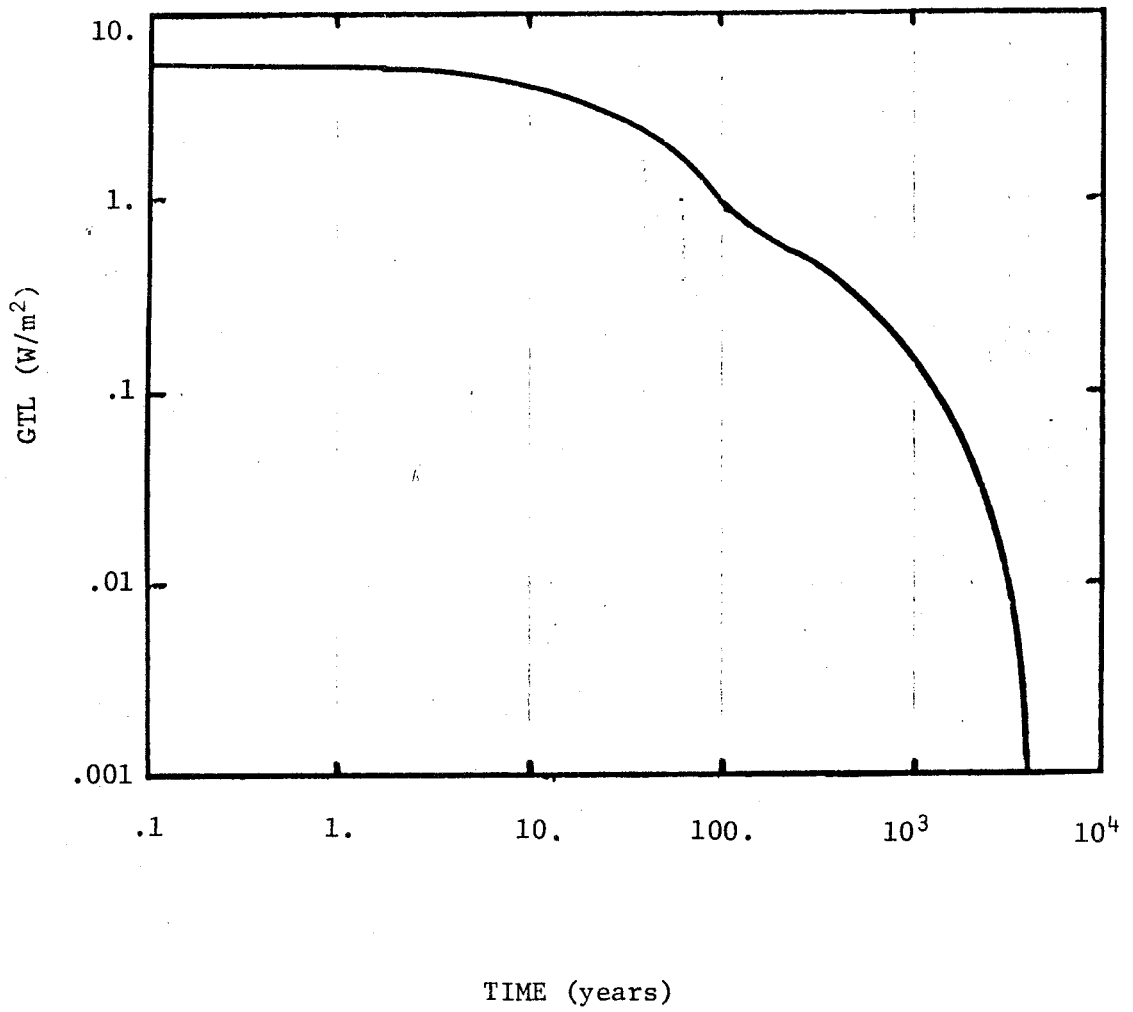
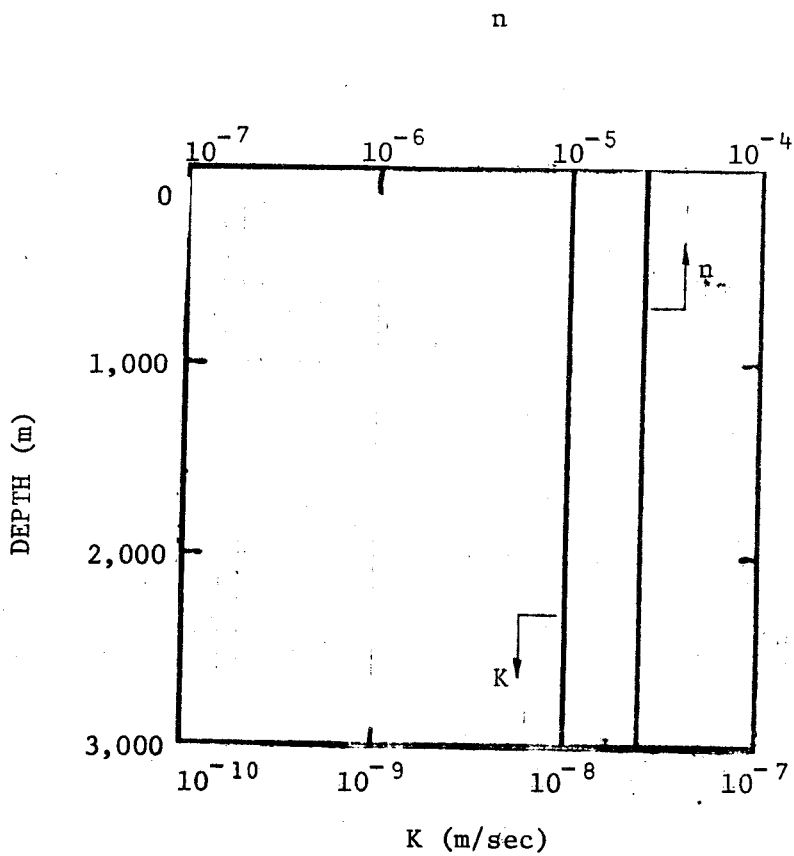
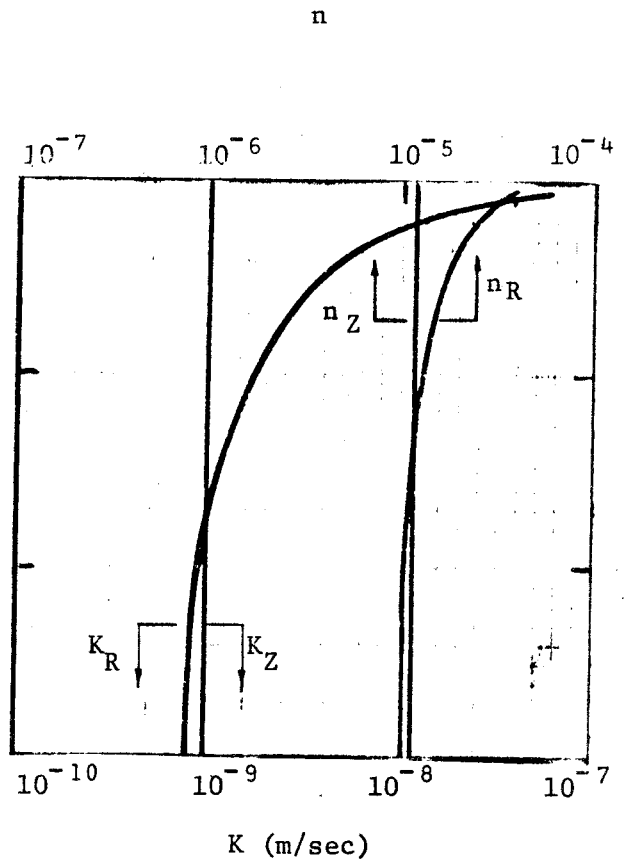


Figure 1 - Decay of GTL for 40 year old HLW



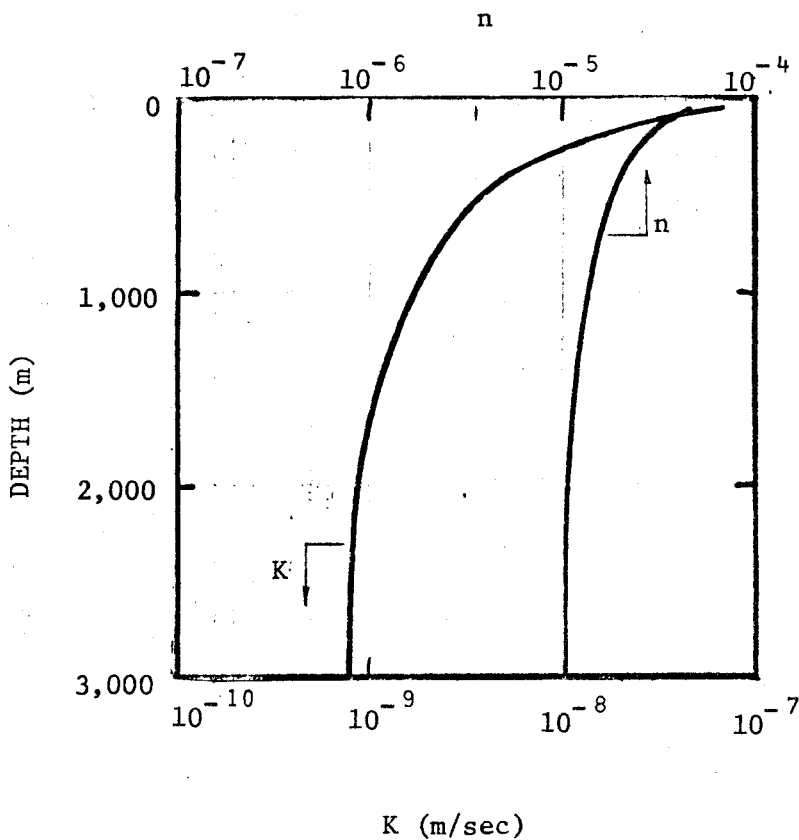
Case 1: K homogeneous, isotropic



Anisotropic, non-homogeneous

Case 3: $K_R(Z)$, K_Z uniform

R = horizontal
 Z = vertical
 S = Fracture spacing = 1.8 m



Case 2: K(Z)

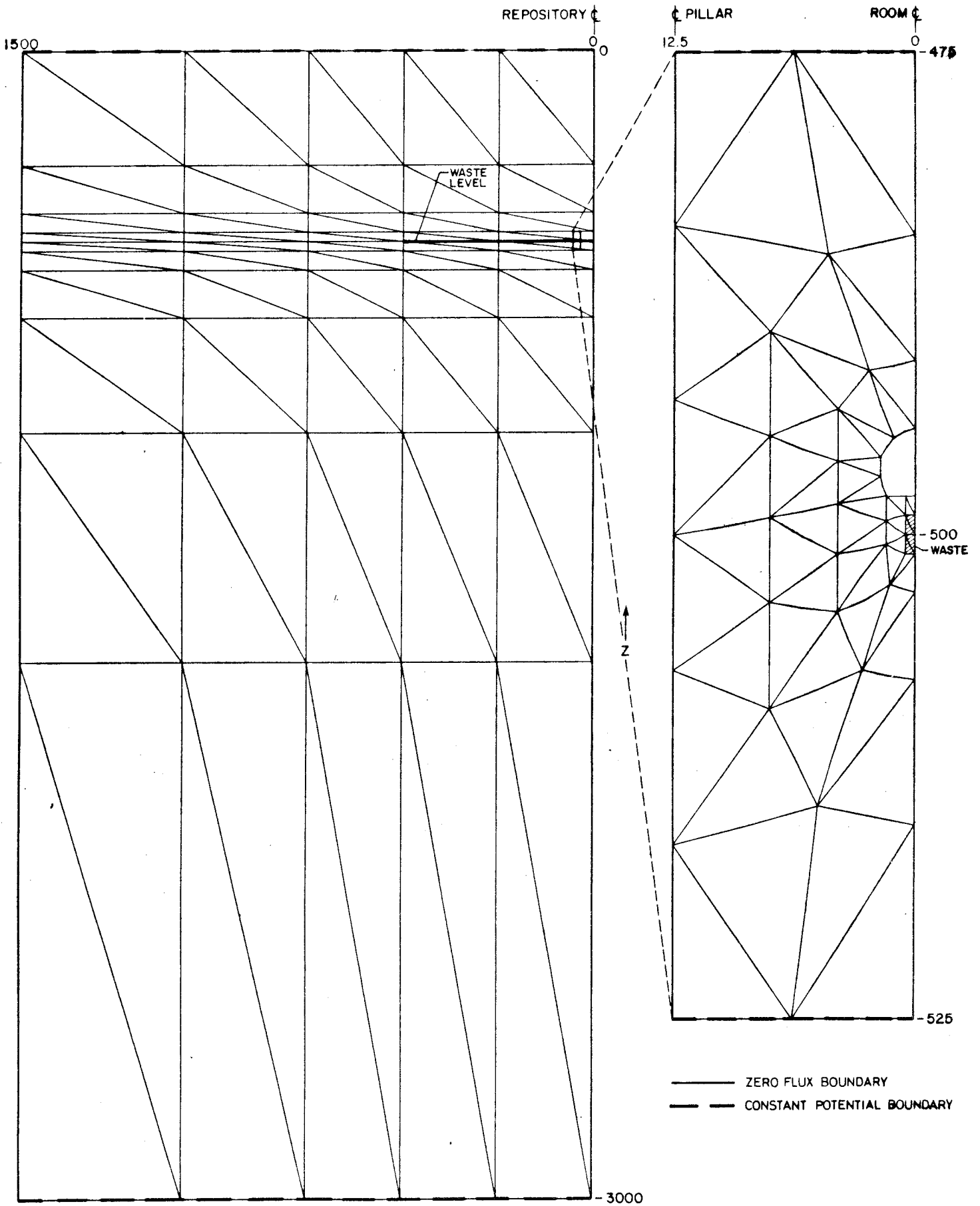
Isotropic, non-homogeneous

FIGURE 2: Distributions of Permeability (K) and Porosity (n) with depth (Z)

Figure 3 :Material Properties

Property	Symbol	Units	Host rock	Backfill
Thermal				
Thermal Conductivity (bulk)	K^T	W/m ^{°C}	2.05	1.5
Density - water	ρ	kg/m ³	1,000	1,000
- bulk	$\bar{\rho}$		2,800	2,070
Specific Heat - water	c_v	J /kg,°C	4,180	4,180
- bulk	\bar{c}_v		735	936
Flow				
Permeability	K	m/s	*	10 ⁻¹⁰
Porosity	n	—	*	0.37
Volumetric Expansion coefficient of water at 20°C	$-\beta^T$	°C ⁻¹	-2.07 x 10 ⁻⁴	-2.07 x 10 ⁻⁴

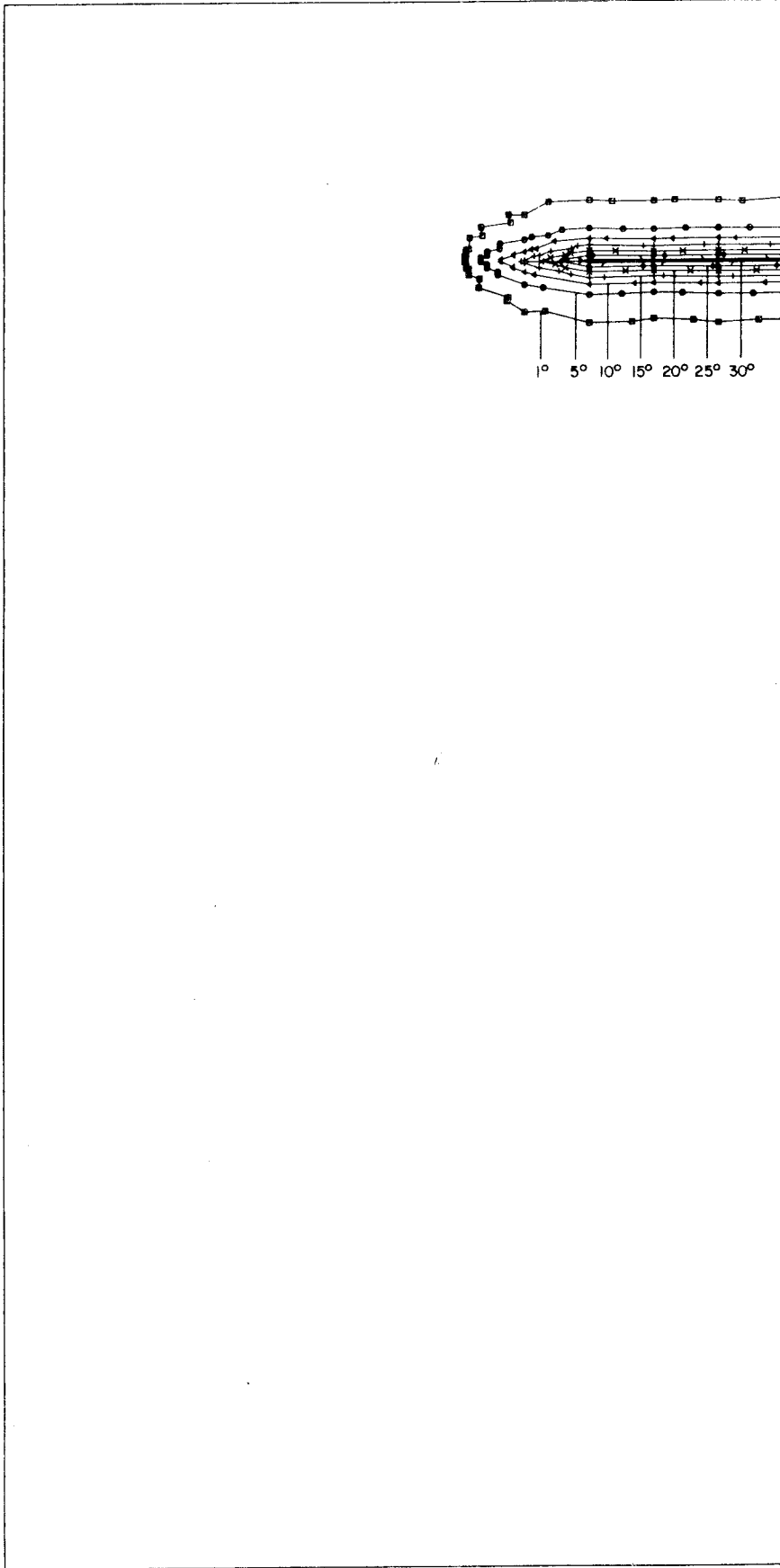
* Varies See Section 2.2 of this report.



(a) REPOSITORY DOMAIN HALF MESH

(b) LOCAL HALF MESH

FIGURE 4. FINITE ELEMENT MODELS FOR FLOW ANALYSES

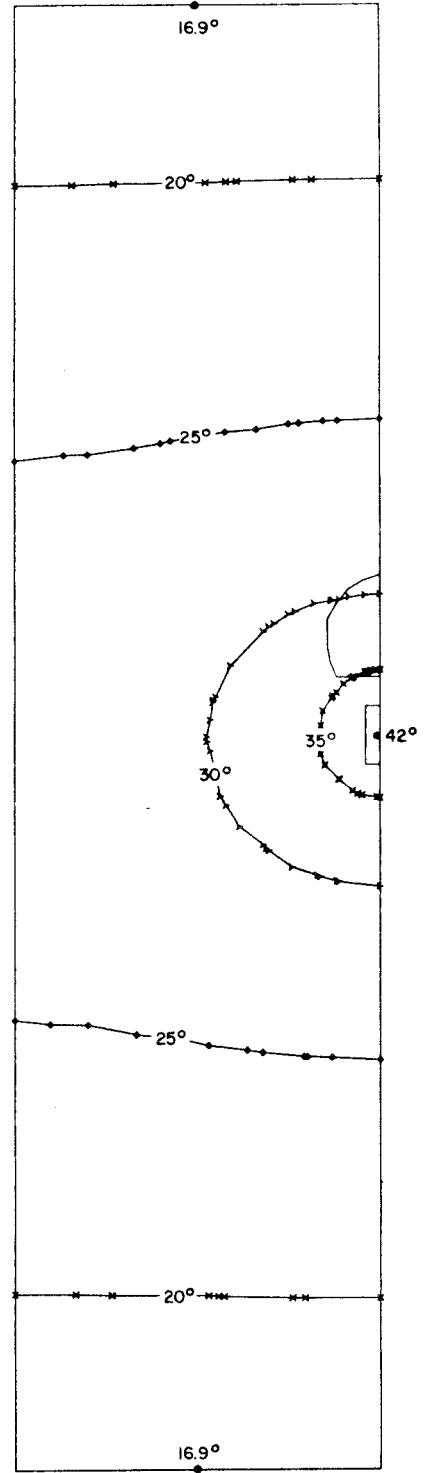


KBS HYDROTHERMAL RUN GLOBAL I
CONDUCTION BASELINE

CONTOUR PLOT

GEOMETRY SCALE 0 500 M

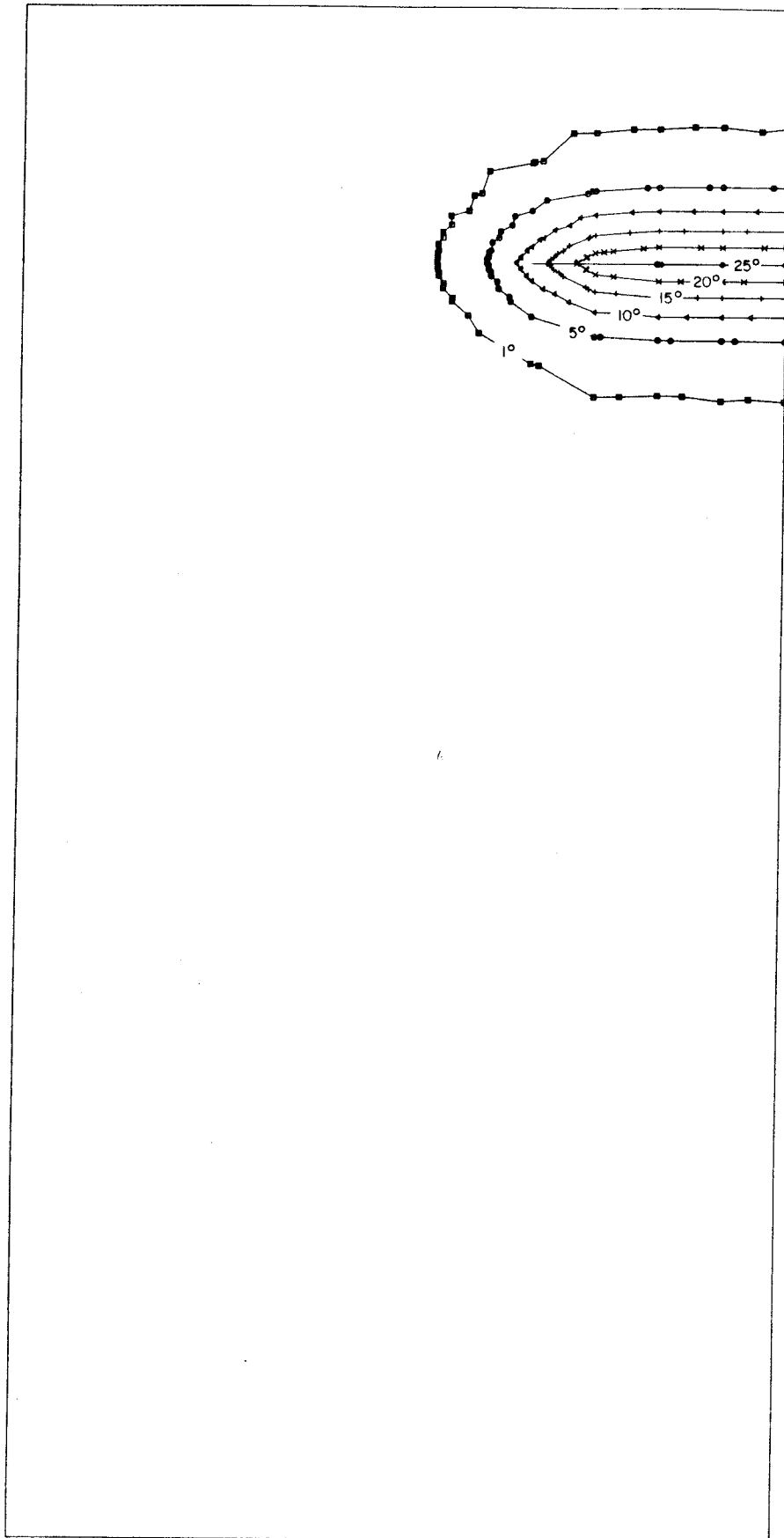
TEMPERATURE CONTOURS IN DEGREES CELSIUS
40 YEARS



LOCAL I

0 5 10 M

FIGURE 5

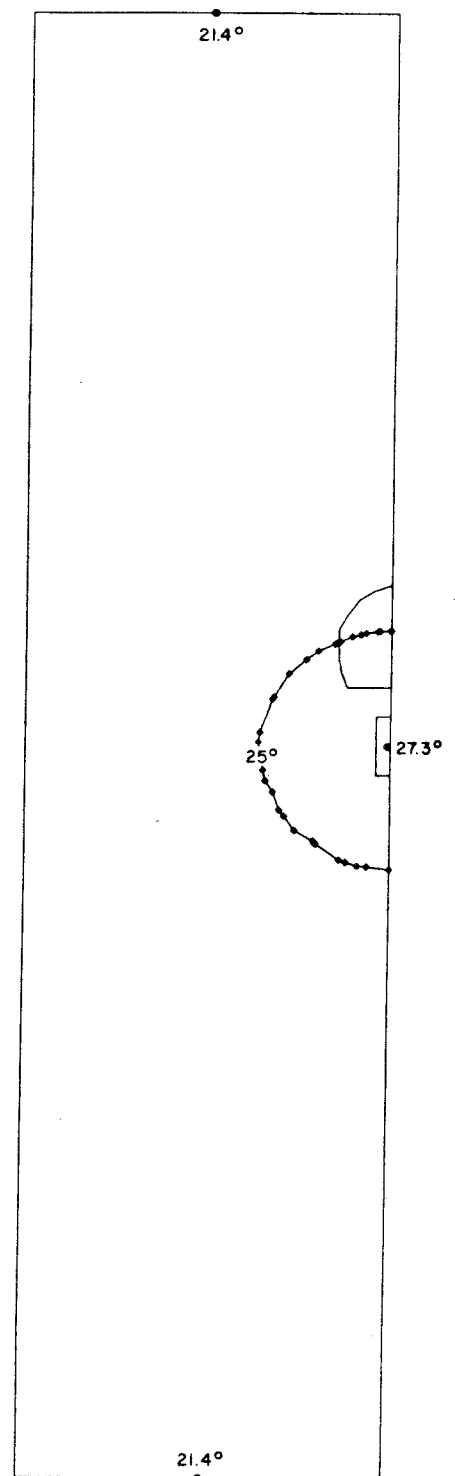


KBS HYDROTHERMAL RUN GLOBAL I
CONDUCTION BASELINE

CONTOUR PLOT

GEOMETRY SCALE 0 500 M

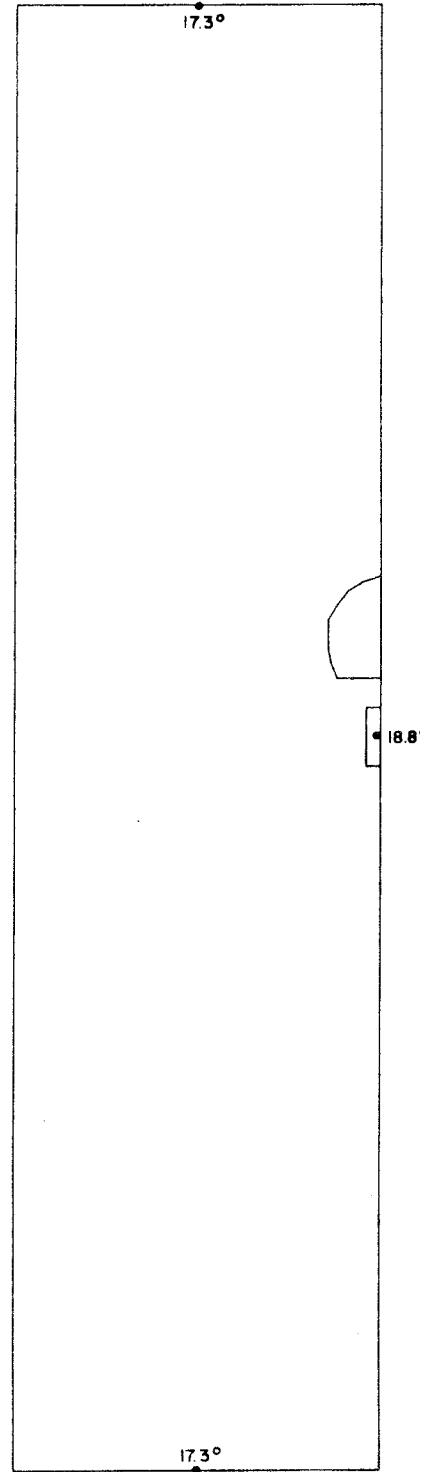
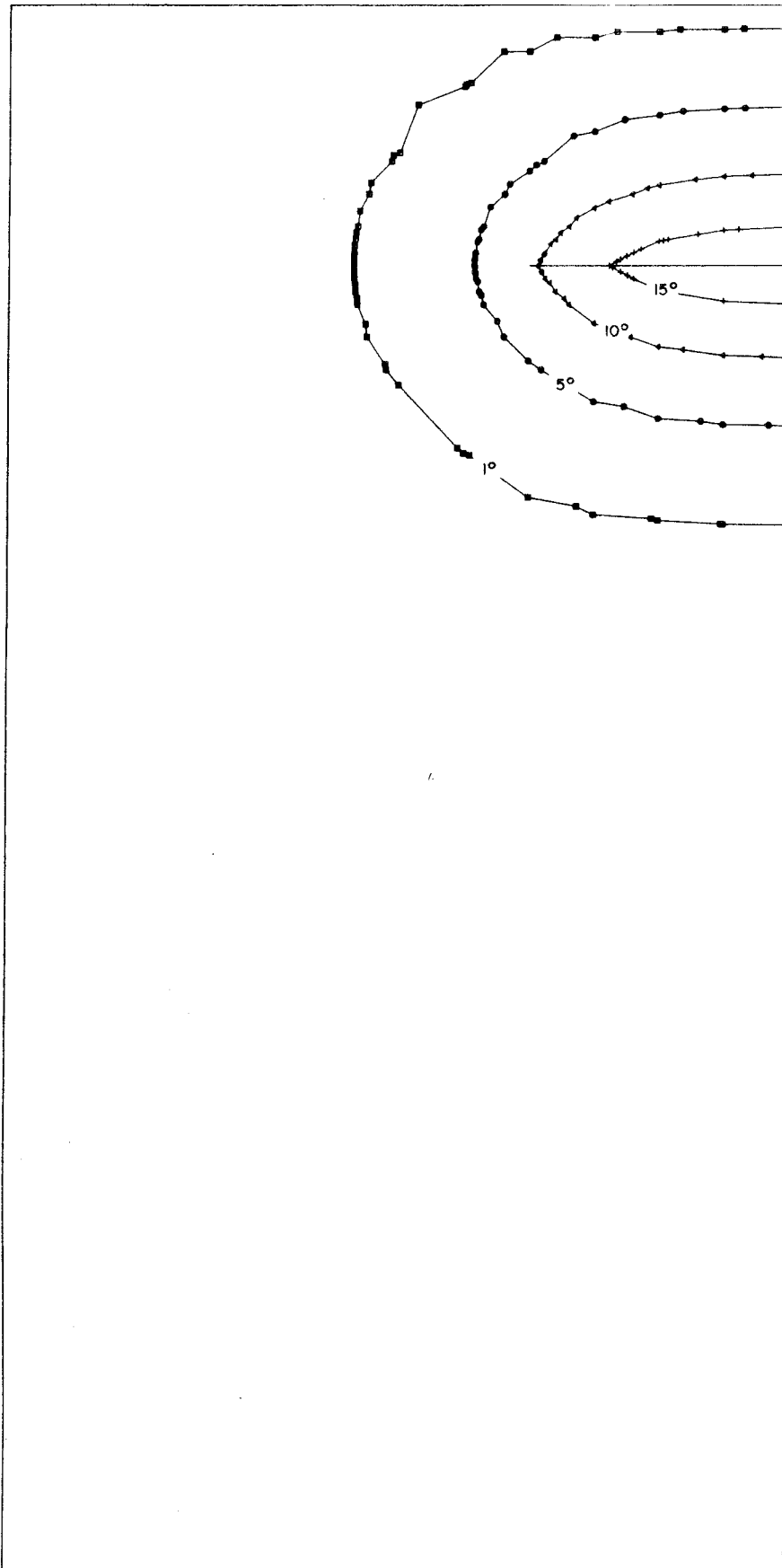
TEMPERATURE CONTOURS IN DEGREES CELSIUS
200 YEARS



LOCAL I

0 5 10 M

FIGURE 6



KBS HYDROTHERMAL RUN GLOBAL I
CONDUCTION BASELINE

LOCAL I

CONTOUR PLOT

GEOMETRY SCALE 0 500 M

0 5 10 M

TEMPERATURE CONTOURS IN DEGREES CELSIUS
1000 YEARS

FIGURE 7

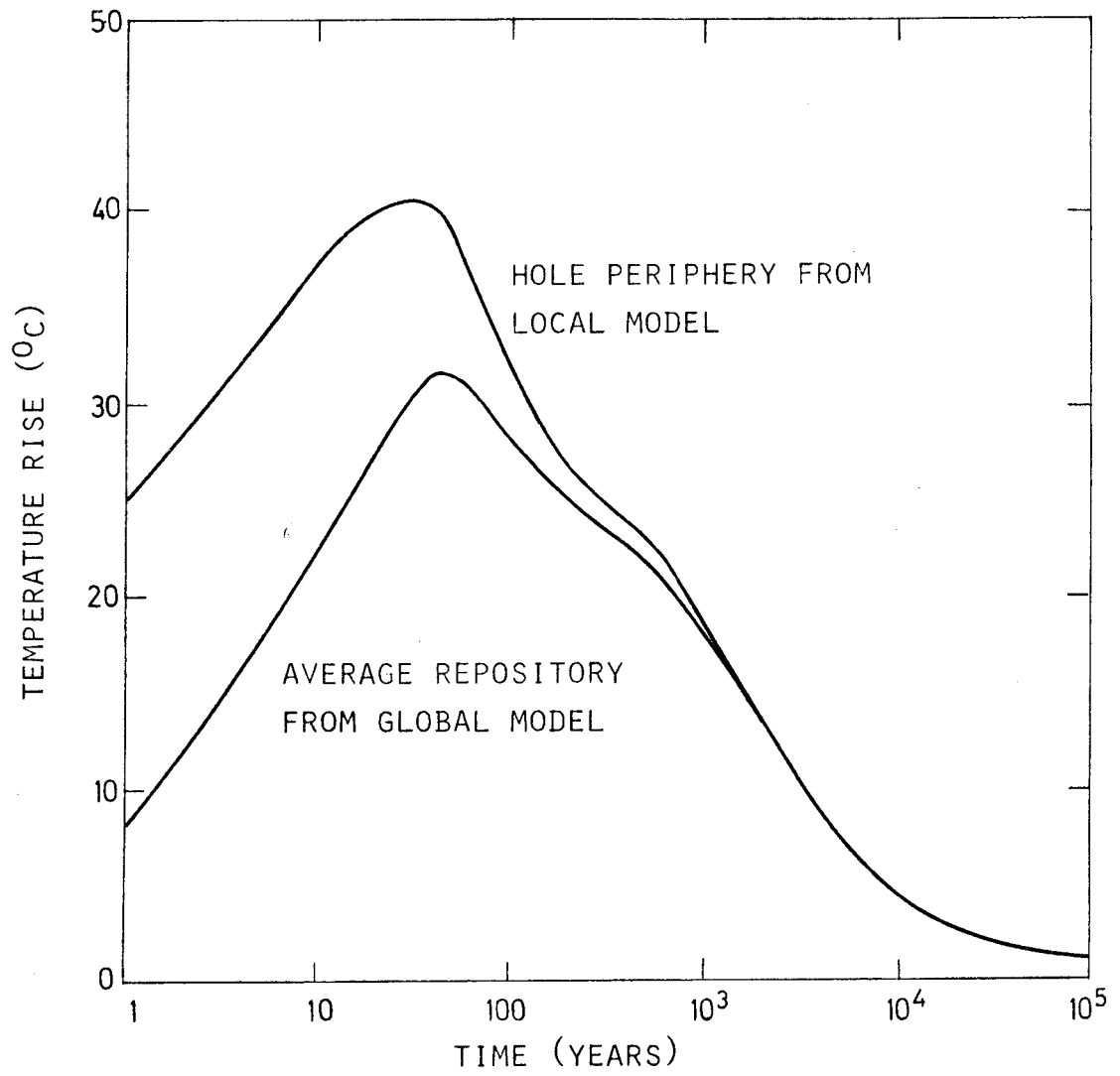
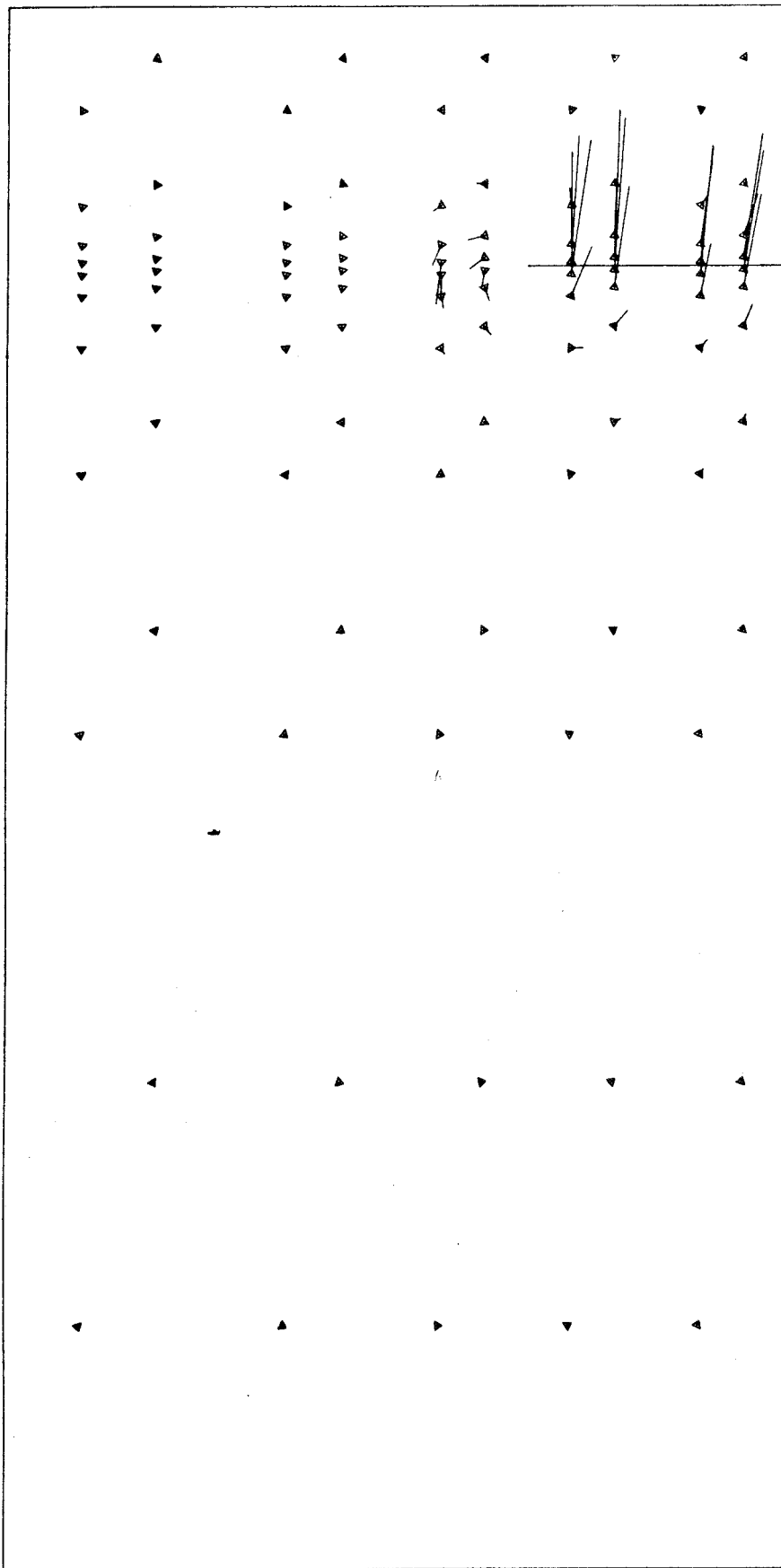


FIGURE 8. CONDUCTION TEMPERATURE HISTORY IN GLOBAL AND LOCAL MODELS

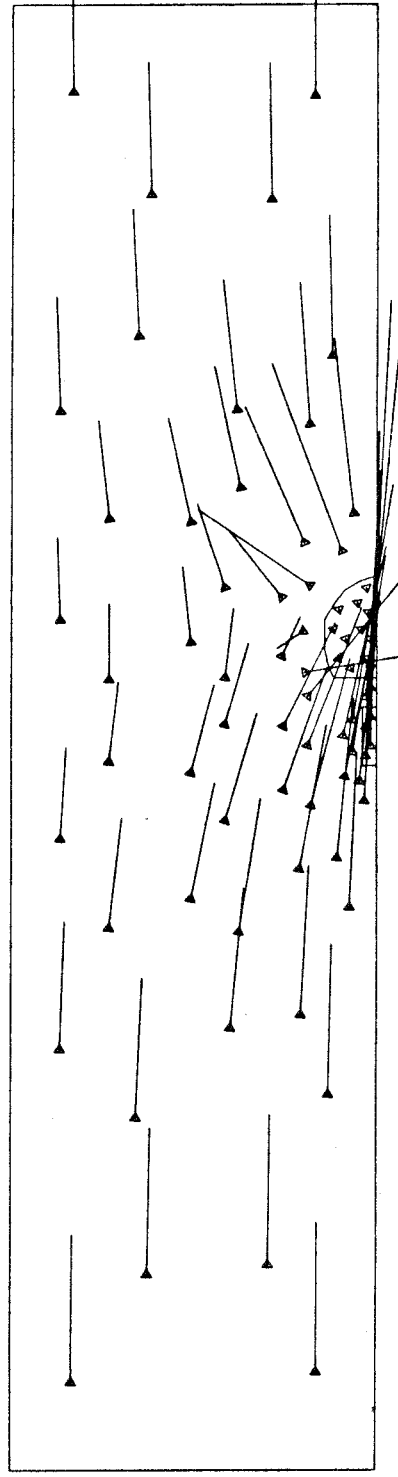


KBS HYDROTHERMAL RUN GLOBAL 2
 K HOMOGENEOUS ISOTROPIC

VELOCITY PLOT

GEOMETRY SCALE 0 500 M
 VELOCITY SCALE $\rightarrow = 0.4 * 10^{**} - 6$ M/SEC

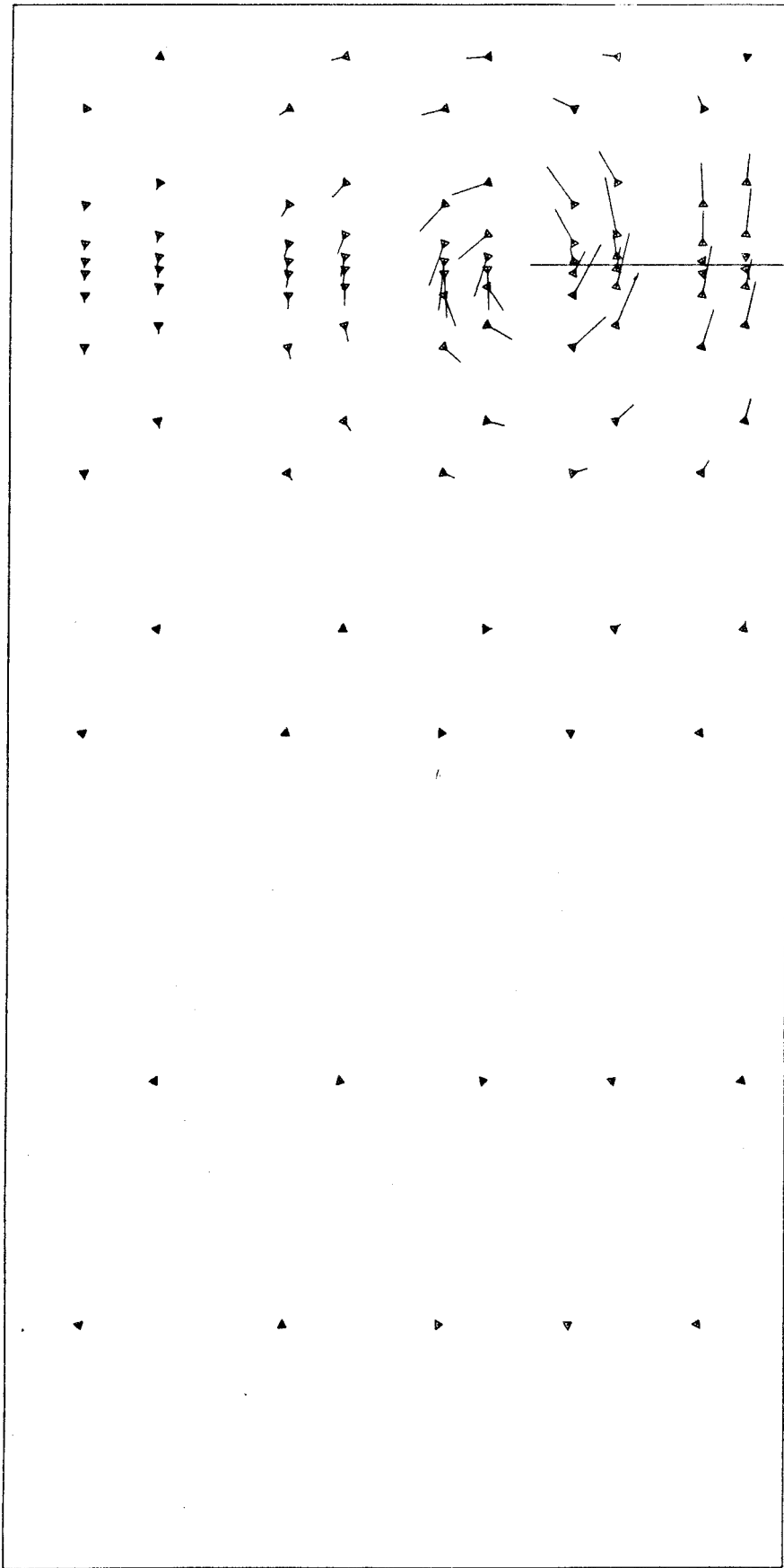
40 YEARS



LOCAL 2

0 5 10 M

FIGURE 9

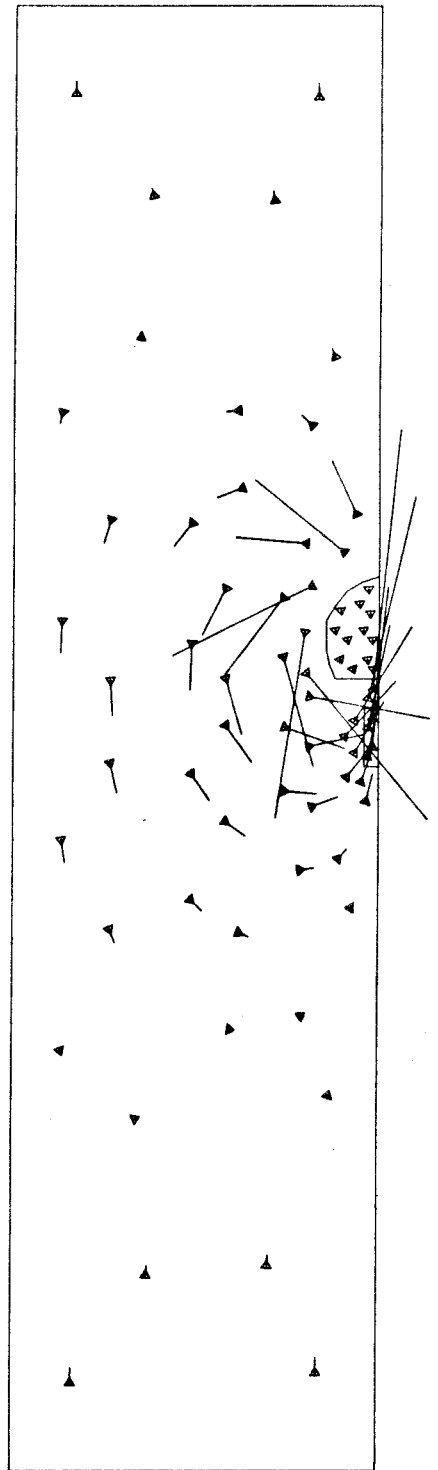


KBS HYDROTHERMAL RUN GLOBAL 2
 K HOMOGENEOUS ISOTROPIC

VELOCITY PLOT

GEOMETRY SCALE $\overline{\hspace{1.5cm}}$ 0 500 M
 VELOCITY SCALE $\overline{\hspace{1.5cm}}$ = 0.4 * 10 ** -6 M/SEC

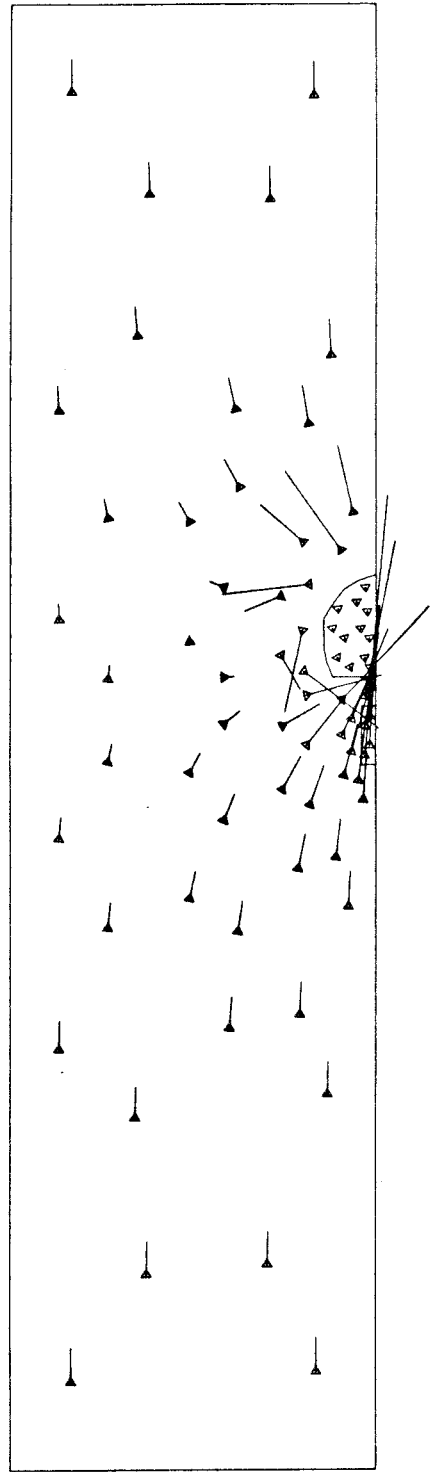
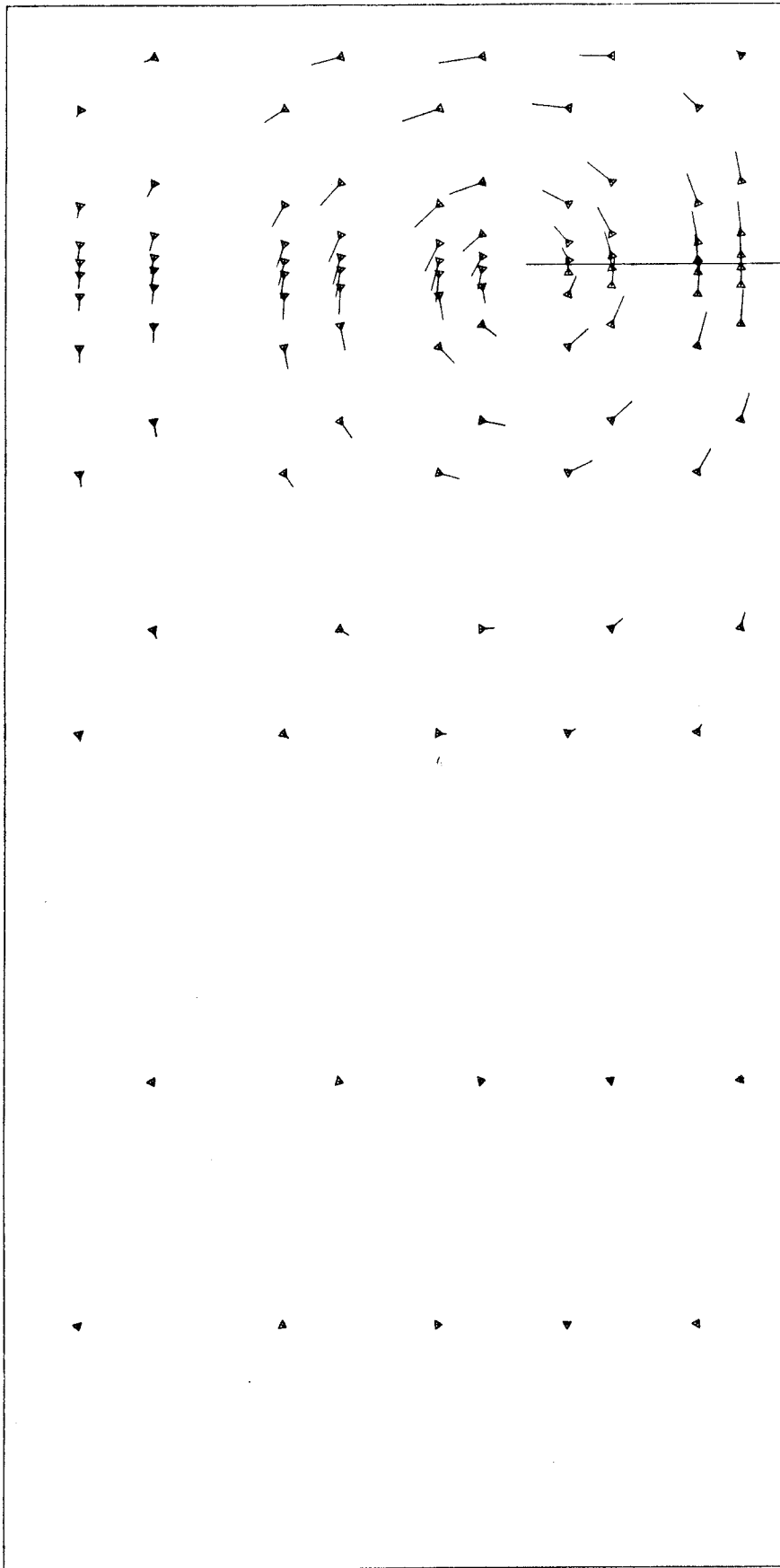
200 YEARS



LOCAL 2

0 5 10 M

FIGURE 10



KBS HYDROTHERMAL RUN GLOBAL 2
K HOMOGENEOUS ISOTROPIC

VELOCITY PLOT

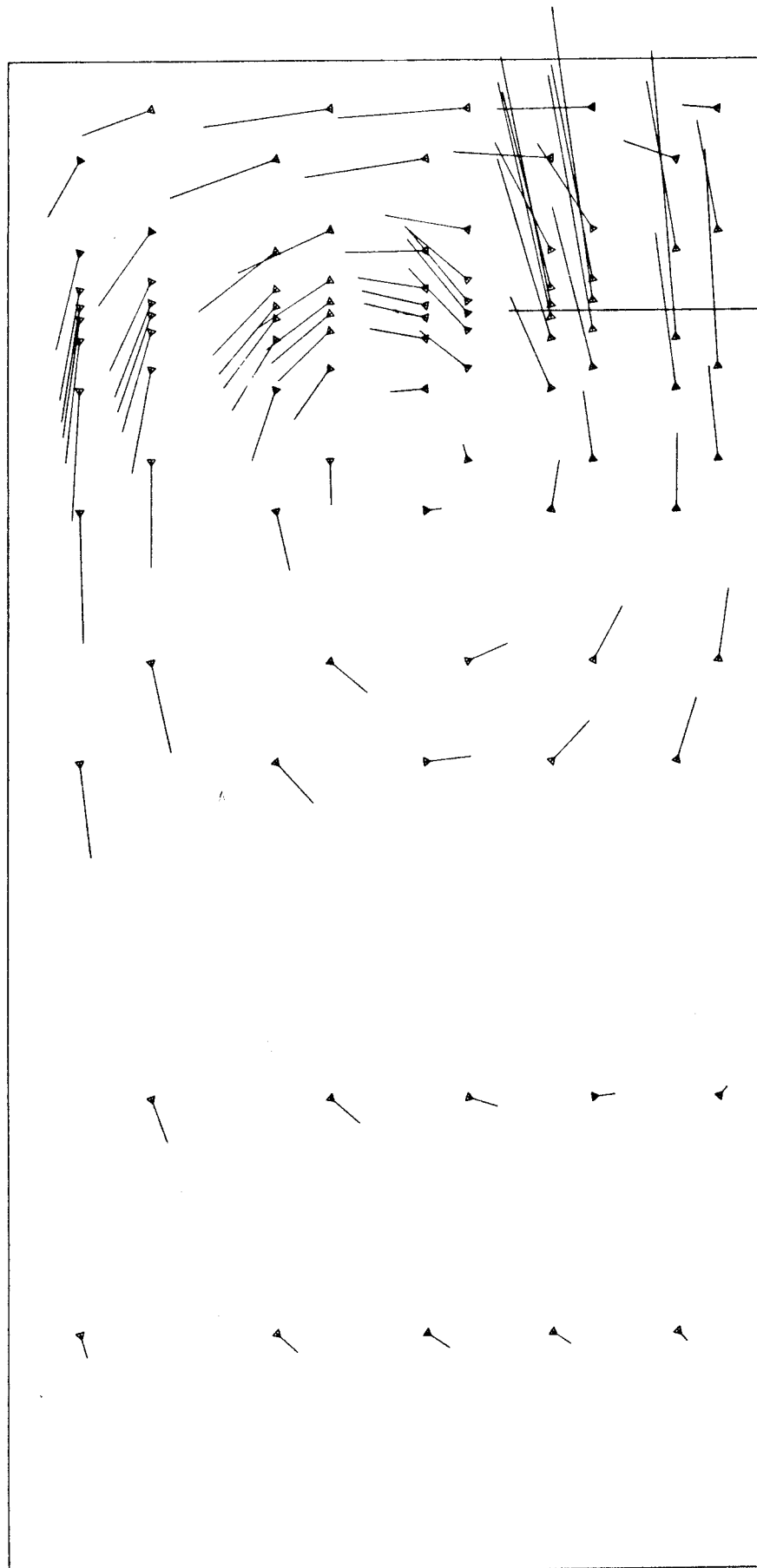
GEOMETRY SCALE 0 500 M
VELOCITY SCALE $\rightarrow = 0.4 * 10^{-6}$ M/SEC

1000 YEARS

LOCAL 2

0 5 10 M

FIGURE 11

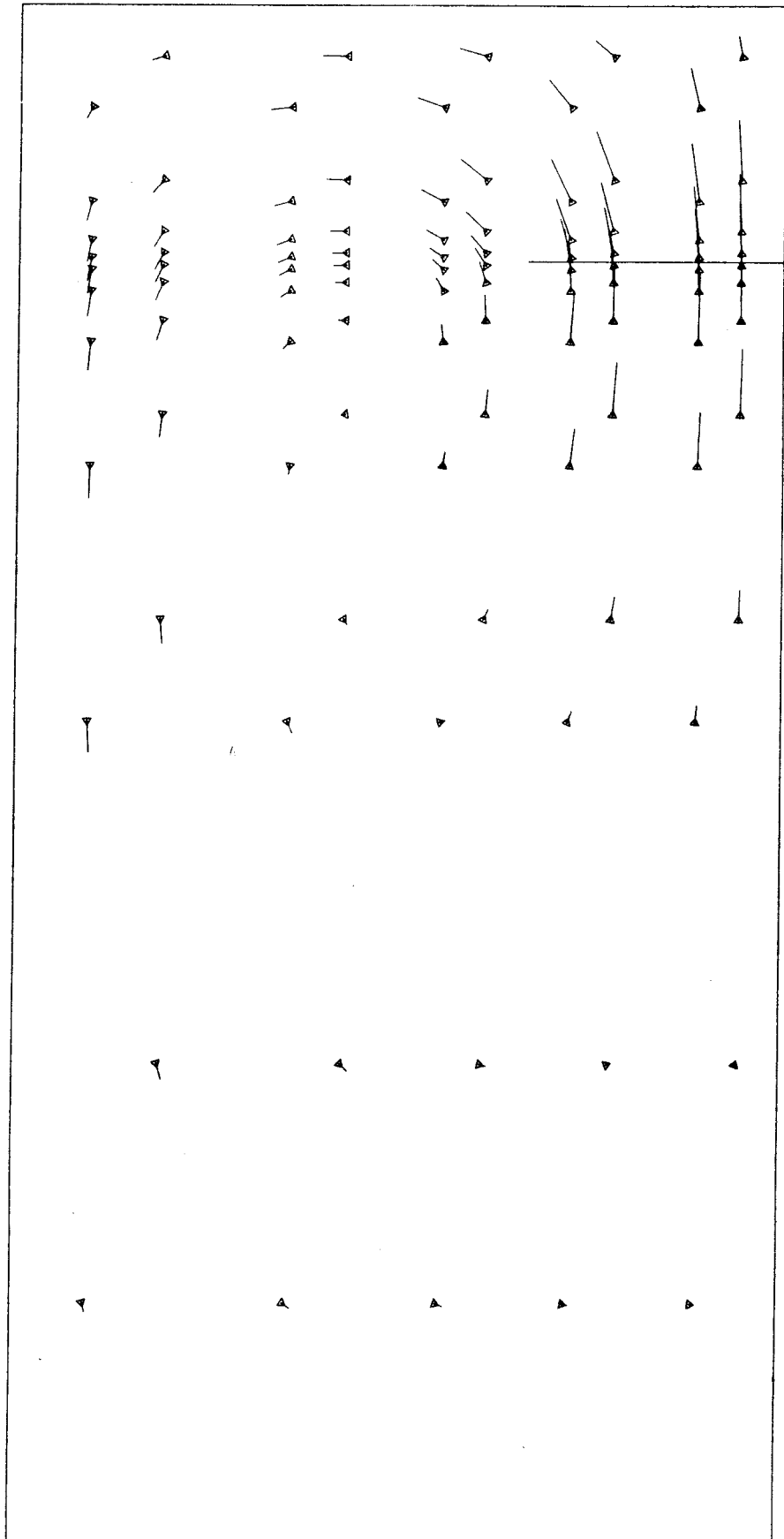


KBS HYDROTHERMAL RUN GLOBAL 2
K HOMOGENEOUS ISOTROPIC

VELOCITY PLOT

GEOMETRY SCALE $\overline{\hspace{1.5cm}}$ 0 500 M
VELOCITY SCALE $\overline{\hspace{1.5cm}}$ = 0.4 * 10 ** - 7 M/SEC

10 000 YEARS

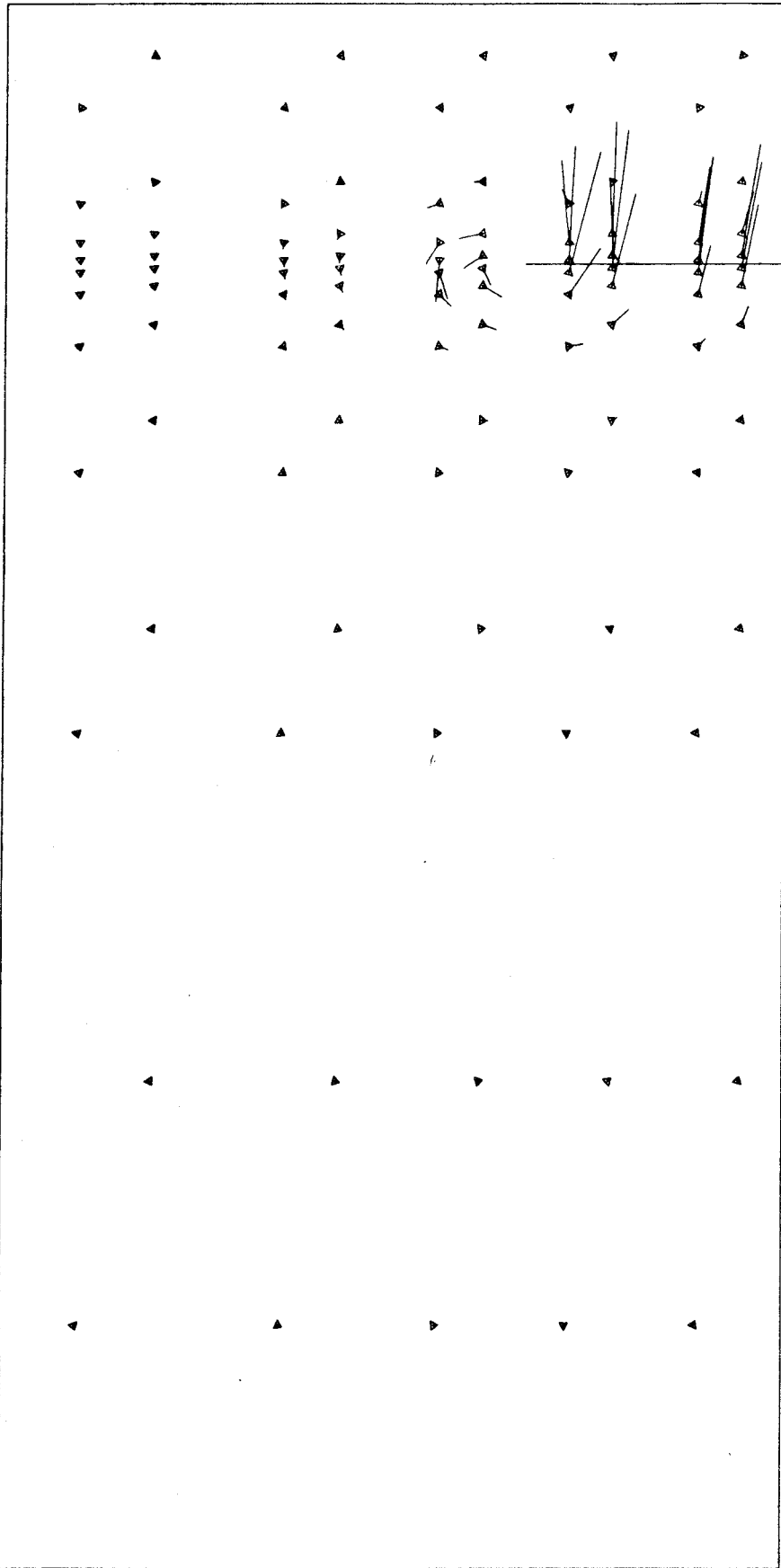


KBS HYDROTHERMAL RUN GLOBAL 2
 K HOMOGENEOUS ISOTROPIC

VELOCITY PLOT

GEOMETRY SCALE $\overset{0}{\rule{1.5cm}{0.4pt}}$ 500 M
 VELOCITY SCALE $\rule{1.5cm}{0.4pt} = 0.4 \times 10^{-7}$ M/SEC

100 000 YEARS

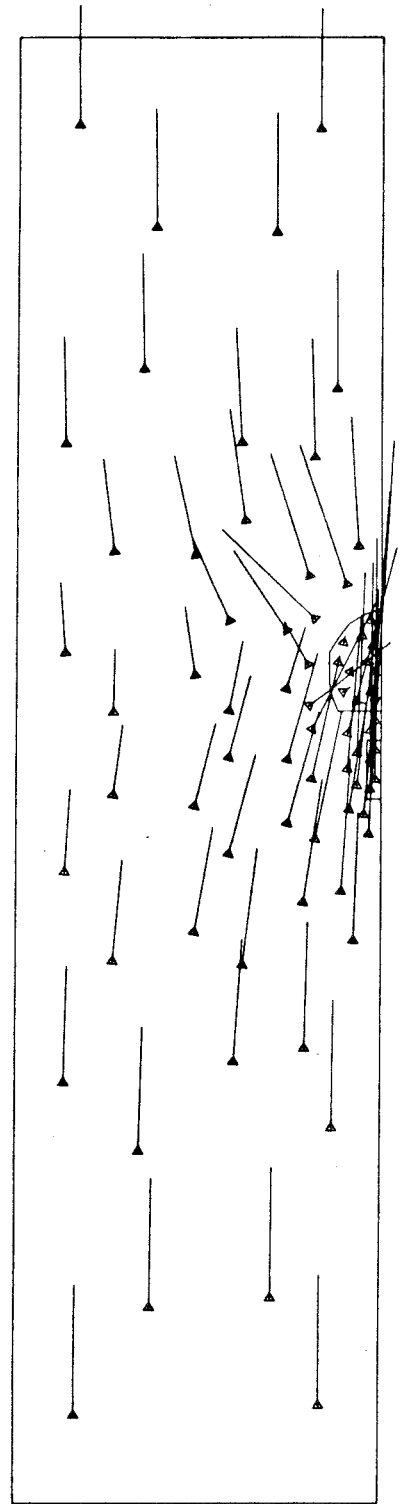


KBS HYDROTHERMAL RUN GLOBAL 3
K (Z) ANISOTROPIC

VELOCITY PLOT

GEOMETRY SCALE $\begin{array}{|c|c|c|c|c|c|} \hline 0 & & & & & 500 \text{ M} \\ \hline \end{array}$
VELOCITY SCALE $\begin{array}{|c|c|c|} \hline \text{---} & \text{---} & \text{---} \\ \hline \end{array} = 0.8 * 10^{**} - 7 \text{ M/SEC}$

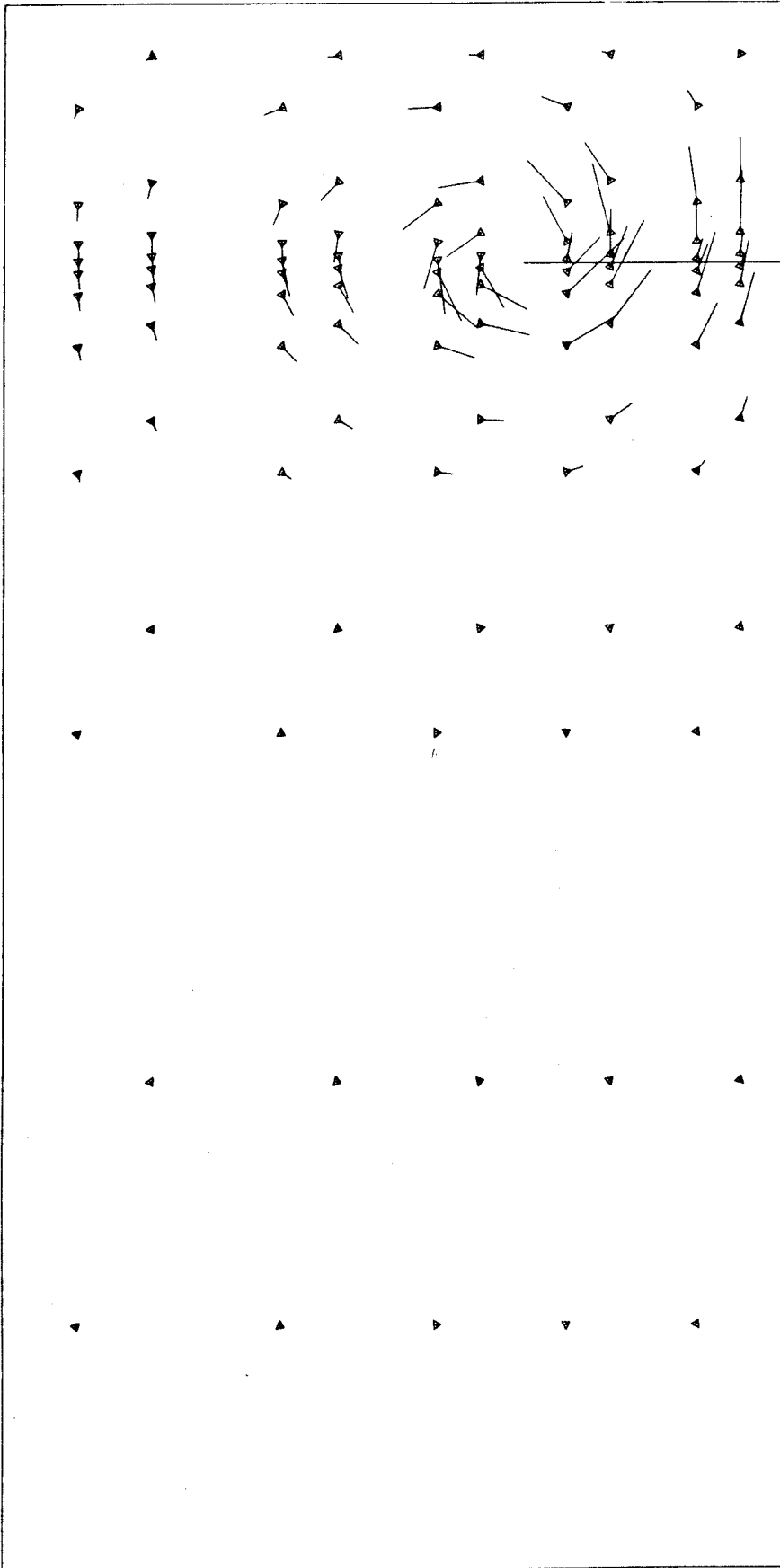
40 YEARS



LOCAL 3

GEOMETRY SCALE $\begin{array}{|c|c|c|c|} \hline 0 & & 5 & 10 \text{ M} \\ \hline \end{array}$

FIGURE 14

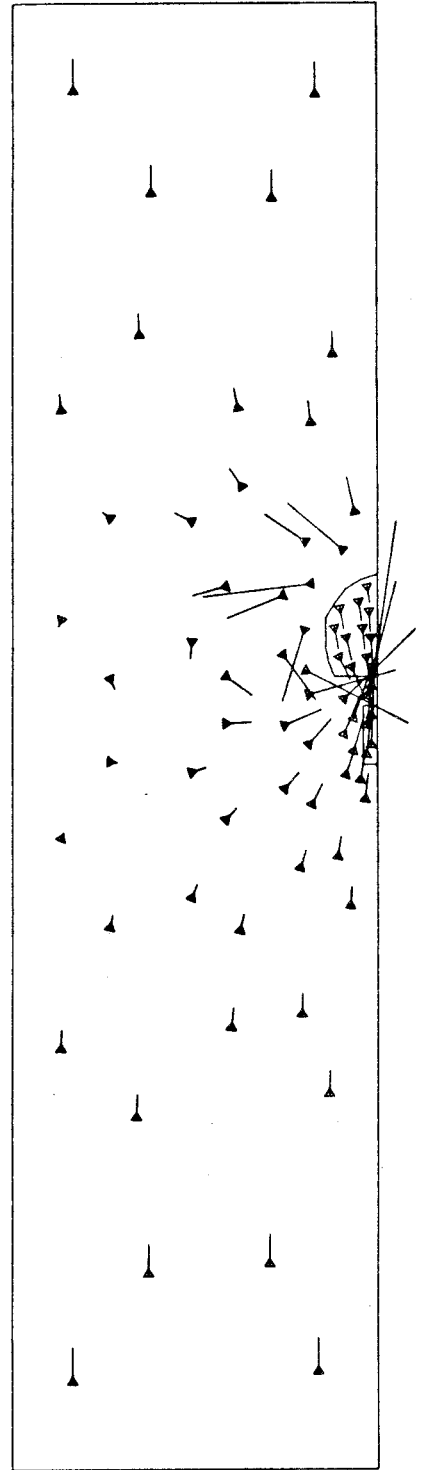


KBS HYDROTHERMAL RUN GLOBAL 3
K(Z) ANISOTROPIC

VELOCITY PLOT

GEOMETRY SCALE 0 ————— 500 M
VELOCITY SCALE |————| = $0.8 * 10 * * - 7$ M/SEC

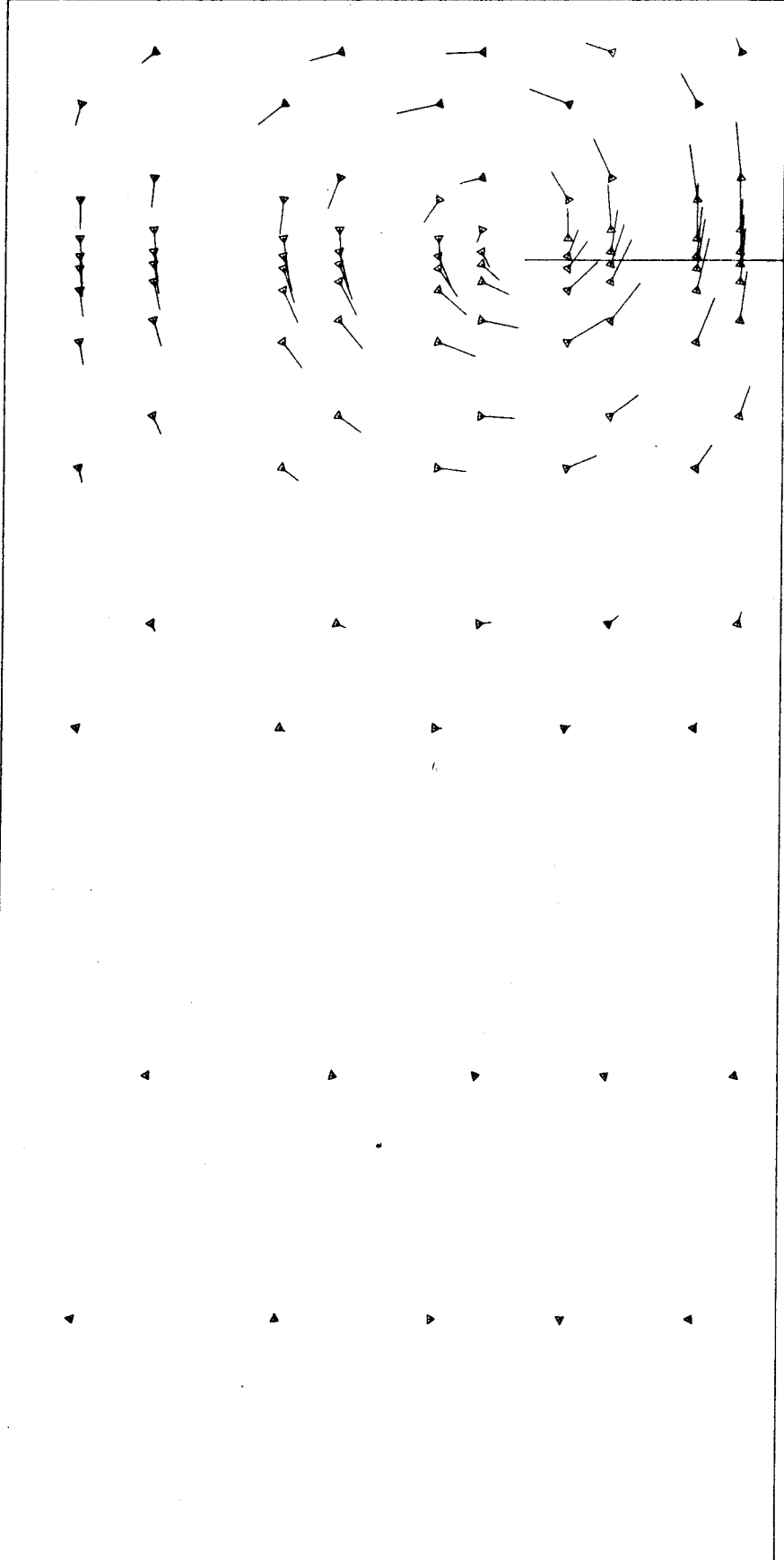
200 YEARS



LOCAL 3

0 ————— 5 ————— 10 M

FIGURE 15

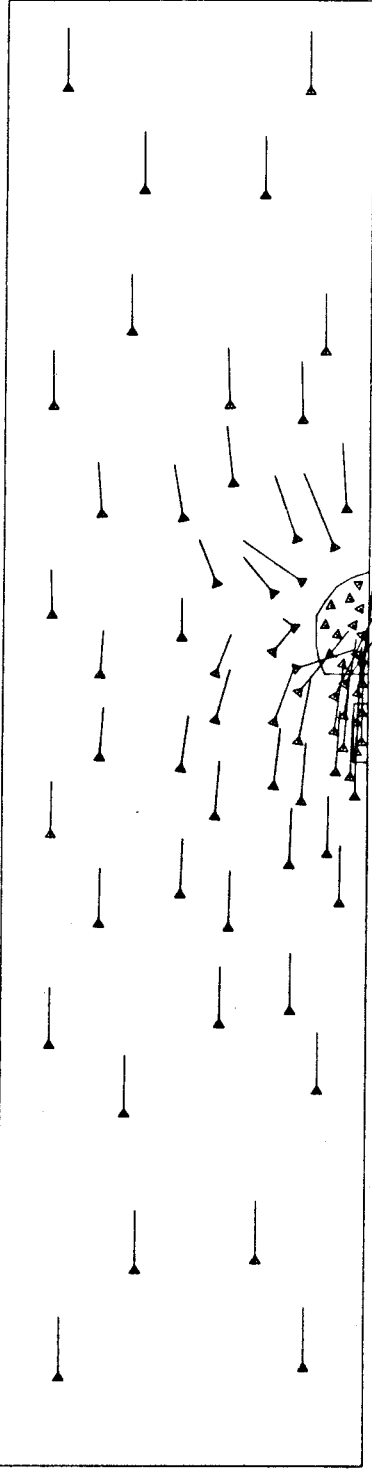


KBS HYDROTHERMAL RUN GLOBAL 3
K(Z) ANISOTROPIC

VELOCITY PLOT

GEOMETRY SCALE 0 500 M
VELOCITY SCALE $\text{---} = 0.8 \times 10^{**} \text{---} = 7 \text{ M/SEC}$

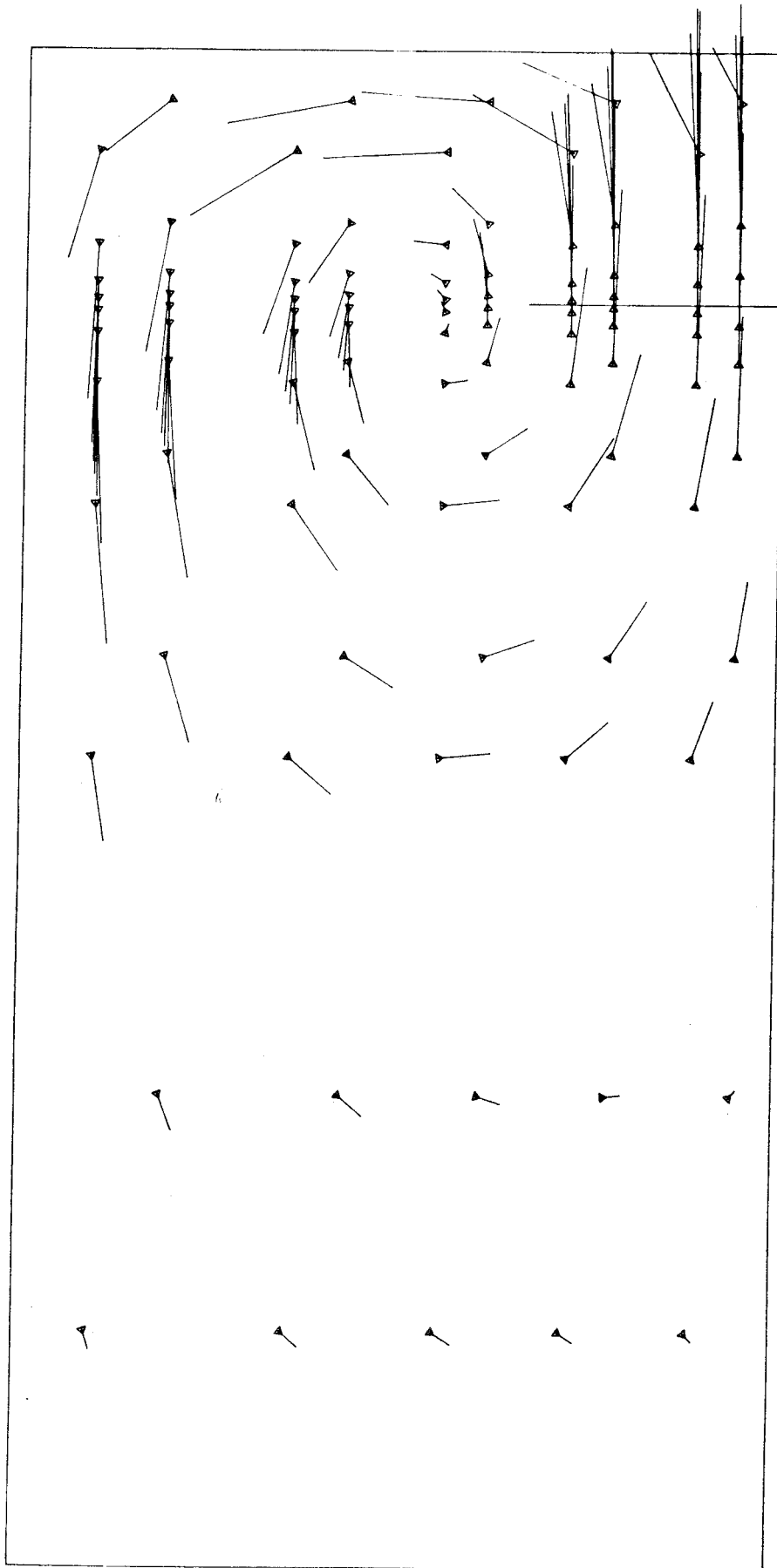
1000 YEARS



LOCAL 3

0 5 10 M

FIGURE 16



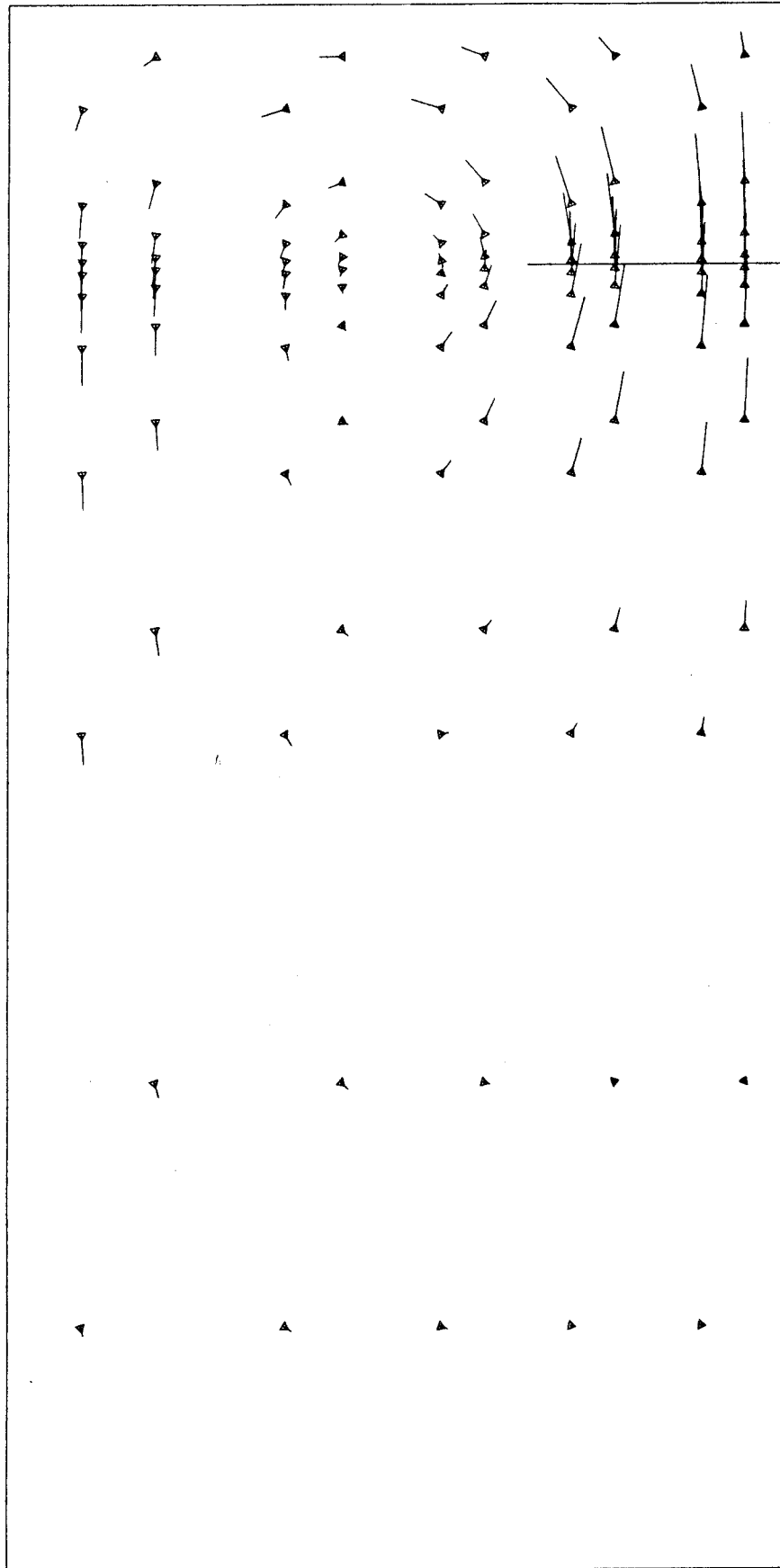
KBS HYDROTHERMAL RUN GLOBAL 3
 K(Z) ANISOTROPIC

VELOCITY PLOT

GEOMETRY SCALE 0 500 M

VELOCITY SCALE \longleftarrow = $0.8 * 10^{**} - 8$ M/SEC

10 000 YEARS

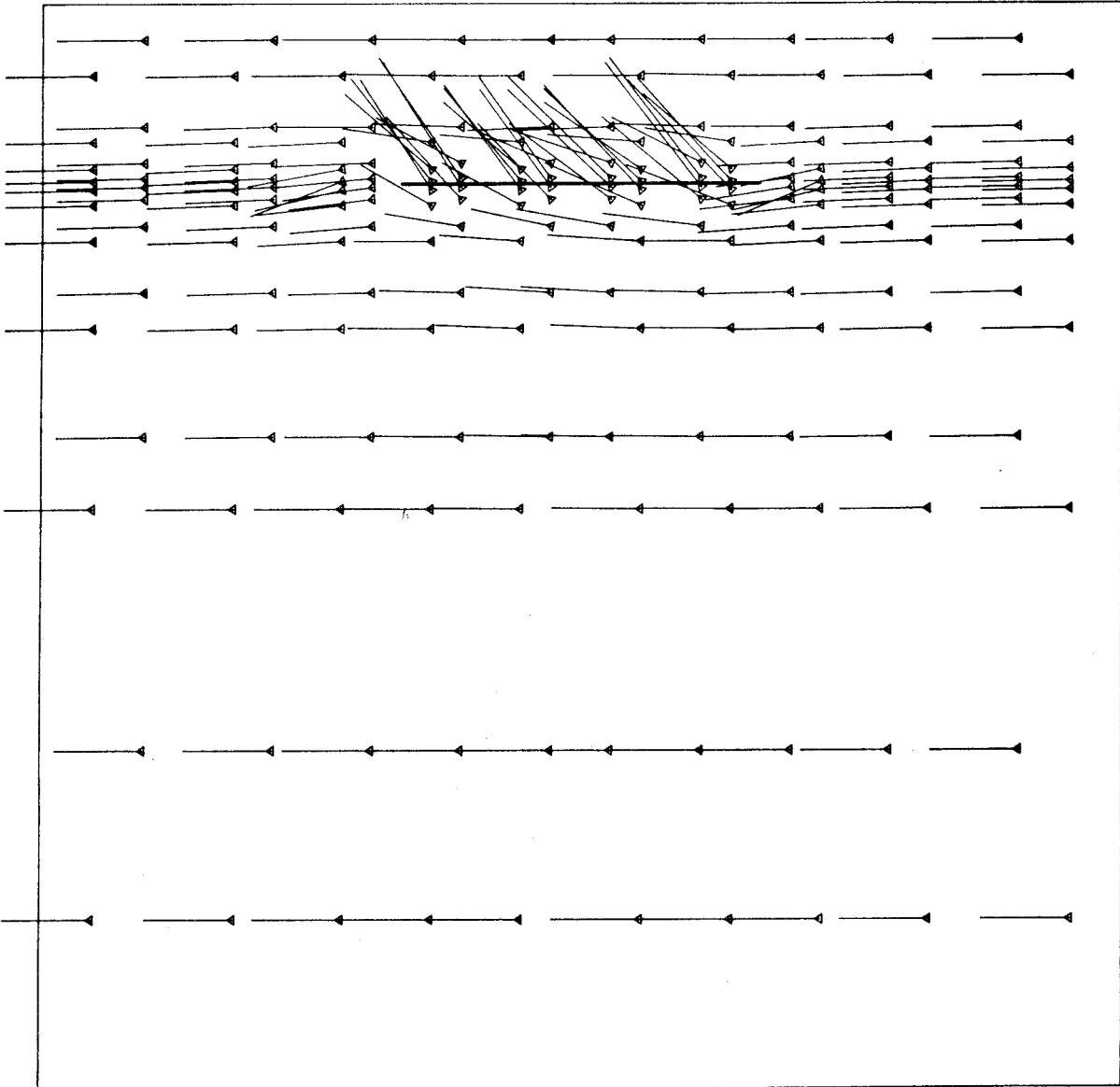


KBS HYDROTHERMAL RUN GLOBAL 3
 K(Z) ANISOTROPIC

VELOCITY PLOT

GEOMETRY SCALE $\overline{\quad\quad\quad}$ 0 500 M
 VELOCITY SCALE $\overline{\quad\quad\quad}$ = $0.8 * 10^{**} - 8$ M/SEC

100 000 YEARS

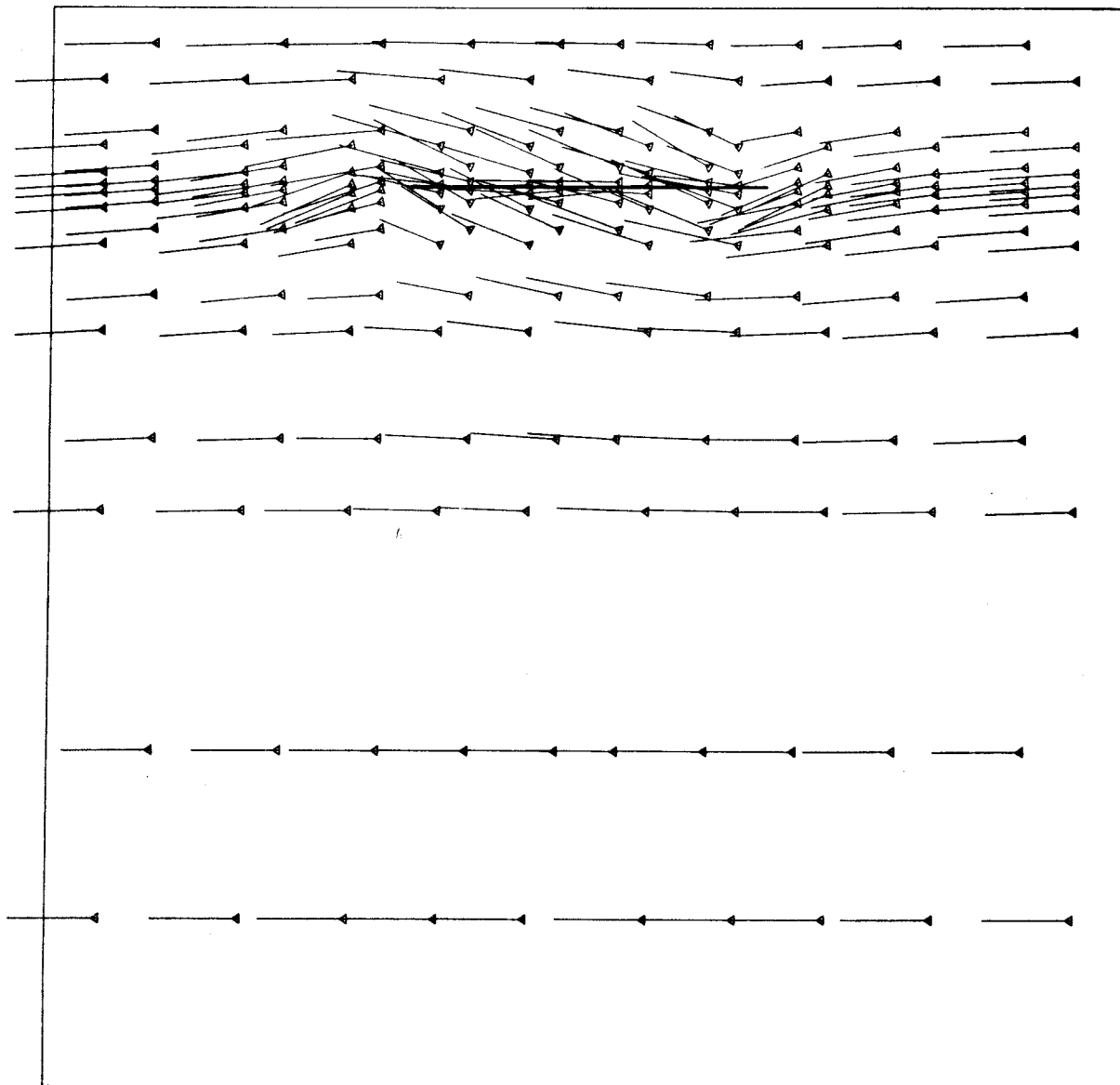


KBS HYDROTHERMAL RUN GLOBAL 2 WITH CROSSFLOW
 K HOMOGENEOUS ISOTROPIC

VELOCITY PLOT

GEOMETRY SCALE 0 500 M
 VELOCITY SCALE \rightarrow = 0.5×10^{-6} M/SEC

40 YEARS

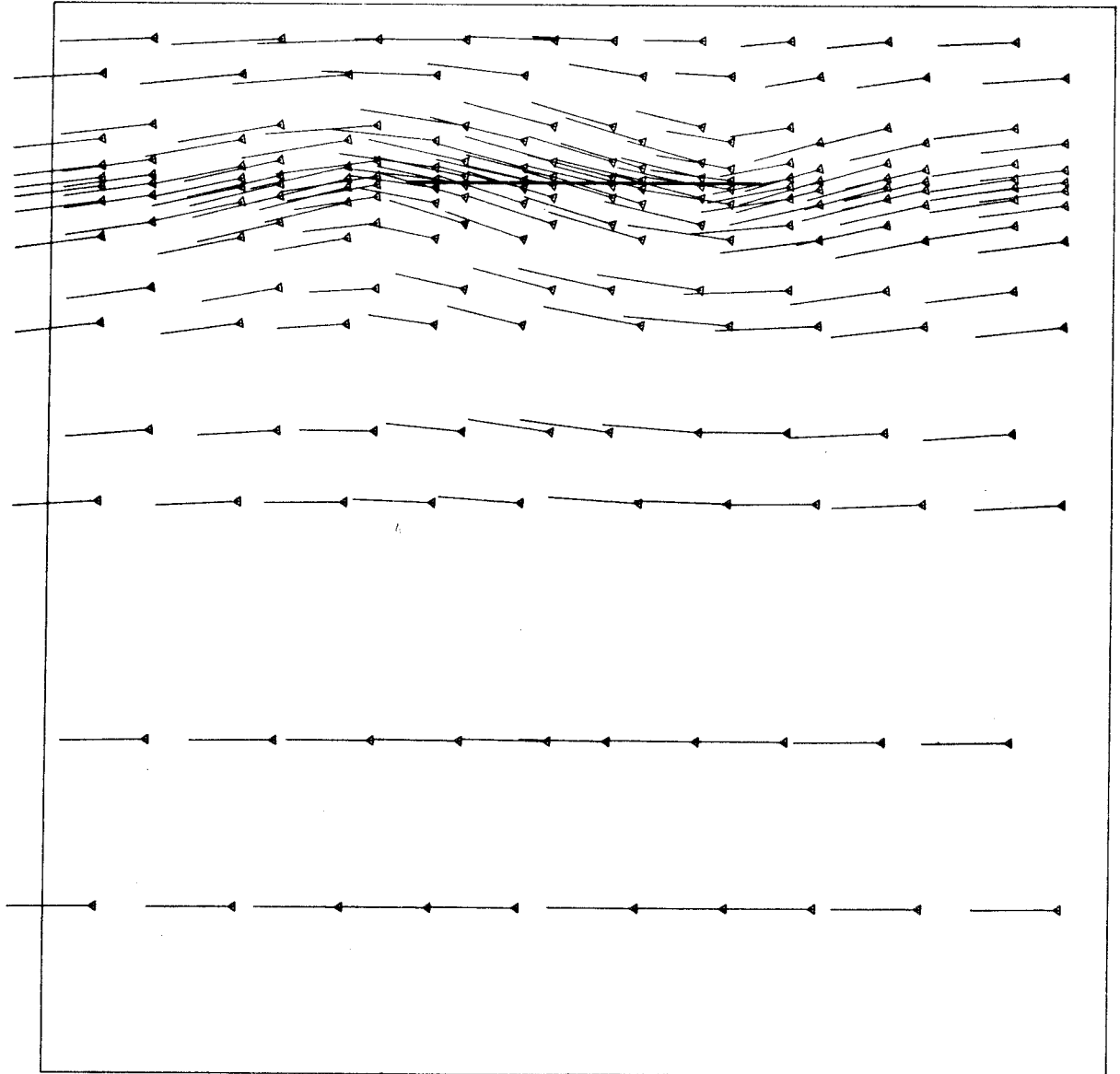


KBS HYDROTHERMAL RUN GLOBAL 2 WITH CROSSFLOW
 K HOMOGENEOUS ISOTROPIC

VELOCITY PLOT


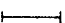
GEOMETRY SCALE $\overline{\hspace{1.5cm}}$ 0 500 M
 VELOCITY SCALE $\overline{\hspace{1.5cm}}$ = 0.5×10^{-6} M/SEC

200 YEARS

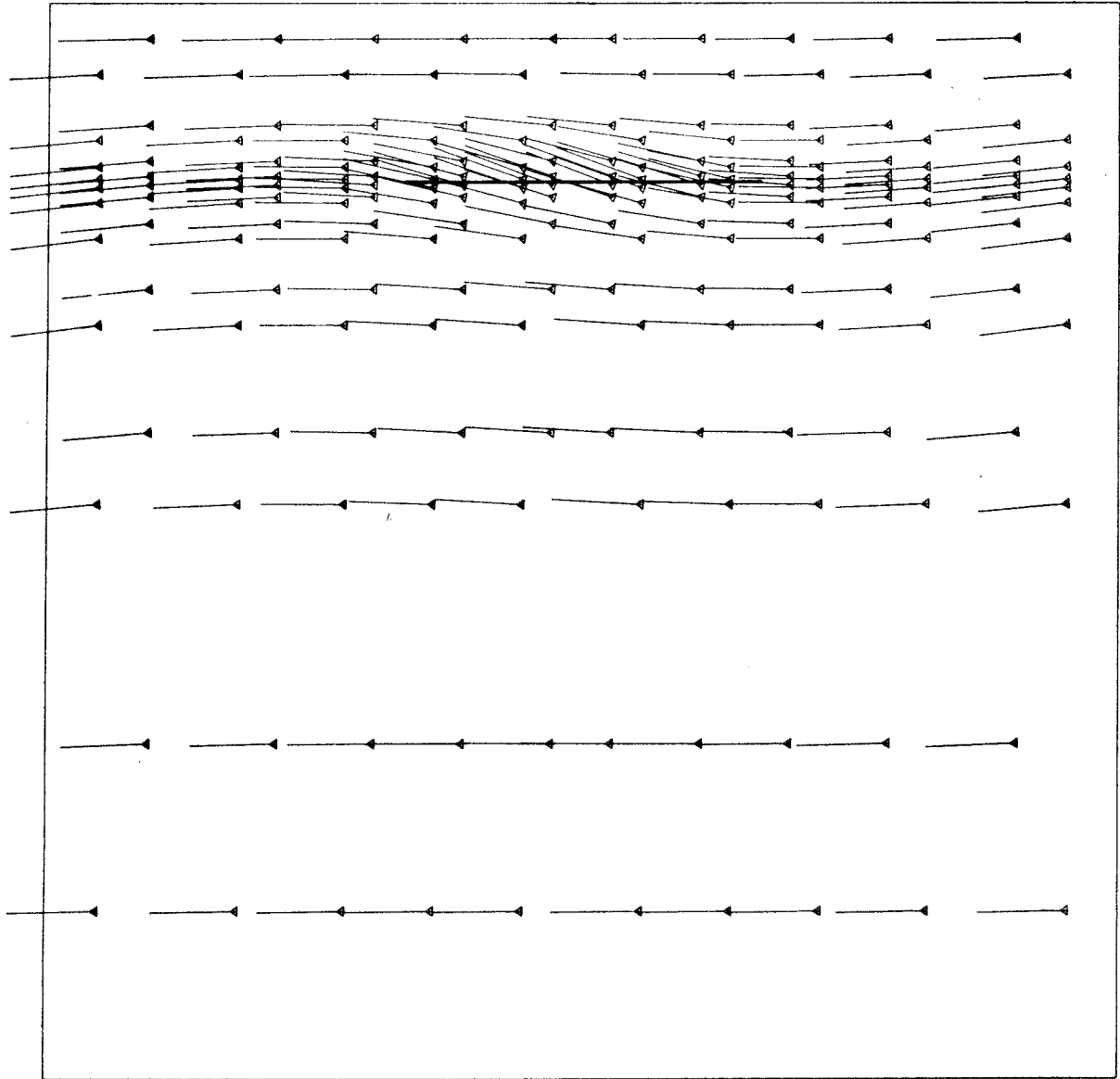


KBS HYDROTHERMAL RUN GLOBAL 2 WITH CROSSFLOW
 K HOMOGENEOUS ISOTROPIC

VELOCITY PLOT


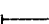
GEOMETRY SCALE  0 500 M
 VELOCITY SCALE  = 0.5 * 10 ** -6 M/SEC

1000 YEARS

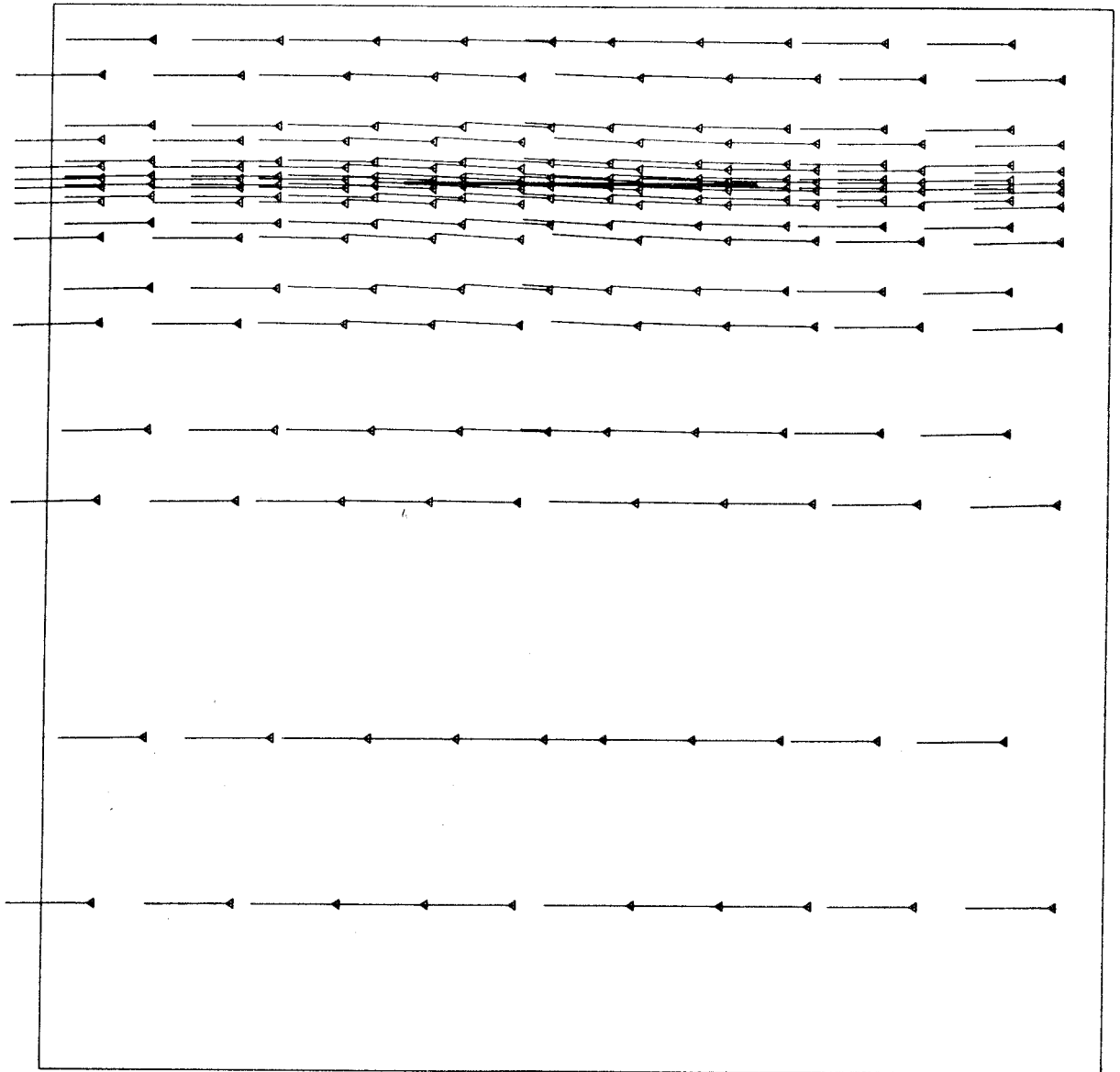


KBS HYDROTHERMAL RUN GLOBAL 2 WITH CROSSFLOW
 K HOMOGENEOUS ISOTROPIC

VELOCITY PLOT

GEOMETRY SCALE  500 M
 VELOCITY SCALE  = 0.5×10^{-6} M/SEC

10 000 YEARS

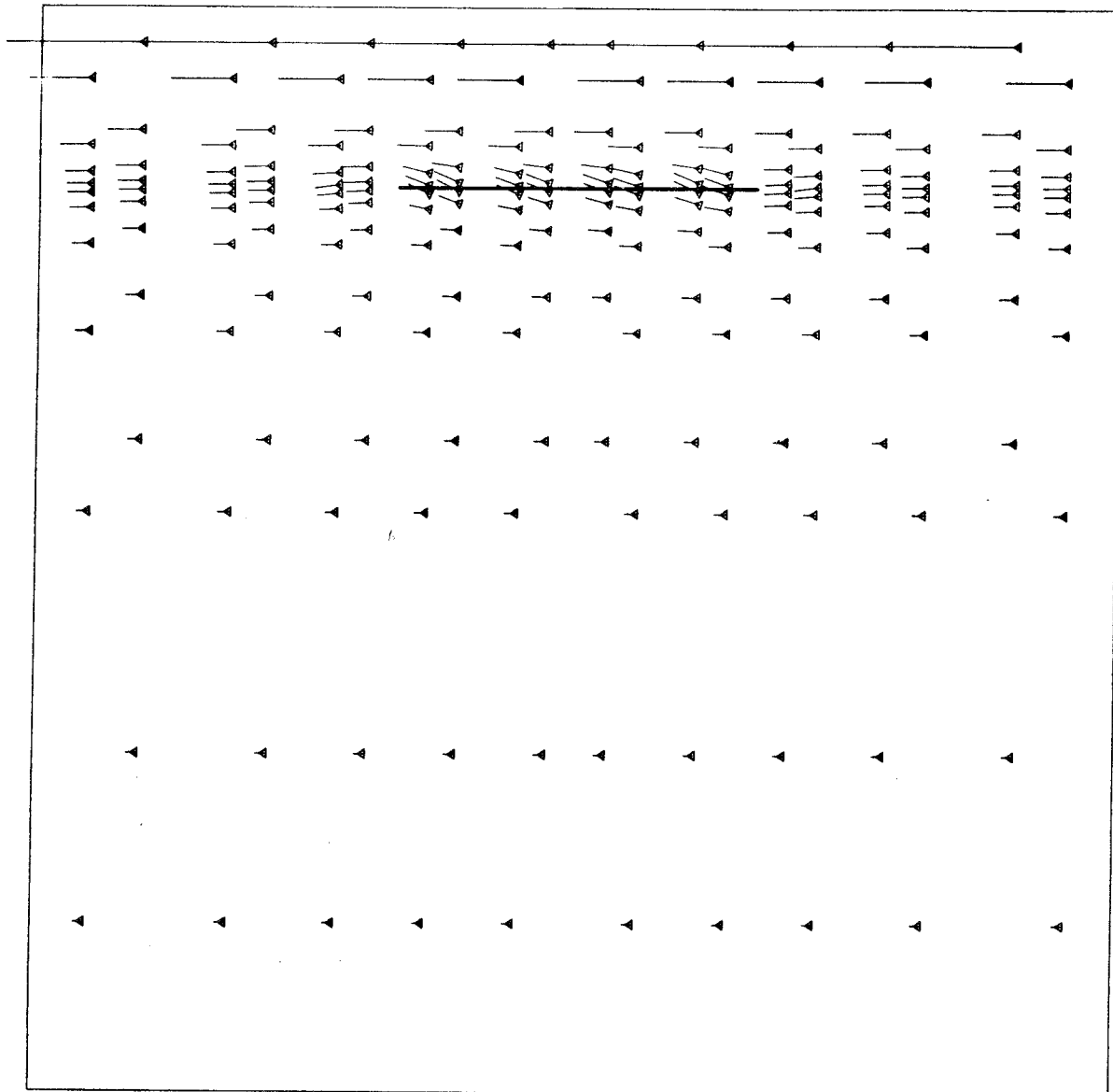


KBS HYDROTHERMAL RUN GLOBAL 2 WITH CROSSFLOW
K HOMOGENEOUS ISOTROPIC

VELOCITY PLOT

GEOMETRY SCALE $\overline{\quad\quad\quad}$ 0 $\overline{\quad\quad\quad}$ 500 M
VELOCITY SCALE $\overline{\quad\quad\quad}$ = 0.5×10^{-6} M/SEC

100 000 YEARS

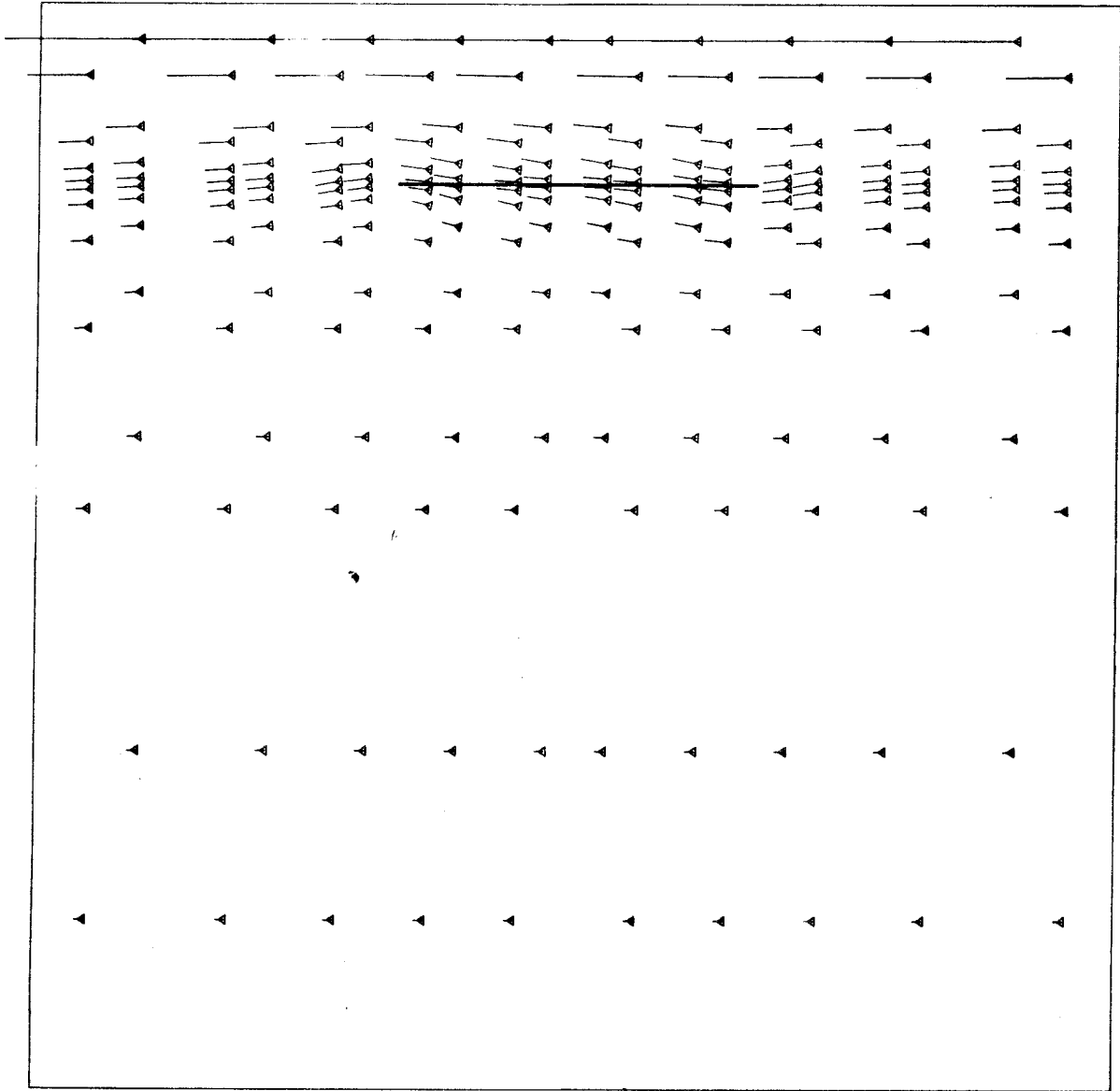


KBS HYDROTHERMAL RUN GLOBAL 3 WITH CROSSFLOW
 K(Z) ANISOTROPIC

VELOCITY PLOT

GEOMETRY SCALE $\begin{array}{|c|c|c|} \hline 0 & \text{---} & 500 \text{ M} \\ \hline \end{array}$
 VELOCITY SCALE $\text{---} = 1.0 * 10^{** -6} \text{ M/SEC}$

40 YEARS

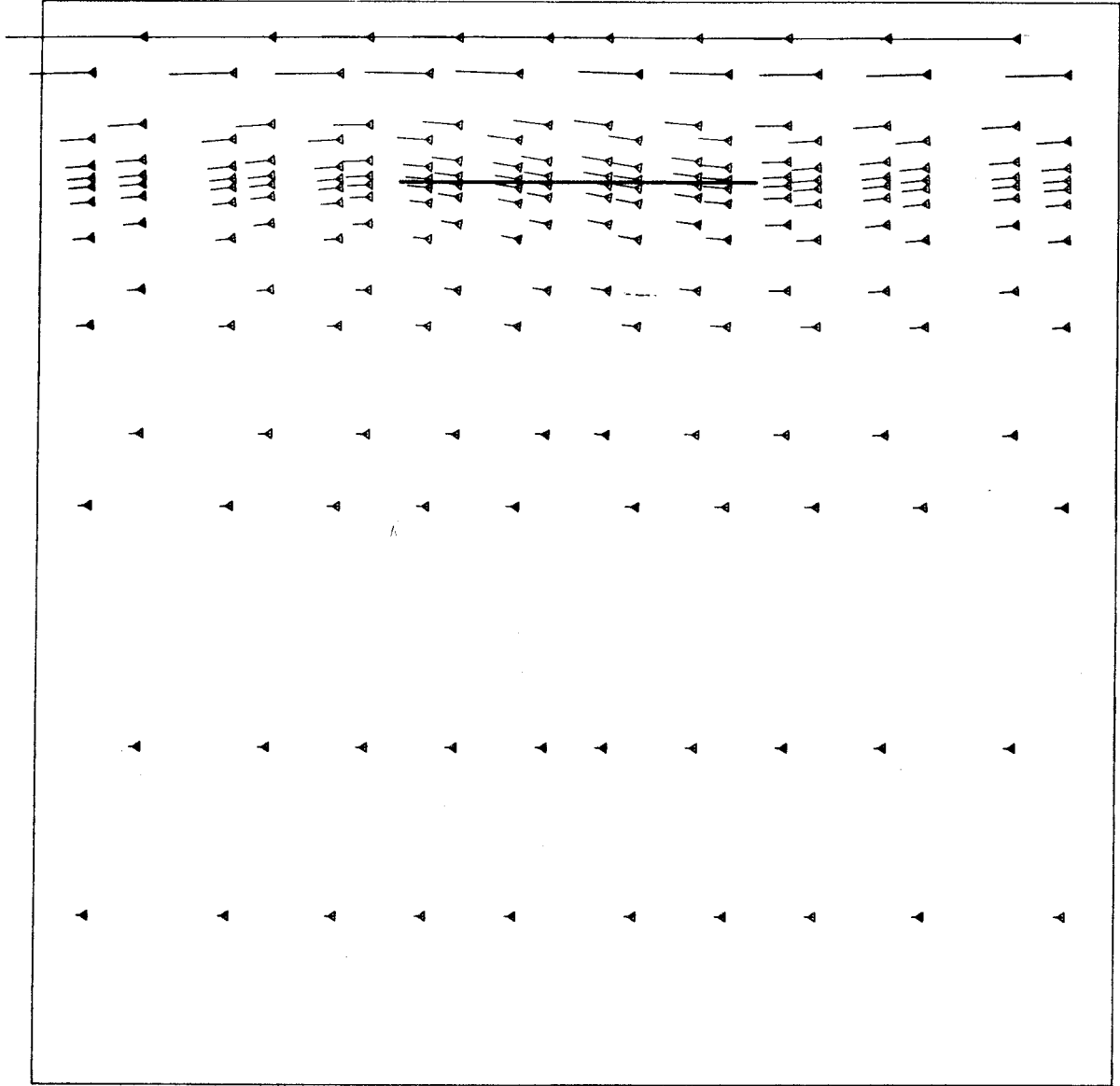


KBS HYDROTHERMAL RUN GLOBAL 3 WITH CROSSFLOW
 K(Z) ANISOTROPIC

VELOCITY PLOT


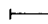
GEOMETRY SCALE 0 500 M
 VELOCITY SCALE \longleftarrow = 1.0×10^{-6} M/SEC

200 YEARS

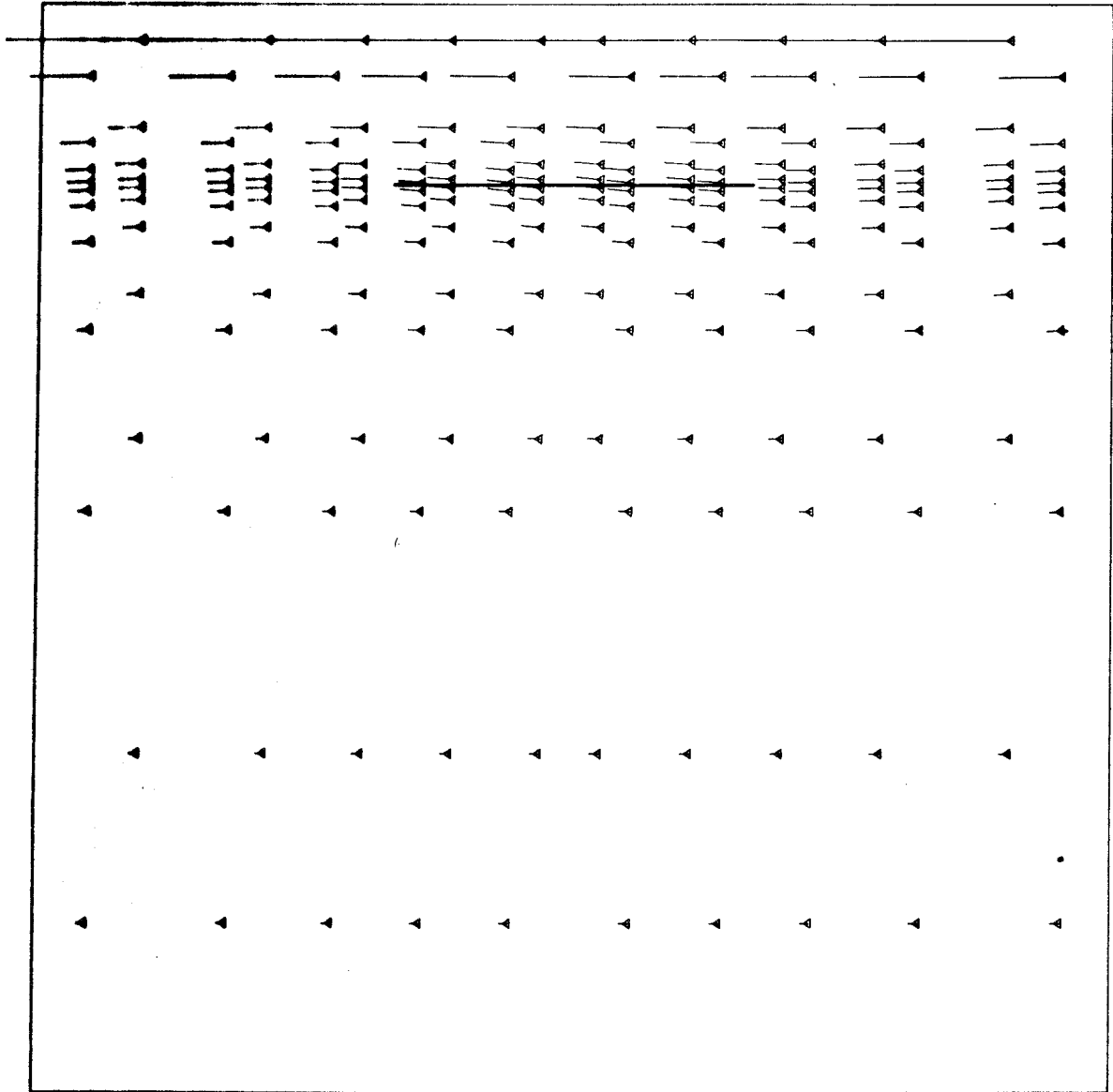


KBS HYDROTHERMAL RUN GLOBAL 3 WITH CROSSFLOW
 K(Z) ANISOTROPIC

VELOCITY PLOT

GEOMETRY SCALE  500 M
 VELOCITY SCALE  = 1.0×10^{-6} M/SEC

1000 YEARS

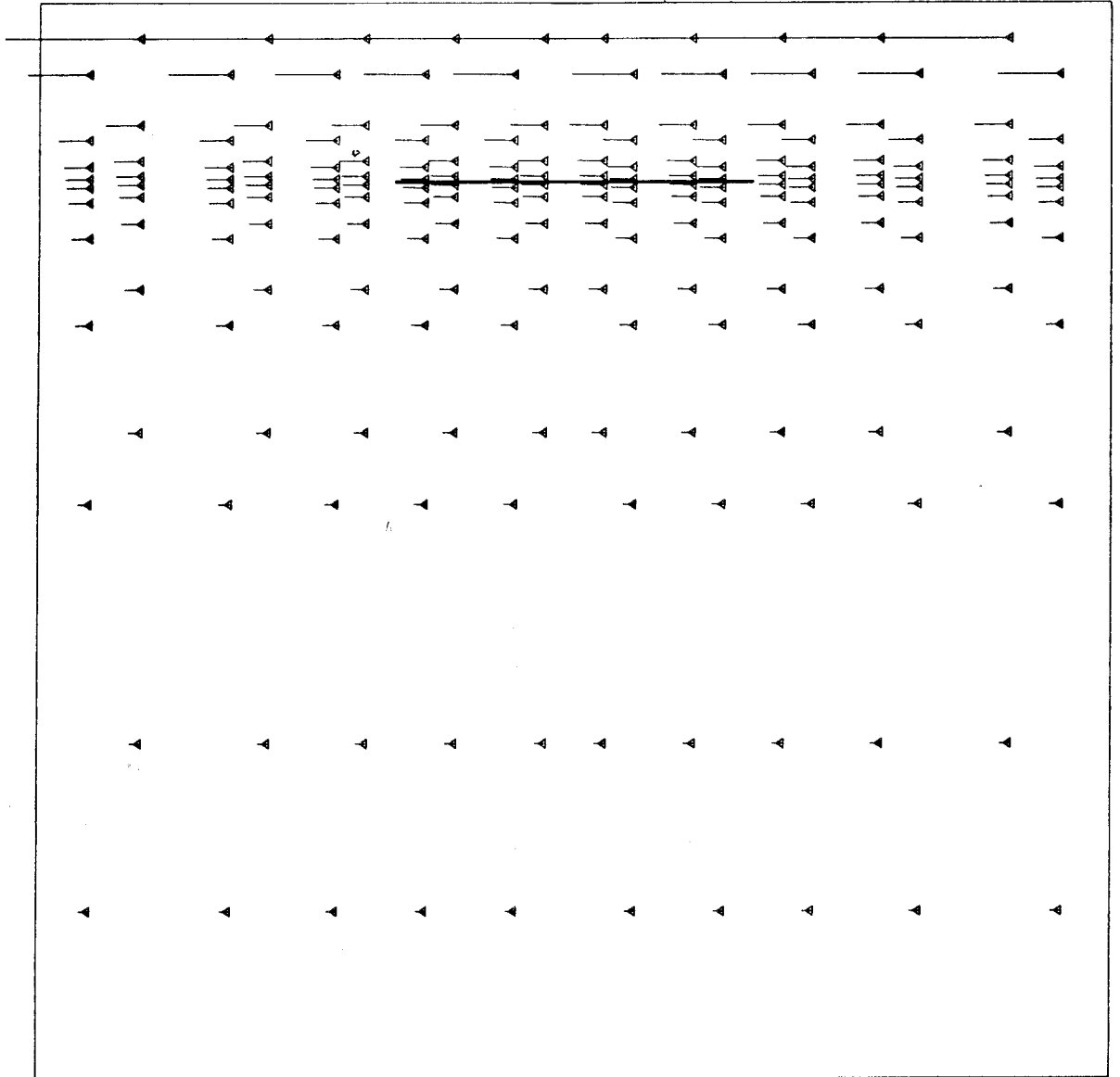


KBS HYDROTHERMAL RUN GLOBAL 3 WITH CROSSFLOW
 K(Z) ANISOTROPIC

VELOCITY PLOT

GEOMETRY SCALE $\overline{\hspace{1.5cm}}$ 0 500 M
 VELOCITY SCALE $\overline{\hspace{1.5cm}}$ = $1.0 * 10^{** -6}$ M/SEC

10 000 YEARS



KBS HYDROTHERMAL RUN GLOBAL 3 WITH CROSSFLOW
 K(Z) ANISOTROPIC

VELOCITY PLOT

GEOMETRY SCALE



VELOCITY SCALE \longleftarrow = 1.0×10^{-6} M/SEC

100 000 YEARS

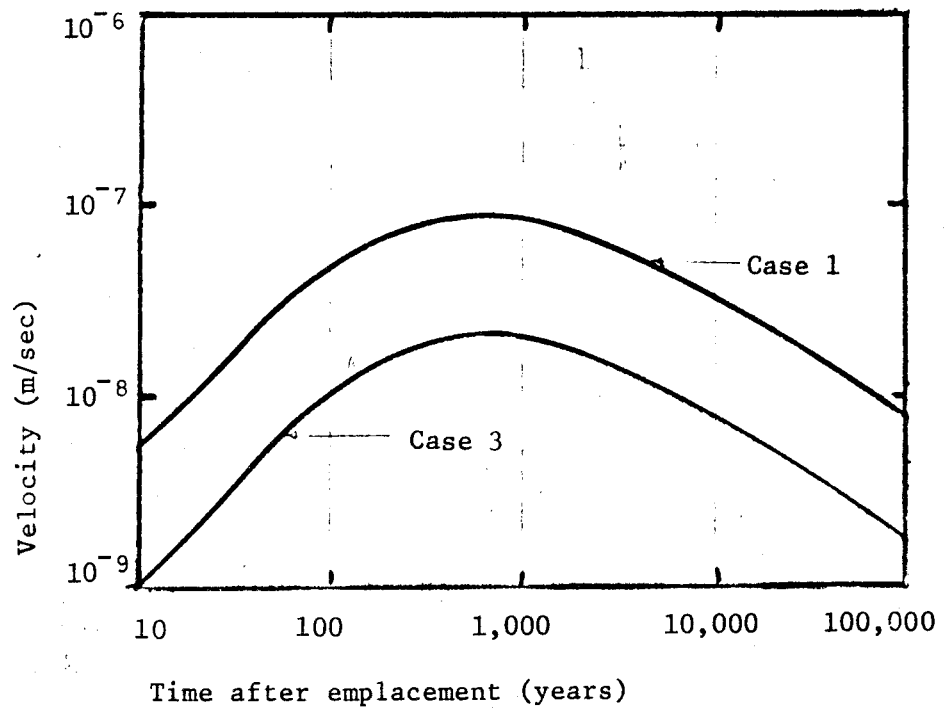


Figure 29. Average hydrothermal vertical velocity above the repository

FÖRTECKNING ÖVER KBS TEKNISKA RAPPORTER

- 01 Källstyrkor i utbränt bränsle och högaktivt avfall från en PWR beräknade med ORIGEN
Nils Kjellbert
AB Atomenergi 77-04-05
- 02 PM angående värmeledningstal hos jordmaterial
Sven Knutsson
Roland Pusch
Högskolan i Luleå 77-04-15
- 03 Deponering av högaktivt avfall i borrhål med buffertsubstans
Arvid Jacobsson
Roland Pusch
Högskolan i Luleå 77-05-27
- 04 Deponering av högaktivt avfall i tunnlar med buffertsubstans
Arvid Jacobsson
Roland Pusch
Högskolan i Luleå 77-06-01
- 05 Orienterande temperaturberäkningar för slutförvaring i berg av radioaktivt avfall, Rapport 1
Roland Blomqvist
AB Atomenergi 77-03-17
- 06 Groundwater movements around a repository, Phase 1, State of the art and detailed study plan
Ulf Lindblom
Hagconsult AB 77-02-28
- 07 Resteffekt studier för KBS
Del 1 Litteraturgenomgång
Del 2 Beräkningar
Kim Ekberg
Nils Kjellbert
Göran Olsson
AB Atomenergi 77-04-19
- 08 Utlakning av franskt, engelskt och kanadensiskt glas med högaktivt avfall
Göran Blomqvist
AB Atomenergi 77-05-20

- 09 Diffusion of soluble materials in a fluid filling a porous medium
Hans Häggblom
AB Atomenergi 77-03-24
- 10 Translation and development of the BNWL-Geosphere Model
Bertil Grundfelt
Kemakta Konsult AB 77-02-05
- 11 Utredning rörande titans lämplighet som korrosionshärdig kapsling för kärnbränsleavfall
Sture Henriksson
AB Atomenergi 77-04-18
- 12 Bedömning av egenskaper och funktion hos betong i samband med slutlig förvaring av kärnbränsleavfall i berg
Sven G Bergström
Göran Fagerlund
Lars Rombén
Cement- och Betonginstitutet 77-06-22
- 13 Urlakning av använt kärnbränsle (bestrålad uranoxid) vid direktdeponering
Ragnar Gelin
AB Atomenergi 77-06-08
- 14 Influence of cementation on the deformation properties of bentonite/quartz buffer substance
Roland Pusch
Högskolan i Luleå 77-06-20
- 15 Orienterande temperaturberäkningar för slutförvaring i berg av radioaktivt avfall
Rapport 2
Roland Blomquist
AB Atomenergi 77-05-17
- 16 Översikt av utländska riskanalyser samt planer och projekt rörande slutförvaring
Åke Hultgren
AB Atomenergi augusti 1977
- 17 The gravity field in Fennoscandia and postglacial crustal movements
Arne Bjerhammar
Stockholm augusti 1977
- 18 Rörelser och instabilitet i den svenska berggrunden
Nils-Axel Mörner
Stockholms Universitet augusti 1977
- 19 Studier av neotektonisk aktivitet i mellersta och norra Sverige, flygbildsgenomgång och geofysisk tolkning av recenta förkastningar
Robert Lagerbäck
Herbert Henkel
Sveriges Geologiska Undersökning september 1977

- 20 Tektonisk analys av södra Sverige, Vättern - Norra Skåne
Kennert Röshoff
Erik Lagerlund
Lunds Universitet och Högskolan Luleå september 1977
- 21 Earthquakes of Sweden 1891 - 1957, 1963 - 1972
Ota Kulhánek
Rutger Wahlström
Uppsala Universitet september 1977
- 22 The influence of rock movement on the stress/strain situation in tunnels or bore holes with radioactive constituents embedded in a bentonite/quartz buffer mass
Roland Pusch
Högskolan i Luleå 1977-08-22
- 23 Water uptake in a bentonite buffer mass
A model study
Roland Pusch
Högskolan i Luleå 1977-08-22
- 24 Beräkning av utlakning av vissa fissionsprodukter och aktinider från en cylinder av franskt glas
Göran Blomqvist
AB Atomenergi 1977-07-27
- 25 Blekinge kustgnejs, Geologi och hydrogeologi
Ingemar Larsson KTH
Tom Lundgren SGI
Ulf Wiklander SGU
Stockholm, augusti 1977
- 26 Bedömning av risken för fördröjt brott i titan
Kjell Pettersson
AB Atomenergi 1977-08-25
- 27 A short review of the formation, stability and cementing properties of natural zeolites
Arvid Jacobsson
Högskolan i Luleå 1977-10-03
- 28 Värmeledningsförsök på buffertsubstans av bentonit/pitesilt
Sven Knutsson
Högskolan i Luleå 1977-09-20
- 29 Deformationer i sprickigt berg
Ove Stephansson
Högskolan i Luleå 1977-09-28
- 30 Retardation of escaping nuclides from a final depository
Ivars Neretnieks
Kungliga Tekniska Högskolan Stockholm 1977-09-14
- 31 Bedömning av korrosionsbeständigheten hos material avsedda för kapsling av kärnbränsleavfall. Lägesrapport 1977-09-27 samt kompletterande yttranden.
Korrosionsinstitutet och dess referensgrupp

- 32 Long term mineralogical properties of bentonite/quartz
buffer substance
Preliminär rapport november 1977
Slutrapport februari 1978
Roland Pusch
Arvid Jacobsson
Högskolan i Luleå
- 33 Required physical and mechanical properties of buffer masses
Roland Pusch
Högskolan Luleå 1977-10-19
- 34 Tillverkning av bly-titan kapsel
Folke Sandelin AB
VBB
ASEA-Kabel
Institutet för metallforskning
Stockholm november 1977
- 35 Project for the handling and storage of vitrified high-level
waste
Saint Gobain Techniques Nouvelles October, 1977
- 36 Sammansättning av grundvatten på större djup i granitisk
berggrund
Jan Rennerfelt
Orrje & Co, Stockholm 1977-11-07
- 37 Hantering av buffertmaterial av bentonit och kvarts
Hans Fagerström, VBB
Björn Lundahl, Stabilator
Stockholm oktober 1977
- 38 Utformning av bergrumsanläggningar
Arne Finné, KBS
Alf Engelbrektson, VBB
Stockholm december 1977
- 39 Konstruktionsstudier, direktdeponering
ASEA-ATOM
VBB
Västerås
- 40 Ekologisk transport och stråldoser från grundvattenburna
radioaktiva ämnen
Ronny Bergman
Ulla Bergström
Sverker Evans
AB Atomenergi
- 41 Säkerhet och strålskydd inom kärnkraftområdet.
Lagar, normer och bedömningsgrunder
Christina Gyllander
Siegfried F Johnson
Stig Rolandson
AB Atomenergi och ASEA-ATOM

- 42 Säkerhet vid hantering, lagring och transport av använt kärnbränsle och förglasat högaktivt avfall
Ann Margret Ericsson
Kemakta november 1977
- 43 Transport av radioaktiva ämnen med grundvatten från ett bergförvar
Bertil Grundfelt
Kemakta november 1977
- 44 Beständighet hos borsilikatglas
Tibor Lakatos
Glasteknisk Utveckling AB
- 45 Beräkning av temperaturer i ett envånings slutförvar i berg för förglasat radioaktivt avfall Rapport 3
Roland Blomquist
AB Atomenergi 1977-10-19
- 46 Temperaturberäkningar för använt bränsle
Taivo Tarandi
VBB
- 47 Teoretiska studier av grundvattenrörelser
Preliminär rapport oktober 1977
Slutrapport februari 1978
Lars Y Nilsson
John Stokes
Roger Thunvik
Inst för kulturteknik KTH
- 48 The mechanical properties of the rocks in Stripa, Kråkemåla, Finnsjön and Blekinge
Graham Swan
Högskolan i Luleå 1977-09-14
- 49 Bergspänningsmätningar i Stripa gruva
Hans Carlsson
Högskolan i Luleå 1977-08-29
- 50 Lakningsförsök med högaktivt franskt glas i Studsvik
Göran Blomqvist
AB Atomenergi november 1977
- 51 Seismotectonic risk modelling for nuclear waste disposal in the Swedish bedrock
F Ringdal
H Gjøystdal
E S Hysebye
Royal Norwegian Council for scientific and industrial research
- 52 Calculations of nuclide migration in rock and porous media, penetrated by water
H Häggblom
AB Atomenergi 1977-09-14

- 53 Mätning av diffusionshastighet för silver i lera-sand-blandning
Bert Allard
Heino Kipatsi
Chalmers tekniska högskola 1977-10-15
- 54 Groundwater movements around a repository
- 54:01 Geological and geotechnical conditions
Håkan Stille
Anthony Burgess
Ulf E Lindblom
Hagconsult AB september 1977
- 54:02 Thermal analyses
Part 1 Conduction heat transfer
Part 2 Advective heat transfer
Joe L Ratigan
Hagconsult AB september 1977
- 54:03 Regional groundwater flow analyses
Part 1 Initial conditions
Part 2 Long term residual conditions
Anthony Burgess
Hagconsult AB oktober 1977
- 54:04 Rock mechanics analyses
Joe L Ratigan
Hagconsult AB september 1977
- 54:05 Repository domain groundwater flow analyses
Part 1 Permeability perturbations
Part 2 Inflow to repository
Part 3 Thermally induced flow
Joe L Ratigan
Anthony S Burgess
Edward L Skiba
Robin Charlwood
- 54:06 Final report
Ulf Lindblom et al
Hagconsult AB oktober 1977
- 55 Sorption av långlivade radionuklider i lera och berg
Del 1 Bestämning av fördelningskoefficienter
Del 2 Litteraturgenomgång
Bert Allard
Heino Kipatsi
Jan Rydberg
Chalmers tekniska högskola 1977-10-10
- 56 Radiolys av utfyllnadsmaterial
Bert Allard
Heino Kipatsi
Jan Rydberg
Chalmers tekniska högskola 1977-10-15

- 57 Stråldoser vid haveri under sjötransport av kärnbränsle
Anders Appelgren
Ulla Bergström
Lennart Devell
AB Atomenergi
- 58 Strålrisker och högsta tillåtliga stråldoser för människan
Gunnar Walinder
FOA 4 november 1977
- 59 Tectonic lineaments in the Baltic from Gävle to Simrishamn
Tom Flodén
Stockholms Universitet 1977-12-15